

6.4.3 Downhole Seismic Surveys

The results of SASW (C) surveys conducted on the crest in the summer 2000 indicated that a high shear-wave velocity gradient may exist in the near-surface rock (Section 6.4.2). It was considered important to acquire near-surface velocity information using an independent approach. Thus, shear- and compression-wave velocities were measured in 8 boreholes along or near the crest of Yucca Mountain by Redpath Geophysics (Figure 202). These downhole velocity surveys were performed in the few open holes above the emplacement area on Yucca Mountain. The procedures, equipment, and analysis techniques of this standard downhole method are described in Section 6.2.5.

Unfortunately, the number of surveyed holes was small and they consisted of neutron-logging holes that are shallow, generally less than 100 ft deep. They also contained a 5-inch ID hanging steel casing that was ungrouted for the entire depth of the borehole. Thus the contact between the casing and the walls of boreholes was unknown and the steel casing prevented the use of the fluxgate compass in the sensor package (Section 6.2.5).

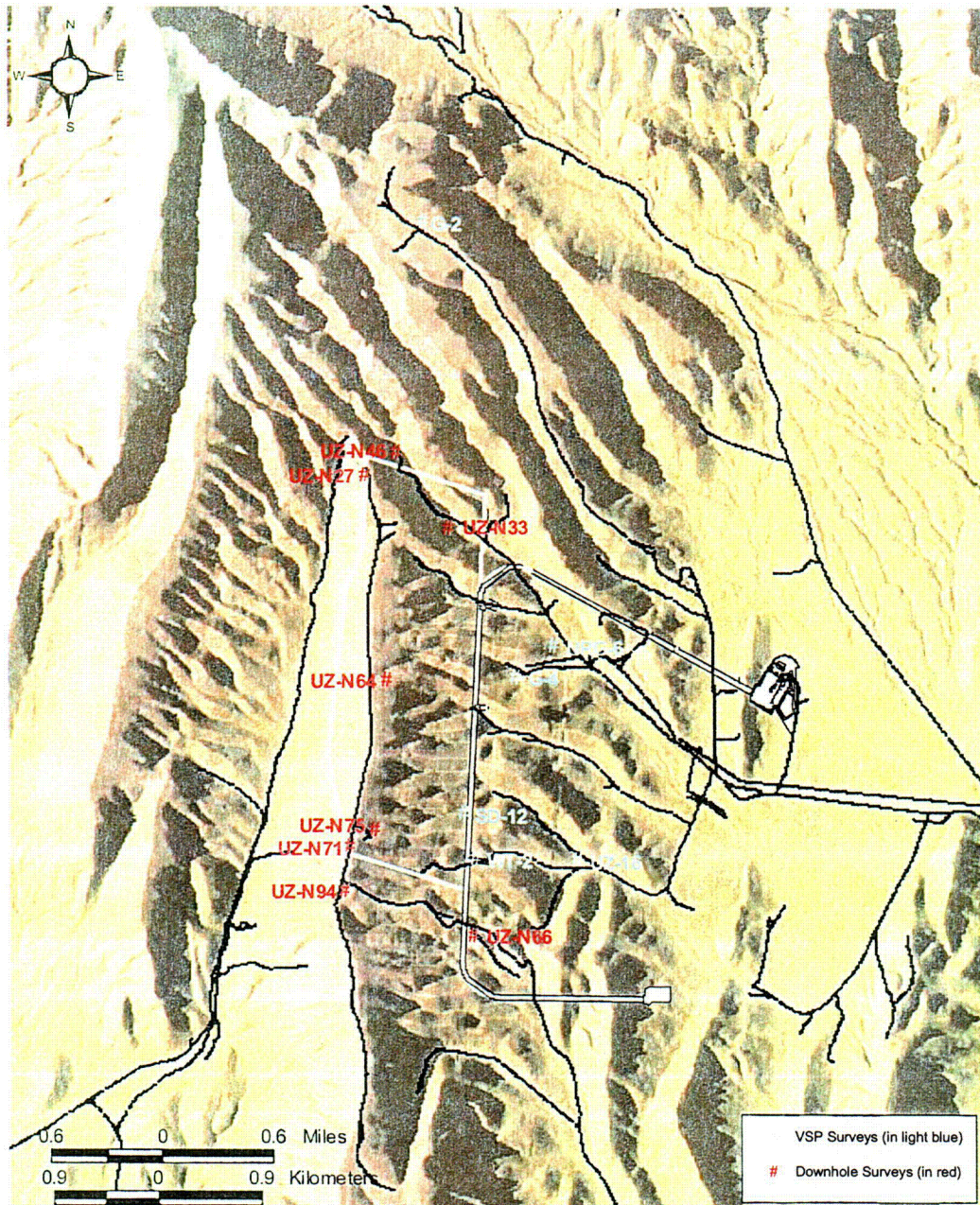
Shear-wave refraction was also attempted. The initial attempt near hole UZ-N27 was not successful, primarily because of a velocity inversion immediately below the surface. Thus, no other refraction surveys were attempted.

Despite the seeming unsuitability of the neutron-logging holes for velocity surveys, the initial results were promising and 8 holes were surveyed. (The results of the downhole and SASW surveys showed that velocity inversions were not unusual in the vicinity of the crest and that further attempts to acquire seismic refraction data were not warranted.) All procedures and relevant calibration information for the downhole measurements at the top of Yucca Mountain are documented in Scientific Notebook SN-M&O-SCI-039-V1 (Redpath 2002). The field work for these investigations was performed from 18 to 23 June 2001. Table 25 lists the neutron-logging holes that were surveyed and their locations are shown on Figure 202.

Table 25. Boreholes Used for Downhole Surveys at Crest of Yucca Mountain

Borehole Number	Elevation Above MSL (ft)	Depth of Survey (ft)
UZ-N27	4857	179
UZ-N33	4329	71
UZ-N46	4501	95
UZ-N64	4789	54
UZ-N66	4358	48
UZ-N71	4925	48
UZ-N75	4799	28
UZ-N94	4926	25

DTN: MO0202DVDWHBSC.002, MO0101COV00396.000



Note: The potential emplacement area as of July 2000 is shown.

Figure 202. Boreholes on or Near the Crest of Yucca Mountain Where Downhole Velocity and VSP Measurements Were Performed

6.4.3.1 Procedures, Equipment, and Analysis

The analysis procedures have been previously described in Section 6.2.5.2. In 7 of the 8 holes, the BHG-2 sensor package was oriented so that one of the horizontal geophones was roughly

aligned with the shear-wave beam. This alignment was done manually since the fluxgate compass in the sensor package could not be used. A half-inch-square piece of reflective tape was attached to the top of the geophone housing. By looking down the borehole with the aid of a flashlight and twisting the connecting cable, the BHG-2 could generally be rotated to an acceptable and known alignment simply by observing the position of the reflected spot of light. Because the lock-in spring is extended at the bottom of the hole and the transducer is dragged up the hole as the survey progresses, the sensor package tended to maintain its initial orientation all the way up the hole. Frequent checks of the orientation were made by looking down the hole and, if necessary, the spring could be released to re-orient the BHG-2. This simple technique was effective even to a depth of 100 ft. UZ-N27 was too deep to use this method so, not knowing the orientation of the BGH-2, the output of both horizontal geophones was recorded.

Travel times were measured from the bottom up at 1-m (3.3 ft) intervals to the surface. An exception to this procedure was made at UZ-N27, in which measurements were made at 2-m (6.6 ft) intervals from 55 to 9 m (180.5 to 29.5 ft) bgs, and then at 1-m (3.3 ft) intervals above that. Although a downhole cable with metric depth markings was used, all results are reported in ft and ft/s.

6.4.3.2 Results

Plots of corrected shear-and compression-wave times vs. depth are shown in Attachment XVI. These plots also show the least-squares values of shear-wave velocities, rounded to the nearest 5-ft/s, and the depths to the interfaces.

Very little of the compression-wave data acquired in these surveys is usable. In almost every instance, a relatively strong signal propagated down the steel casing (labeled as a 'casing wave' on the time vs. depth plots in Attachment XVI) and obscured the compression wave traveling through the rock. A good example of this phenomenon can be seen in the compression-wave records for UZ-N27 (Redpath 2002, Attachment A). A casing wave is dominant down to about 15 m (~ 50 ft), but below this depth, the true compression wave can be seen. The offset of the compression source from the hole collar was increased in an effort to enhance the actual compression wave, but this was not effective. In general, only data points for the shallowest and for the very deepest measurement points are considered valid. An exception is hole UZ-N46, for which the compression-wave velocity seems plausible for the entire depth of the hole.

The question as to why the shear-wave data are considered valid and most of the compression signals are considered to be unreliable can only be answered intuitively. The contact between the steel casing and the surrounding rock is probably not continuous and frictional rather than a solid, uniform, cemented bond as would be the case had it been grouted. A compression wave propagating down through the rock must excite the casing along its axis, *i.e.*, in its stiff direction, in order to be detected by the vertically-sensitive geophone locked inside the casing. It is suspected that it is difficult for a compression wave with sufficient amplitude to be transmitted across the friction contact between the rock and steel pipe. Conversely, a downward traveling shear wave excites the casing in its radial or flexible direction, and any slippage along the length of the casing at the boundary would not be an issue.

The final values of shear-wave velocities are listed in Table 26 and shown in Figures 203 to 210. Also shown is the generalized lithology based on an examination and re-evaluation of the borehole logs. The re-evaluation of these mainly pre-1989 boreholes was required largely because of a change in lithostratigraphic nomenclature. The nomenclature used in this report is based on Buesch et al. (1996). In general, there is only a weak correlation between the velocity layers and the lithology (e.g., UZ-N46). All profiles are shown in Figure 211, illustrating the large variability in shear-wave velocities. Note that there are considerable differences in elevation of the ground surface at these boreholes (maximum of 597 ft; Table 25). The median and plus and minus one standard deviation profiles for the 8 profiles are shown in Figure 212. Compression-wave velocities are not tabulated because of the spotty and questionable results due to interference from the casing wave.

In general, the overall quality of the shear-wave arrival times is surprisingly good considering the uncertainty regarding the contacts between the casing and borehole wall. There is little scatter of the data points about their respective trend lines (Attachment XVI). The scatter is most probably attributable to the absence of grout and the intermittent contact between the steel casing and the rock. The scatter is not due to insufficient signal amplitudes, to noise from extraneous sources such as nearby machinery, nor to some systemic flaw in the recording instrumentation or procedures.

The most questionable data were acquired in UZ-N71, and two attempts were required to obtain plausible shear signals. The shear waves collected in the first attempt were judged to be non-identifiable, and the source was moved to another location for the second try, which resulted in marginally acceptable signals.

The near-surface velocity inversion at UZ-N27, noted earlier as an impediment to a refraction survey, is shown on the plot of travel times against depth for that hole (Figure XVI-1). The inversion exists immediately below a thin (~ 5 ft), relatively fast ($v_s \sim 2200$ ft/s) layer of rock present right at the surface. In an attempt to collect shear-wave refraction data at UZ-N27, usable signals would not propagate beyond about 100 ft, despite many blows to the shear-wave beam, and only the velocity of the thin layer at the surface was evident on the time vs. distance plot.

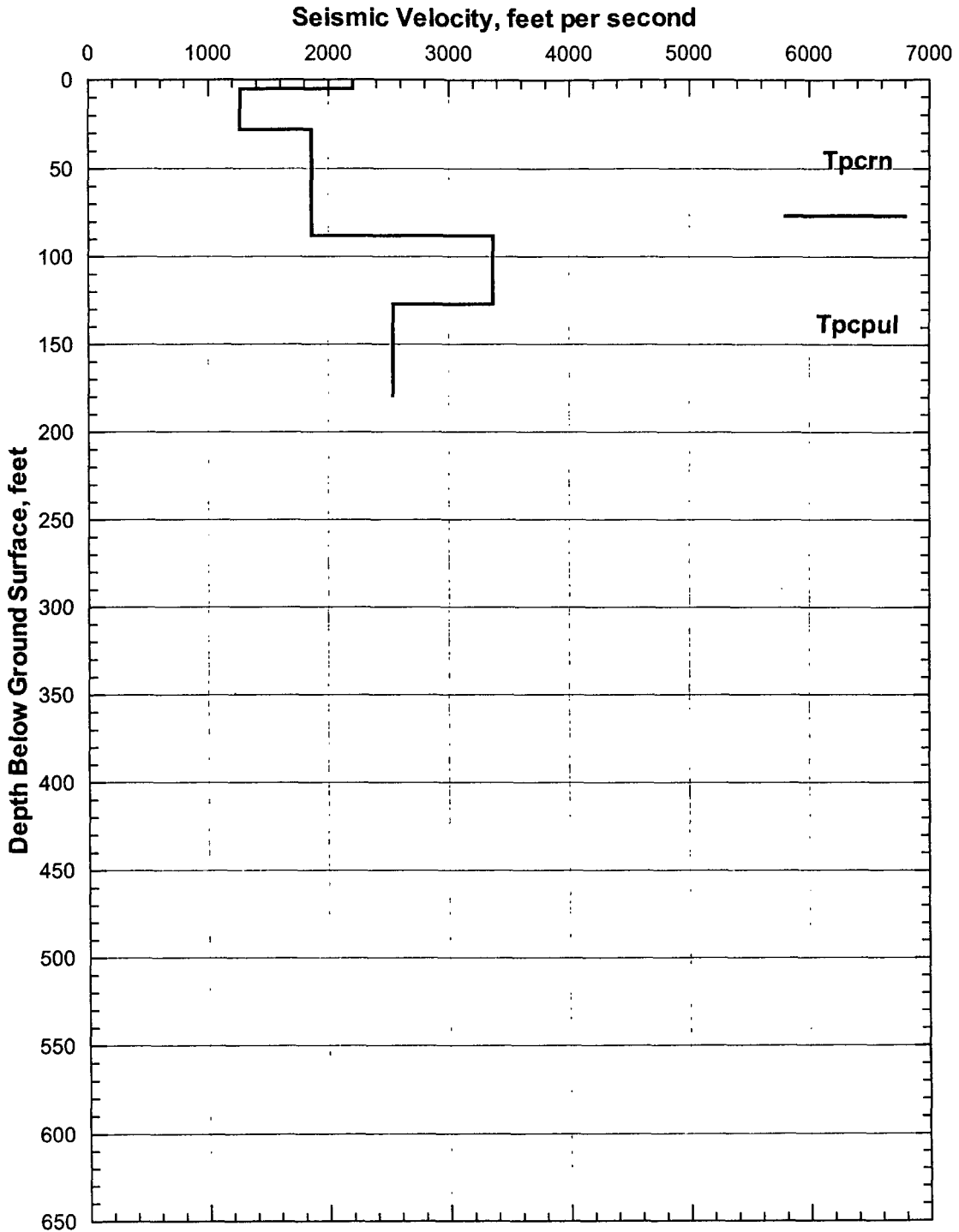
As previously mentioned, there is always some judgement involved when assigning travel-time data points to a layer. Often the change of slope of the data points is not especially pronounced when crossing the boundary between one velocity zone and the one immediately below, and the exact depth of the boundary becomes somewhat uncertain due to the inherent scatter in the data. Nevertheless, least-squares calculations of slopes were used to determine shear-wave velocities in each hole.

An examination of Figure 211, which shows all the velocity profiles, indicates considerable variability in the top 50 ft. A significant velocity contrast is observed in UZ-N46 and UZ-N71. A significant high-velocity spike (?) is observed in UZ-N64. This variability is reflected in the mean, median, and plus and minus one standard deviation profiles shown in Figure 212. The wide range in the values of shear-wave velocities and the apparent lack of stratigraphic correlation between holes (Figures 203 to 210) demonstrate the heterogeneous nature of the volcanic deposits that comprise the Yucca Mountain site.

Table 26. Downhole Shear-Wave Velocities at Crest of Yucca Mountain

UZ-N27	Depth Range (ft)	Velocity (ft/s)
	1.5 - 5	2,200
	5 - 28	1,265
	28 - 88	1,860
	88 - 127	3,365
127 - 179	2,535	
UZ-N33	Depth Range (ft)	Velocity (ft/s)
	1.5 - 9	1,245
	9 - 71	2,790
UZ-N46	Depth Range (ft)	Velocity (ft/s)
	2 - 31	1,275
	31 - 81	1,580
81 - 95	5,500 ±	
UZ-N64	Depth Range (ft)	Velocity (ft/s)
	2 - 8	1,735
	8 - 31	2,140
	31 - 41	3,995
41 - 54	2,190	
UZ-N66	Depth Range (ft)	Velocity (ft/s)
	2 - 5	1,525
	5 - 31	2,650
31 - 48	1,280	
UZ-N71	Depth Range (ft)	Velocity (ft/s)
	2 - 22	1,735
	22 - 48	5,000 ±
UZ-N75	Depth Range (ft)	Velocity (ft/s)
	1.5 - 10	2,065
10 - 28	2,680	
UZ-N94	Depth Range (ft)	Velocity (ft/s)
	1.5 - 25	2,835

DTN: MO0202DVDWHBSC.002



DTNs: MO0202DVDWHBSC.002, GS940208314211.004

Figure 203. UZ-N27 Shear-Wave Velocities from Downhole Measurements and Generalized Lithology

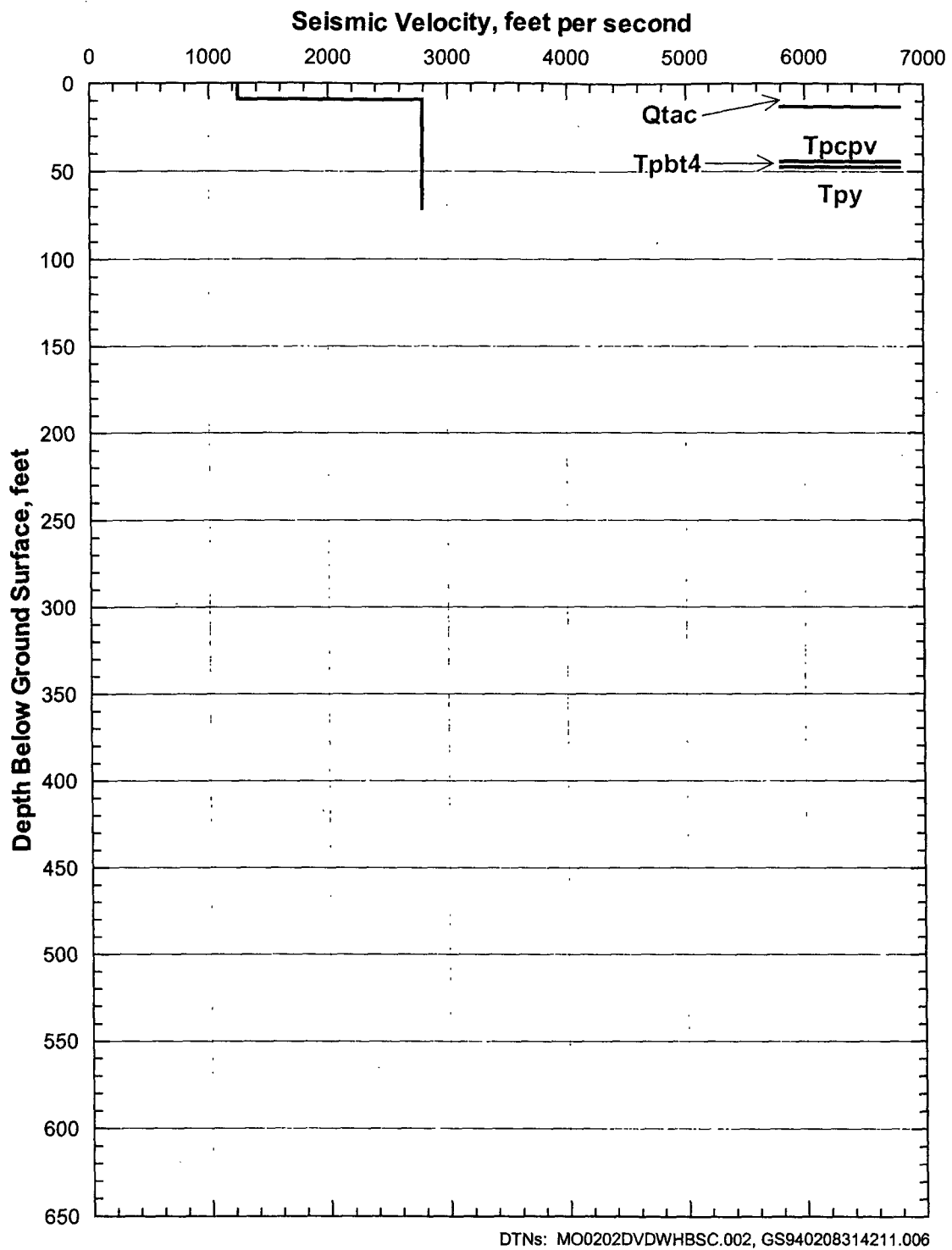
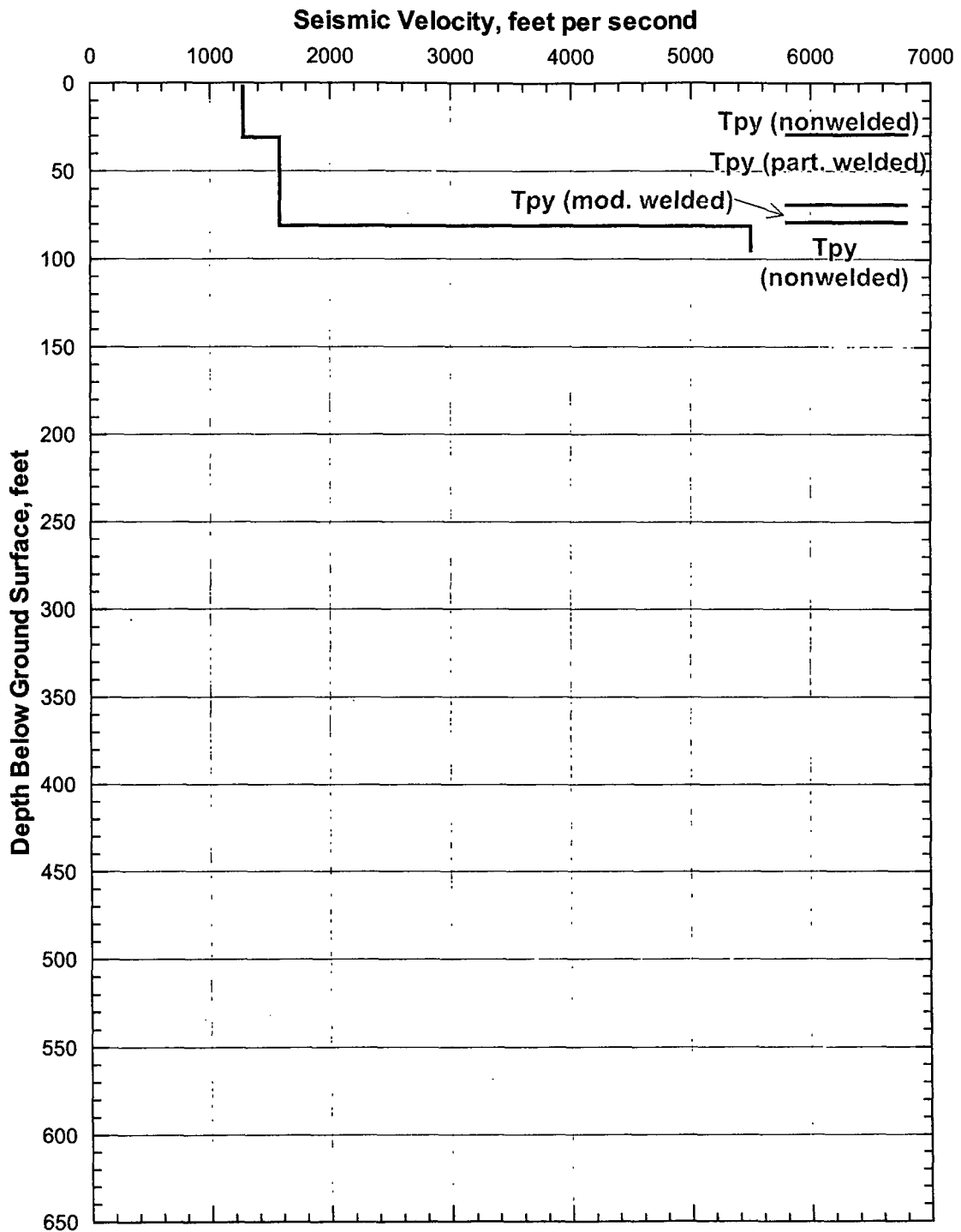


Figure 204. UZ-N33 Shear-Wave Velocities from Downhole Measurements and Generalized Lithology



Sources: DTN: MO0202DVDWHBSC.002, Blout et al. (1994, page 51)

Figure 205. UZ-N46 Shear-Wave Velocities from Downhole Measurements and Generalized Lithology

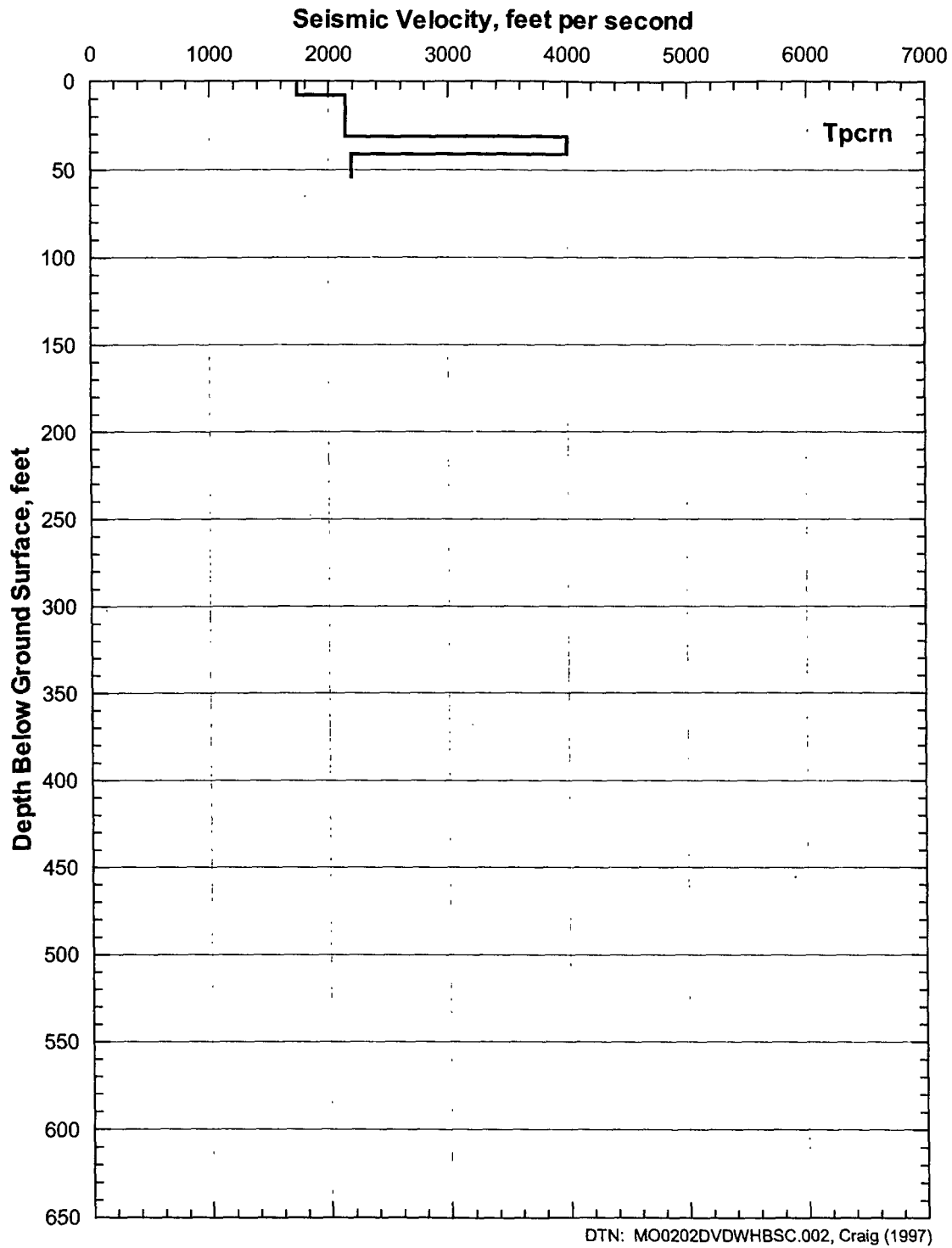


Figure 206. UZ-N64 Shear-Wave Velocities from Downhole Measurements and Generalized Lithology

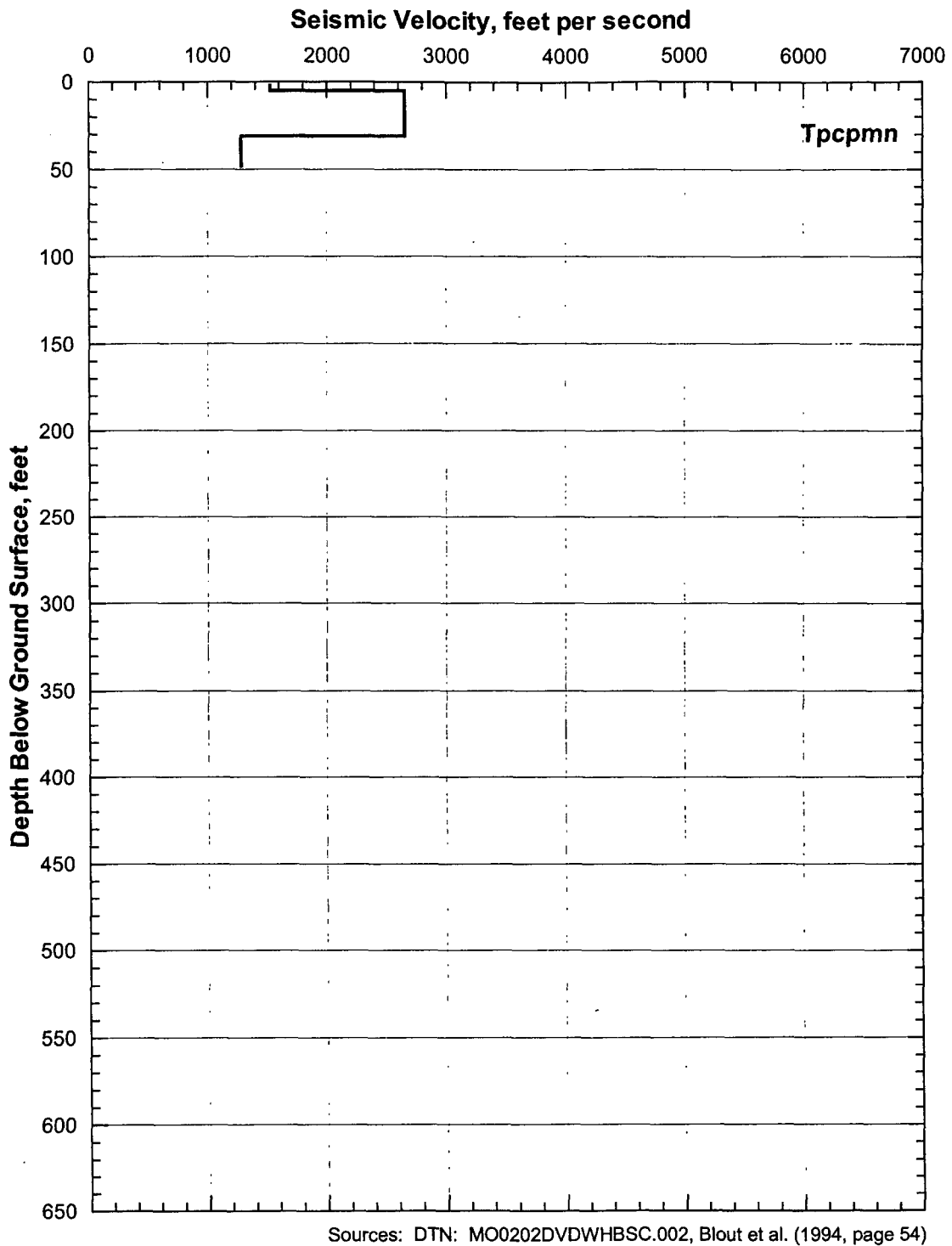
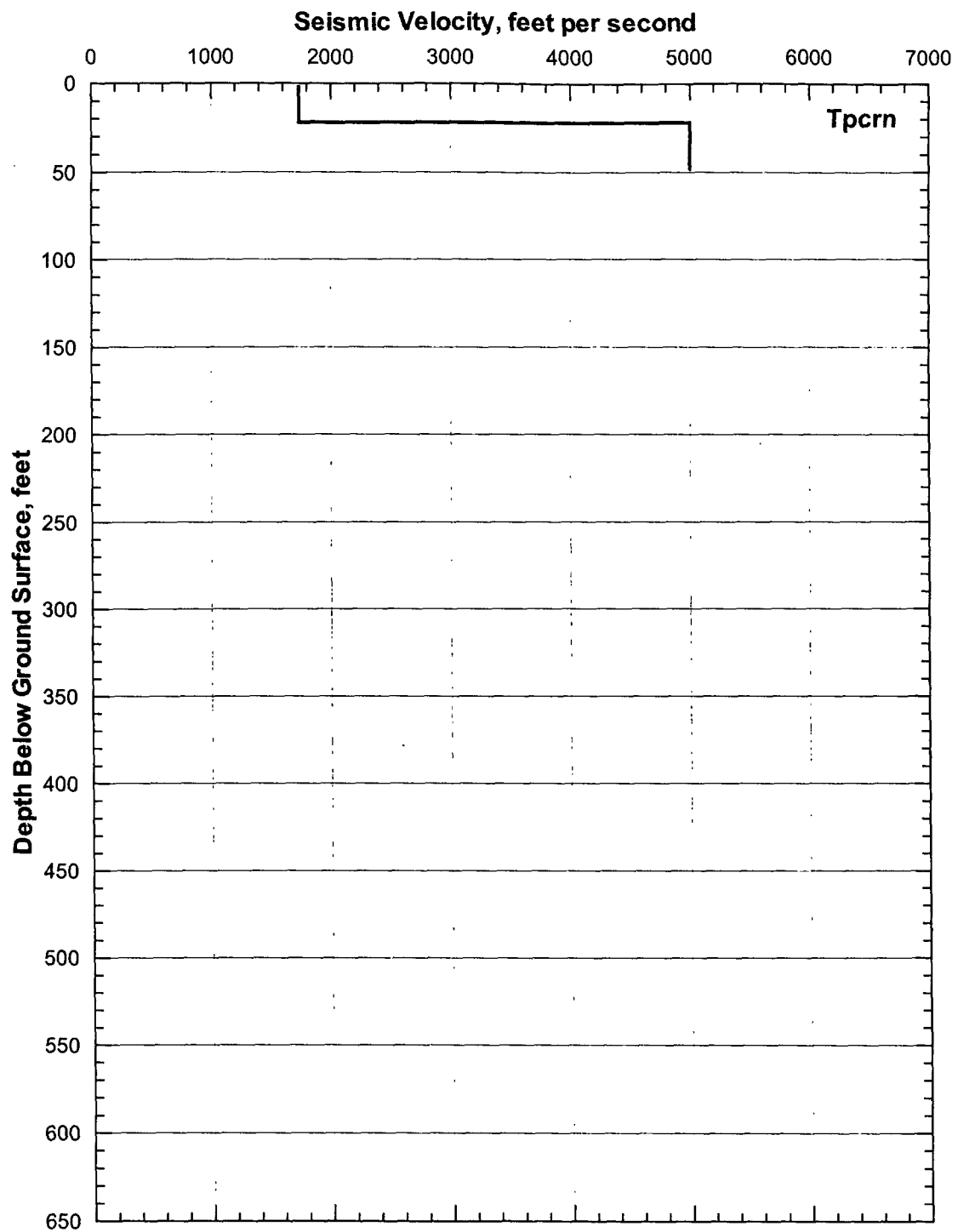


Figure 207. UZ-N66 Shear-Wave Velocities from Downhole Measurements and Generalized Lithology



Sources: DTN: MO0202DVDWHBSC.002, Blout et al. (1994, page 55)

Figure 208. UZ-N71 Shear-Wave Velocities from Downhole Measurements and Generalized Lithology

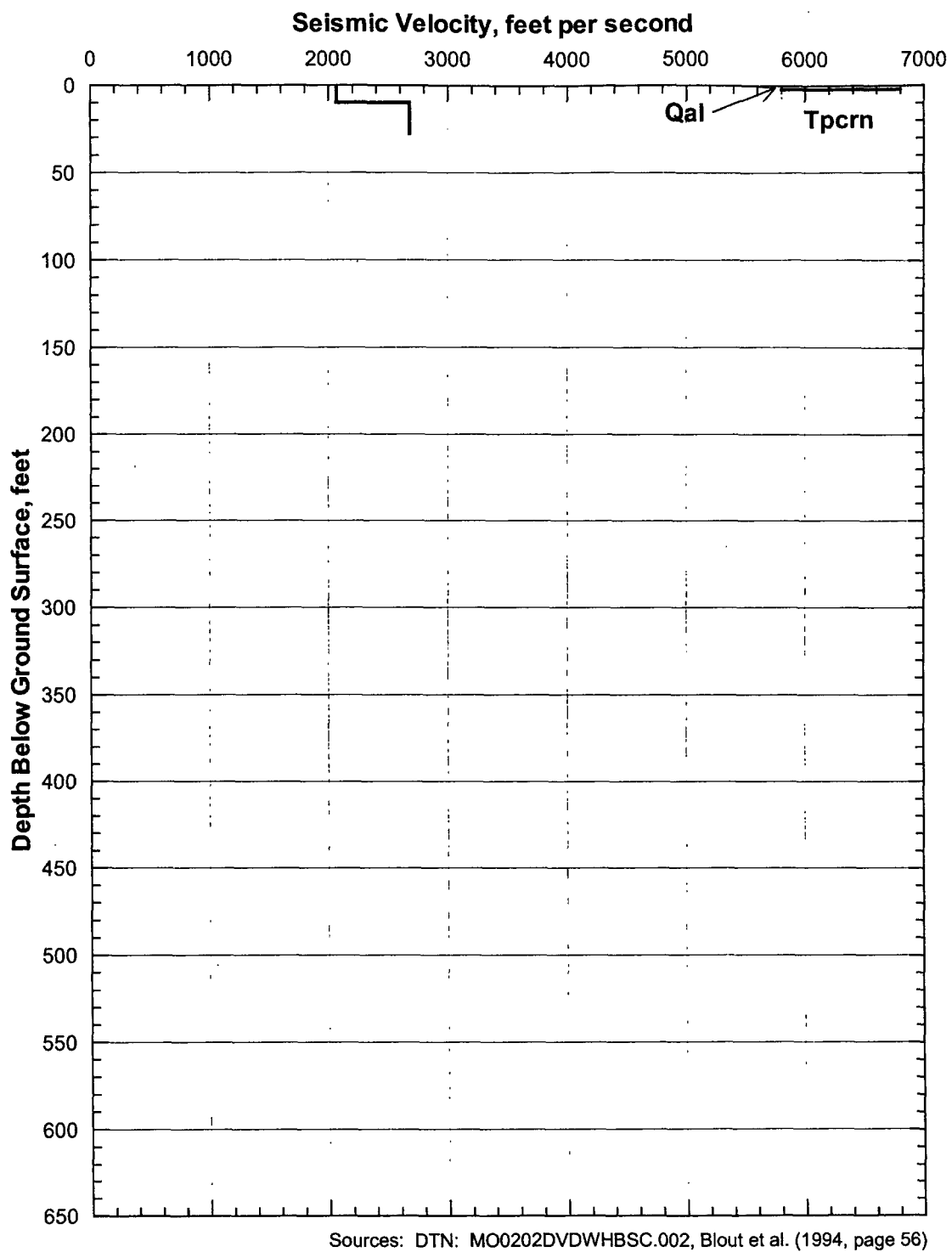
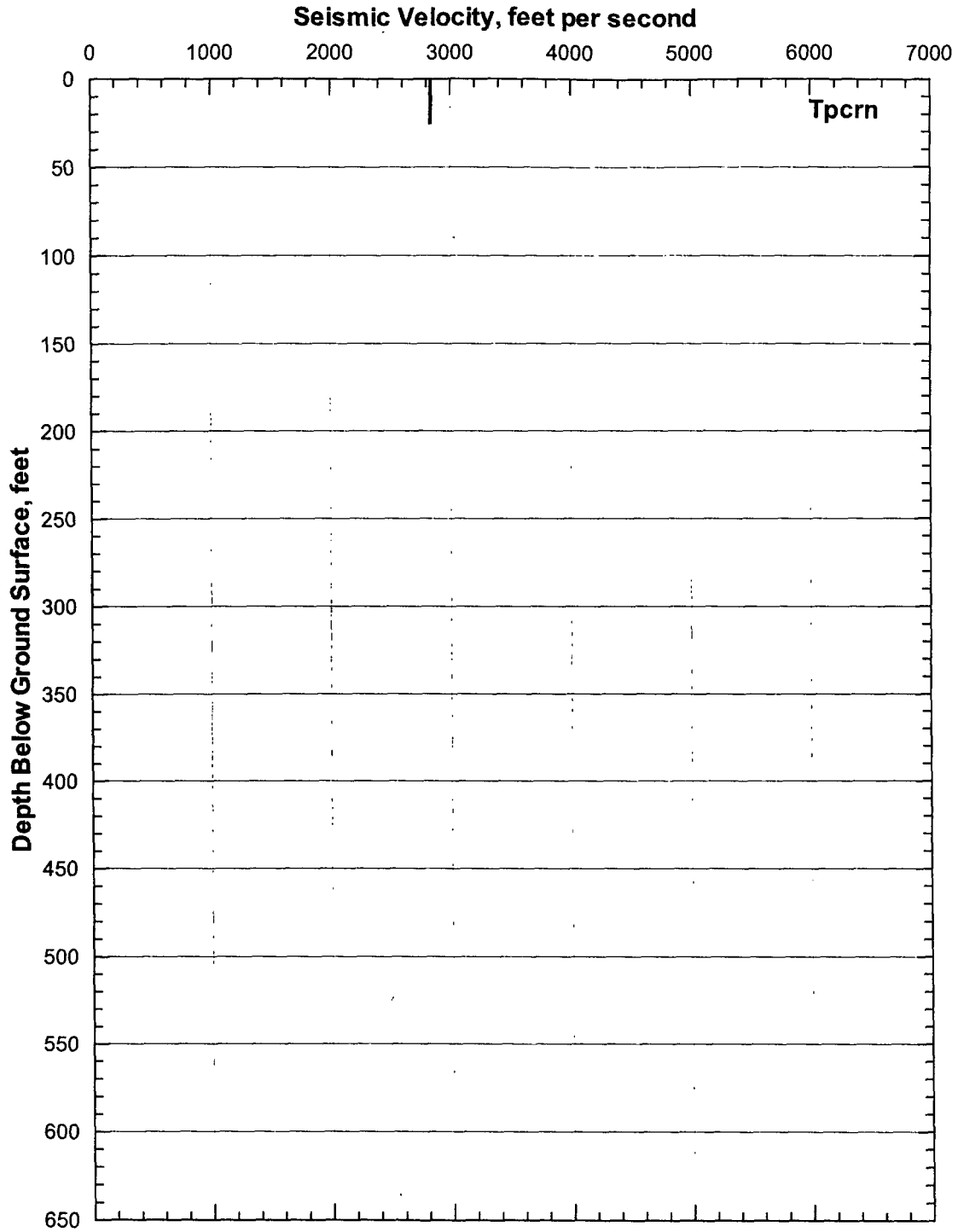


Figure 209. UZ-N75 Shear-Wave Velocities from Downhole Measurements and Generalized Lithology



Sources: DTN: MO0202DVDWHBSC.002, Blout et al. (1994, page 63)

Figure 210. UZ-N94 Shear-Wave Velocities from Downhole Measurements and Generalized Lithology

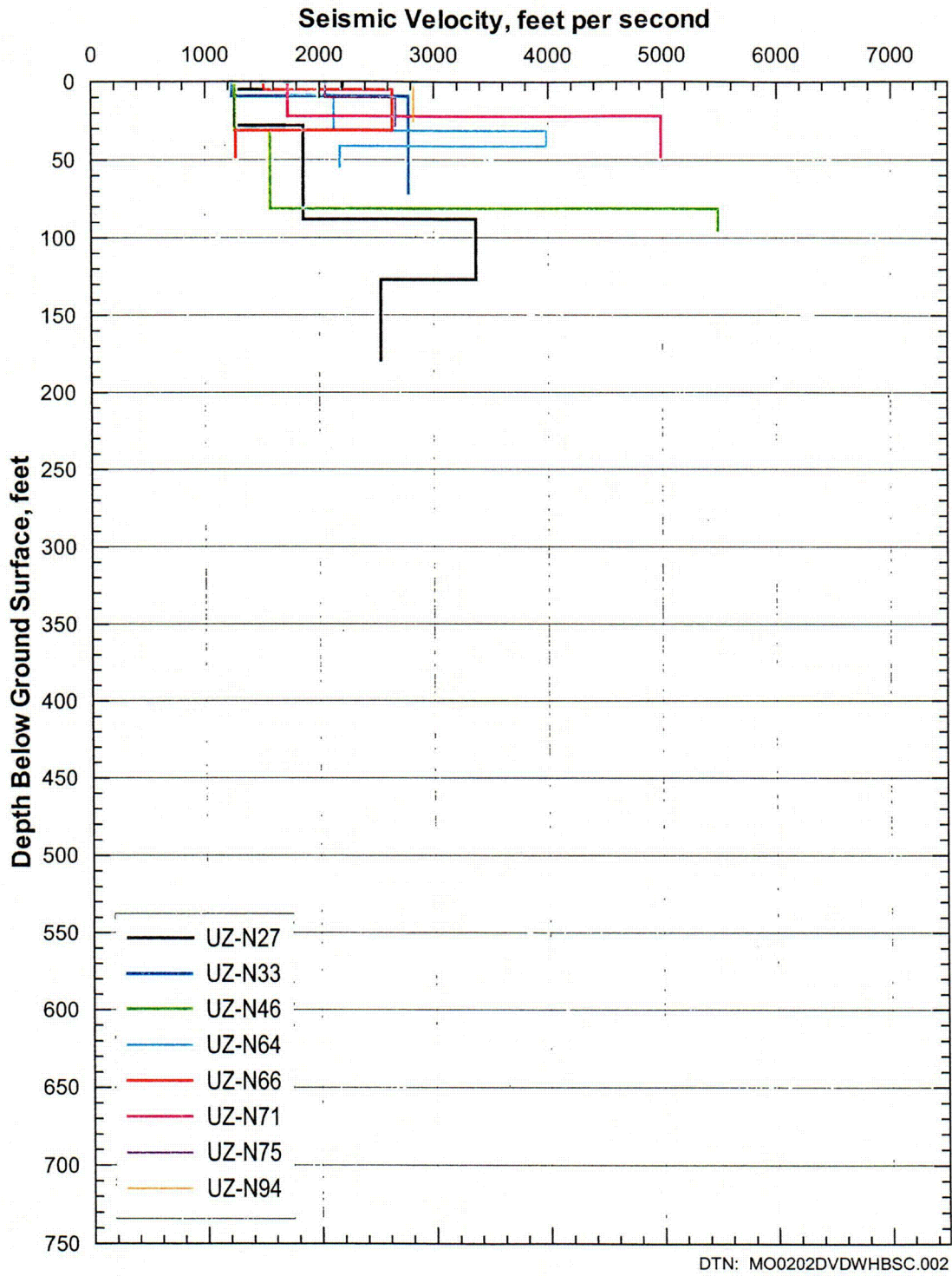
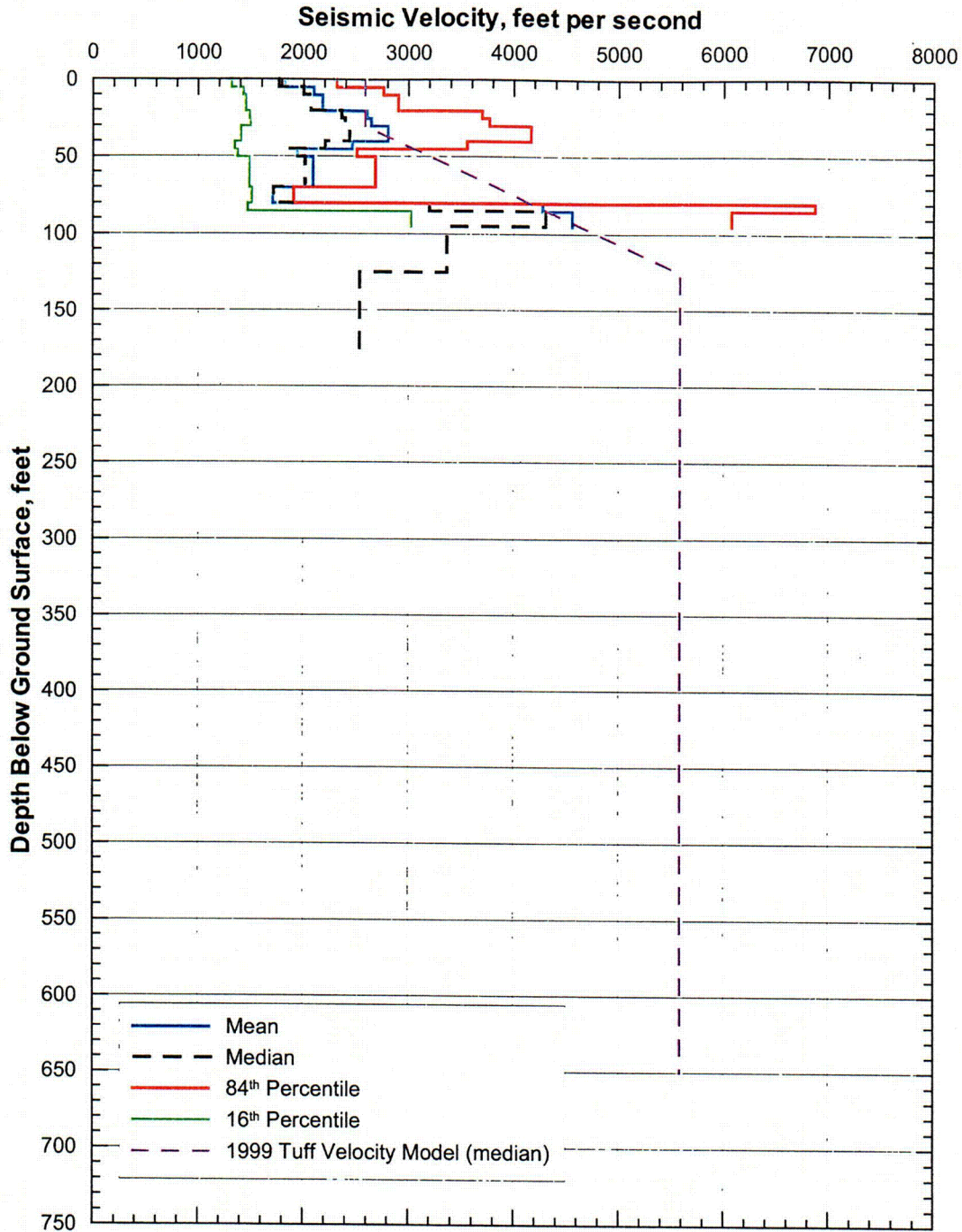


Figure 211. Shear-Wave Velocities from Downhole Measurements at Crest of Yucca Mountain



DTN: MO98PRECLOSURE.000

Note: These statistics have been calculated for illustrative purposes only. Final statistics calculated for use in the forthcoming scientific analysis entitled *Development of Seismic Design Input Ground Motions for a Geologic Repository at Yucca Mountain* will be submitted to the TDMS.

Figure 212. Statistical Analyses of Shear-Wave Velocities from Downhole Measurements at Crest of Yucca Mountain

6.5 DATA ACQUIRED FOR BORROW MATERIAL

6.5.1 Overview

Four samples of potential borrow material from an existing borrow area called Fran Ridge Borrow Area, whose general outlines as of November 2001 are shown on Figure 213. The objective was to evaluate the borrow area as a potential source for the engineered fill for the future North Portal surface facilities. The four samples were taken at the widely spaced locations shown on Figure 213. The samples were collected with a shovel; four sacks were taken at each of the four locations.

6.5.2 Geotechnical Laboratory Static Testing

Testing in Denver, CO - The four samples of potential borrow material from the Fran Ridge Borrow Area were combined following USBR 5205-89, *Procedure for Preparing Soil Samples by Splitting or Quartering*. The Denver, CO, laboratory performed some tests on the material, including a gradation analysis test and maximum/minimum density tests. These test results are summarized in Table 27. The sample classifies as a poorly graded sand (SP) according to the USCS; however, with 48.8% sand-size particles and 48.3% gravel-size particles, the material is nearly a poorly graded gravel (GP) and could be assigned a borderline classification of SP/GP.

The particles retained on a 19.0 mm (¾-inch) sieve were then removed from the material and the remaining material was split in accordance with USBR 5205-89 at the Denver, CO geotechnical laboratory and a part of the sample was sent to a geotechnical laboratory in Santa Ana, CA. A second part was sent to a geotechnical laboratory in Austin, Texas. The testing performed in Austin, Texas is discussed in Section 6.5.3, while the testing performed by the Santa Ana, CA and the Denver, CO laboratories is discussed in this section. The Denver, CO geotechnical laboratory also performed specific gravity tests on the sand fraction (the part of the sample passing the No. 4 sieve), and specific gravity and absorption tests on the fine gravel (fraction passing the ¾-inch sieve and retained on the No. 4 sieve) and coarse gravel (fraction passing the 3-inch sieve and retained on the ¾-inch sieve). Liquid limit and plastic limit tests were performed and the sample found to be non-plastic (Table 27). Note that the value of the specific gravity of the minus No. 4 sieve fraction in Table 27, 2.52, is the same as the average of the values in Table 13 for the samples from the test pits in the WHB Area. This is not a surprising result, given that the materials from both locations are alluvium derived from similar source material.

Testing in Santa Ana, CA - Testing in Santa Ana, California was performed in accordance with YMP Line Procedure LP-GEO-001Q-M&O, *Laboratory Geotechnical Testing of Soil, Rock and Aggregate Samples*. Testing consisted of particle-size distribution tests, a compaction characteristics test using modified effort and triaxial compression tests, performed in accordance with Sections 5.5.5, 5.5.7, and 5.5.12, respectively, of LP-GEO-001Q-M&O.

Particle-size distribution tests were performed on the sample in three conditions: (1) as received (including materials greater than ½-inch in size); (2) after scalping on the ½-inch sieve and prior to compaction, and (3) after the compaction test on the ½-inch minus material. Note that

Section 5.5.5 of LP-GEO-001Q-M&O allows the choice of two different test methods to measure

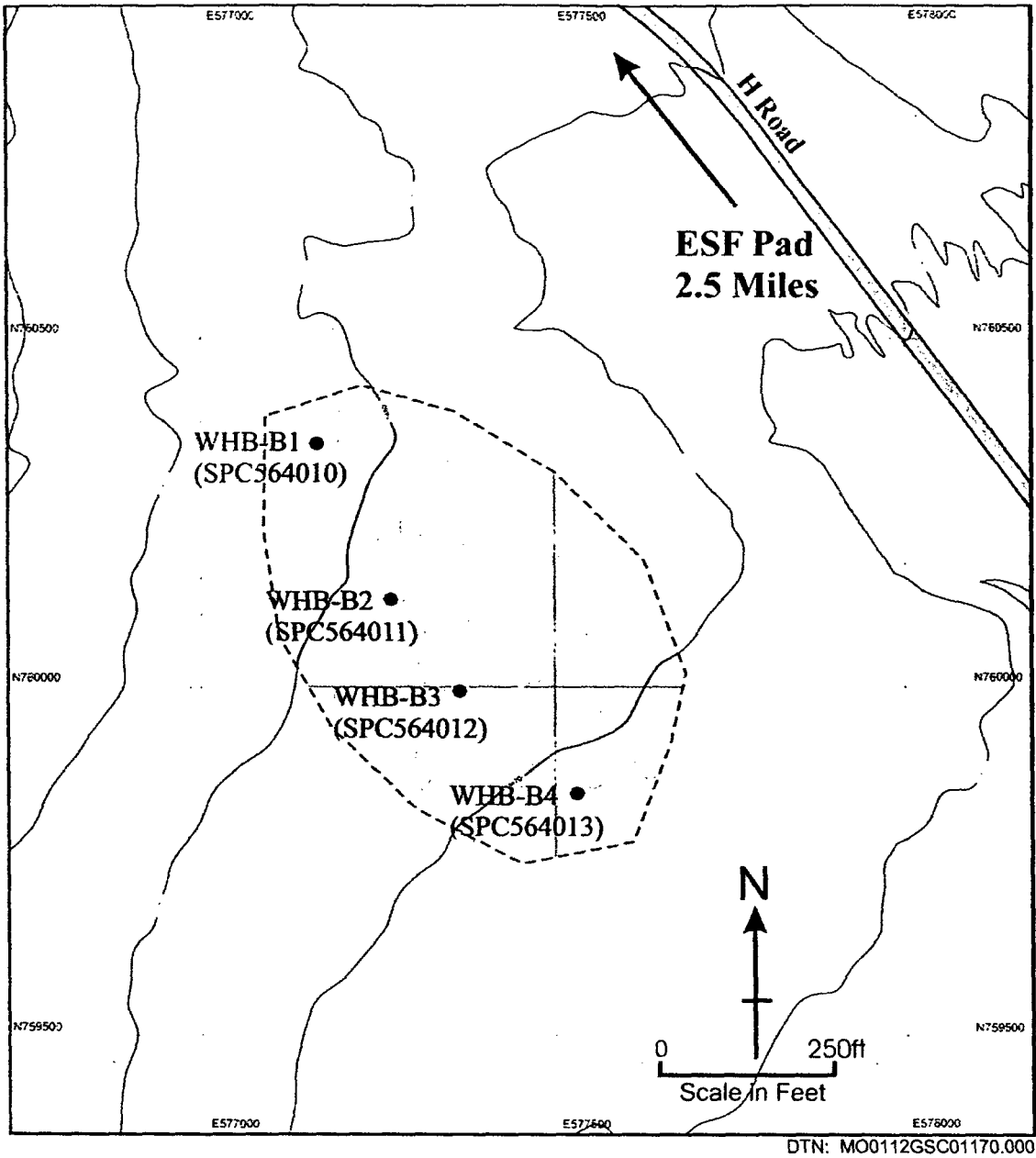


Figure 213. Location of Fran Ridge Borrow Samples

Table 27. Tests Performed in Denver, CO, on a Composite Sample of Fran Ridge Materials

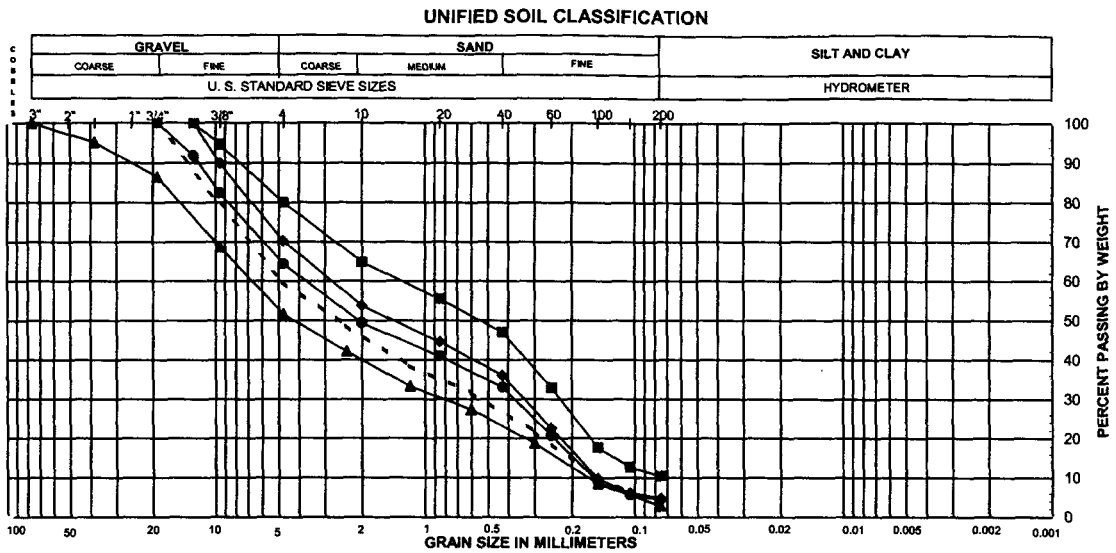
Test	Result
Particle-size distribution per USBR 5325-89 and 5335-89	100% passing 3" sieve; 95.2% passing 1½" sieve; 86.5% passing ¾" sieve; 68.8% passing 3/8" sieve; 51.7% passing No. 4 sieve; 42.1% passing No. 8 sieve; 33.2% passing No. 16 sieve; 27.4% passing No. 30 sieve; 18.8% passing No. 50 sieve; 8.5% passing No. 100 sieve; 2.9% passing No. 200 sieve
Maximum and minimum index unit weights of the particles passing the 3-inch sieve per USBR 5525-89 and 5530-89	Maximum 112.4 pcf (dry method) Minimum 94.0 pcf
Specific gravity and absorption of the particles retained on the ¾-inch sieve and passing the 3-inch sieve per USBR 5320-89 (volume method)	2.39 apparent 2.24 bulk (saturated surface dry) 2.13 bulk (oven dry) 5.3% absorption
Specific gravity and absorption of the particles retained on the 4.75 mm (No. 4) sieve and passing the 19.0 mm (¾-inch) sieve per USBR 5320-89 (suspension method)	2.45 apparent 2.24 bulk (saturated surface dry) 2.10 bulk (oven dry) 6.9% absorption
Specific gravity of the particles passing the 4.75 mm (No. 4) sieve per USBR 5320-89 (volume method)	2.52
Liquid and plastic limits per USBR 5350-89	Nonplastic
Unified Soil Classification System per USBR 5000-86	SP

DTN: MO0206EBSFRBLT.018

particle-size distribution; for these tests, ASTM C 136-96a, *Standard Test Method for Sieve Analysis of Fine and Coarse Aggregates*, was used.

The results of the particle-size distribution tests are presented on Figure 214 and on the bottom half of Figure 215. Note that the percent of particles passing the No. 200 sieve increased from 4.9 percent before the compaction test to 10.5 percent after the compaction test, which causes the USCS group name/symbol to change from poorly graded sand with gravel (SP) to poorly graded sand with silt and gravel (SP-SM). Figure 214 also shows the particle-size distribution curve for the test at the geotechnical laboratory in Denver, CO on the sample before scalping and splitting and the theoretical particle-size distribution curve (dashed line) representing perfect scalping and splitting of the sample before processing.

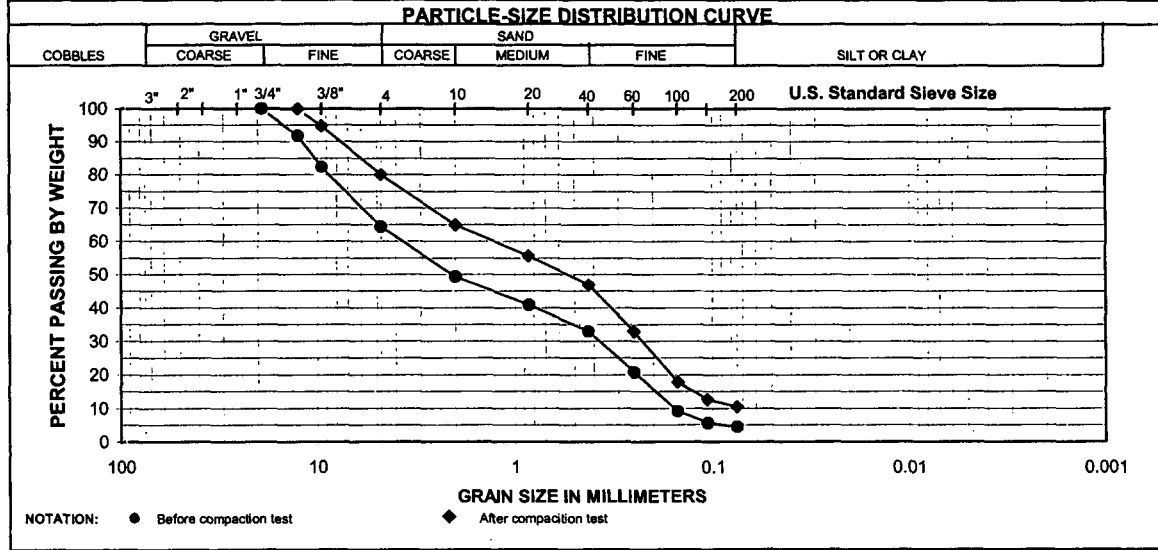
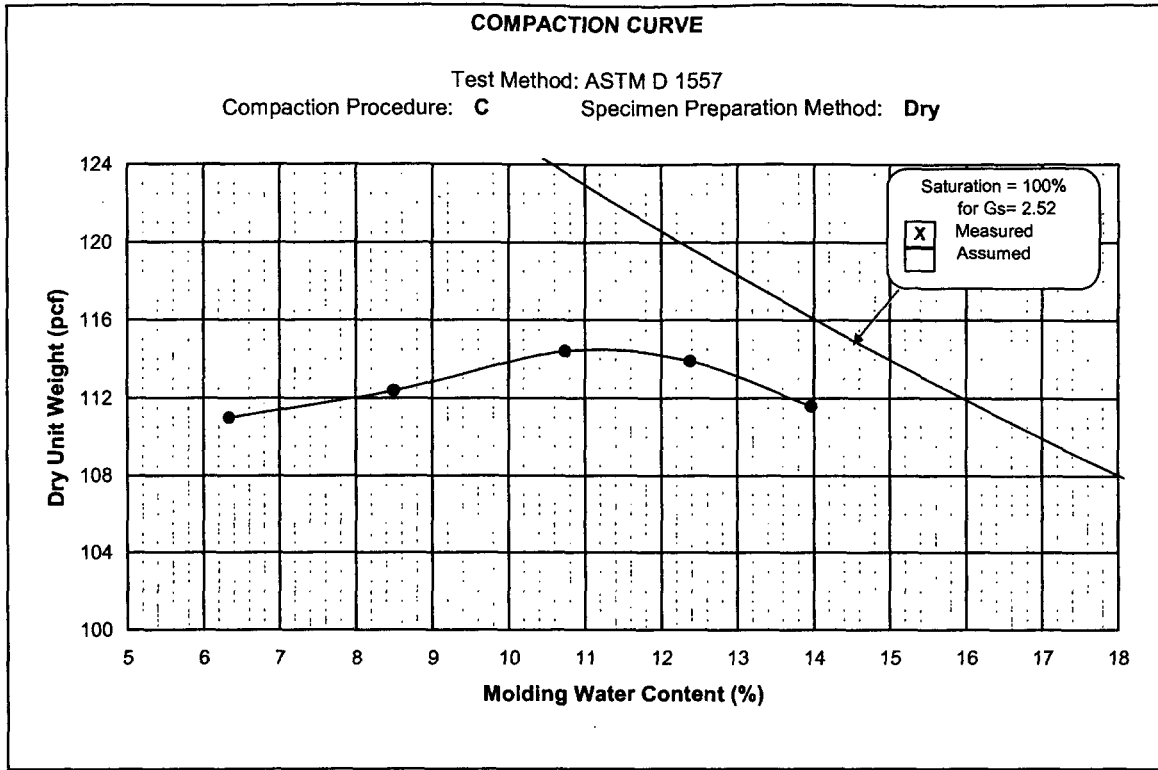
The compaction characteristics were measured in accordance with ASTM D 1557-91 (1998), *Standard Test Method for Laboratory Compaction Characteristics of Soil Using Modified Effort (56,000 ft-lbf/ft³ (2,700 kN-m/m³))*. The compaction characteristics test was performed on the material after it had been scalped on the one-half inch sieve. The one-half inch size corresponds to the maximum particle size that was to be included in the triaxial test specimens tested by the Santa Ana geotechnical laboratory and the resonant column and torsion shear tests conducted in Austin, Texas on a portion of composite sample No. 65A-X613. The results of the compaction test are summarized on the top half of Figure 215 and indicate a maximum dry unit weight of 114.5 pounds-force per cubic foot (pcf or lbf/ft³) and an optimum water content of 11 percent.



Sample No.	SYMBOL	LL	PI	CF	Description and Classification	D ₆₀	D ₃₀	D ₁₀	C _u	C _c
65A-X613 (test by USBR before splitting)	◻	NP	NP		Poorly graded Sand with gravel (SP)	6.9	0.82	0.17	40.6	0.6
65A-X613 (as-received by URS)	●				Poorly graded Sand with gravel (SP)	3.8	0.37	0.16	23.8	0.2
65A-X613 (-1/2 inch, before compaction)	◆				Poorly graded Sand with gravel (SP)	2.8	0.34	0.16	17.5	0.3
65A-X613 (-1/2 inch, after compaction)	■				Poorly graded Sand with silt and gravel (SP-SM)	1.3	0.23	0.07	18.6	0.6
Theoretical curve for 65A-X613 (test by USBR before splitting) scalped on 3/4-inch sieve	--	NP	NP		Poorly graded Sand with gravel (SP)	4.9	0.53	0.16	30.6	0.4

DTN: MO0203EBSCTCTS.016

Figure 214. Particle-Size Distributions – Fran Ridge Borrow Area Composite Sample



Sample No.	Depth (ft)	Opt. Water Content (%)	Max. Dry Unit Weight (pcf)	Description and/or Classification
65A-X613	NA	11.0	114.5	Brown poorly graded Sand with gravel (SP) (before test)

DTN: MO0203EBSCTCTS.016

Figure 215. Compaction Test Results – Fran Ridge Borrow Area Composite Sample

The triaxial tests were performed under isotropically consolidated, drained conditions at confining stresses ranging from 1.18 kips per square foot (ksf) to 8.70 ksf. The initial conditions and results are summarized in Table 28. Plots of axial strain versus deviator stress, change in volume and obliquity (i.e., ratio of major to minor principal stress, σ'_1/σ'_3) are presented on Figure 216. Mohr circles based on the peak deviator stress for each of the confining stresses are shown on Figure 217. Two strength envelopes have been fitted to the data as shown on Figure 217. One of these envelopes is the traditional straight line Mohr-Coulomb failure envelope:

$$\tau_{ff} = c' + \sigma_{ff} \tan \phi' = 1790 \text{psf} + 0.7587 \sigma_{ff} \quad (\text{Eq. 37})$$

where: τ_{ff} is the shear stress acting on the failure plane at failure, i.e., the effective shear strength
 c' is the effective cohesion intercept
 ϕ' is the effective friction angle
 σ_{ff} is the normal stress acting on the failure plane at failure.

The other is a curved failure envelope (with zero cohesion at zero confining pressure) that reflects the important influence of confining pressure on shear strength:

$$\tau_{ff} = \sigma_{ff} \tan(\phi'(\sigma_{ff})) \quad (\text{Eq. 38})$$

where: τ_{ff} and σ_{ff} are as defined previously
 $\phi'(\sigma_{ff})$ is a function defined by Eq. 39.

$$\phi'(\sigma_{ff}) = \phi_1 - \Delta\phi \log\left(\frac{\sigma_{ff}}{p_a}\right) = 54.2^\circ - 16.0^\circ \log\left(\frac{\sigma_{ff}}{p_a}\right) \quad (\text{Eq. 39})$$

where: ϕ_1' is the effective friction angle for $\sigma_{ff} = 1$ atmosphere
 $\Delta\phi'$ is the decrease in ϕ' per log cycle change in σ_{ff}
 p_a is 1 atmosphere (approximately 2,116.22 lbs/ft²).

Either failure envelope may be selected for use in design calculations. However, if the Mohr-Coulomb failure envelope approach is used, the geotechnical engineer may need to modify the values of c' and ϕ' to fit the specific range of confining pressures involved in a particular analysis.

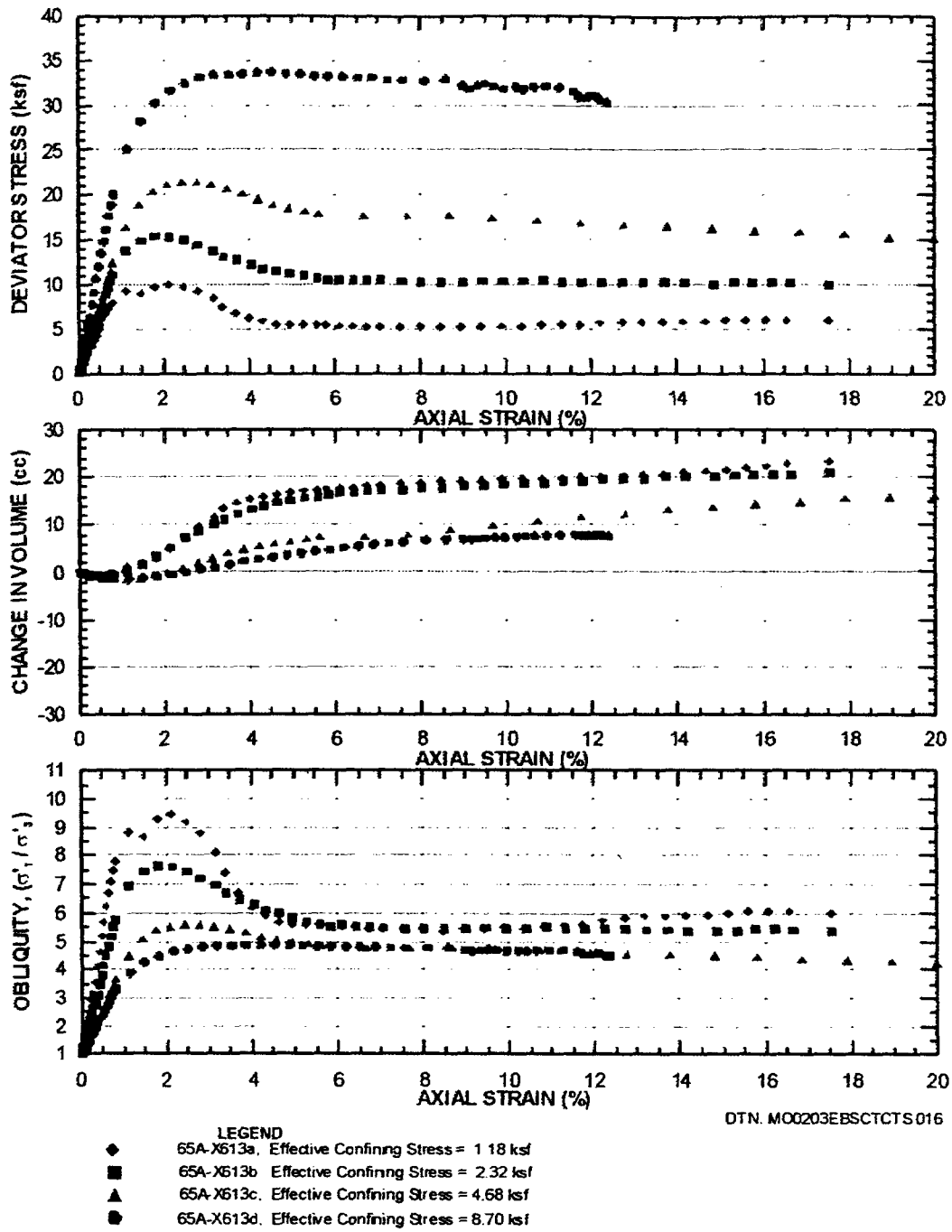
Note that some particle breakage occurred during the compaction characteristics test (Figure 214), which employs a 10-pound-force steel rammer falling 18 inches. The triaxial specimens are compacted in a three-inch diameter mold with a small steel tamper that is manipulated by the laboratory technician. Typically, less particle breakage occurs during triaxial specimen preparation relative to the compaction characteristics test, though some breakage may occur. Thus, it is possible that the material tested (after compaction and consolidation, but before shear) was a poorly graded sand with silt and gravel (SP-SM).

Table 28. Summary of Isotropically Consolidated, Drained Triaxial Compression Tests Performed on Laboratory-Compacted Specimens of the Fran Ridge Borrow Area Composite Sample

Specimen No.	USCS Group Symbol	Compaction Characteristics ⁽⁴⁾		Initial Molding Conditions		w _o	γ _{do}	σ' _{pm}	OCR	ε _{ac}	B factor (%)	at Maximum Deviator Stress					
												at Maximum Obliquity					
												γ _{d,max} (pcf)	w _{opt} (%)	% Comp.	W-W _{opt} (%)	w _c (%)	γ _{dc} (pcf)
65A-X613	SP	114.5	11.0	95.4	1.4	12.4	109.2	—	—	0.41	96.1	2.127	4.999	6.180	9.467	0.500	54.0
a	2.52					18.4	107.7	1.18	1.0	1.43	1.86	—	—	—	—	—	—
65A-X613	SP	114.5	11.0	96.4	1.3	12.3	110.4	—	—	0.43	96.2	1.802	7.687	10.006	7.632	0.221	50.2
b	2.52					17.1	109.6	2.32	1.0	0.71	1.86	—	—	—	—	—	—
65A-X613	SP	114.5	11.0	95.7	1.7	12.7	109.6	—	—	1.30	96	2.439	10.719	15.399	5.581	0.051	44.1
c	2.52					18.8	106.5	4.68	1.0	2.89	2.03	—	—	—	—	—	—
65A-X613	SP	114.5	11.0	95.9	1.7	12.7	109.8	—	—	0.42	98.1	4.201	16.807	25.505	4.865	0.083	41.2
d	2.52					17.0	110.1	8.70	1.0	-0.29	1.74	—	—	—	—	—	—

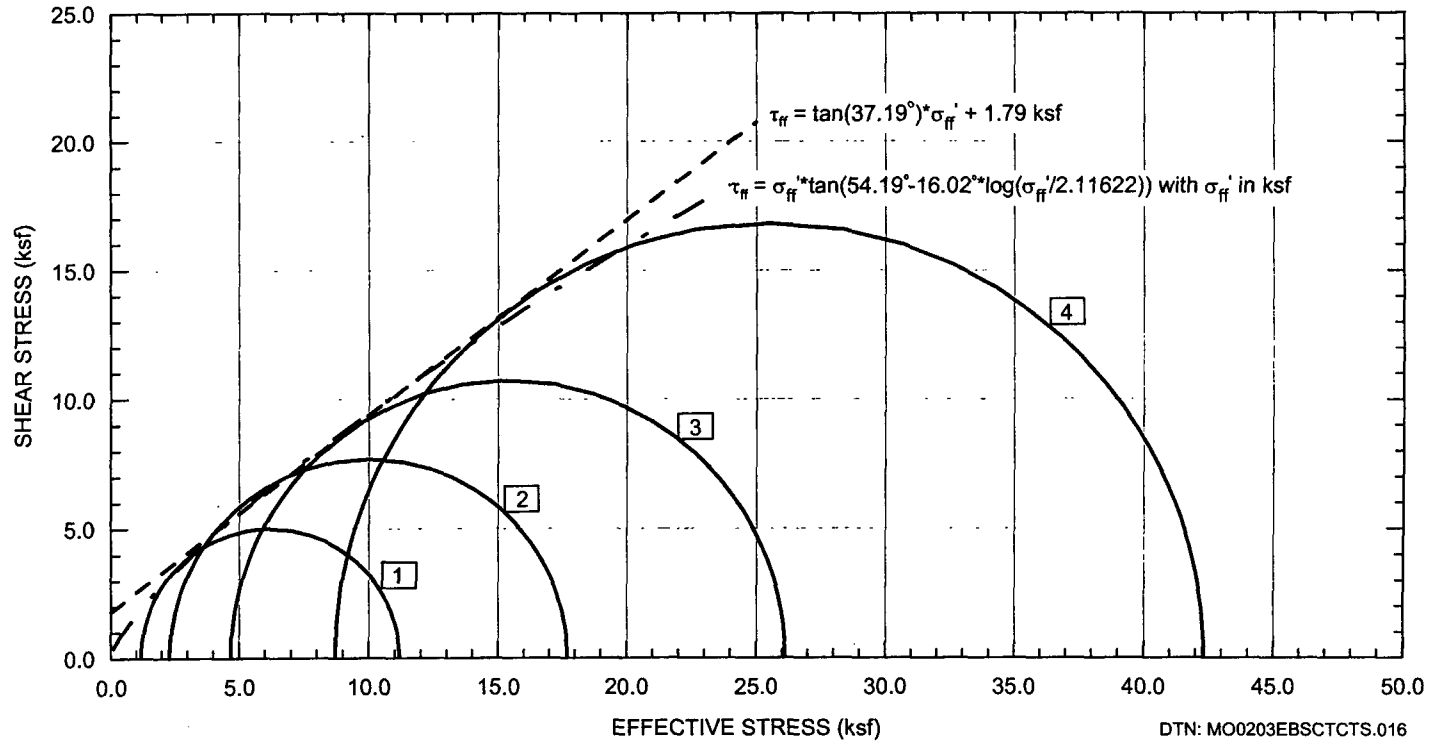
DTN: MO0203EBSCTCTS.016

- NOTES: ⁽¹⁾ Description of the material before compacting the specimens: Brown poorly graded Sand with gravel (SP).
⁽²⁾ The value of specific gravity is for the particles passing the No. 4 sieve and was provided by the Denver CO, laboratory (see Table 27).
⁽³⁾ The value of φ' is based on the Mohr-Coulomb failure criterion with c'=0 and is calculated at peak deviator stress (σ₁-σ₃), which is the same as peak obliquity for a drained test.
⁽⁴⁾ Per ASTM D 1557-91 (1998)



Note: The material used to prepare triaxial specimens was scalped on the 1/2 inch sieve.

Figure 216. Results of Isotropically Consolidated Drained Triaxial Compression Tests - Fran Ridge Borrow Area Composite Sample



LEGEND	
1	65A-X613a, Effective Confining Stress = 1.18 ksf
2	65A-X613b, Effective Confining Stress = 2.32 ksf
3	65A-X613c, Effective Confining Stress = 4.68 ksf
4	65A-X613d, Effective Confining Stress = 8.70 ksf

NOTE: The material used to prepare triaxial specimens was scalped on the 1/2 inch sieve.

Figure 217. Mohr Circles at Peak Deviator Stress for Isotropically Consolidated Drained Triaxial Compression Tests - Fran Ridge Borrow Area Composite Sample

6.5.3 Geotechnical Laboratory Dynamic Testing

The dynamic properties of 10 specimens of the proposed engineered fill material for the WHB foundation were evaluated in the laboratory at the Geotechnical Engineering Center at the University of Texas at Austin using RCTS equipment. The specimens were collected from the Fran Ridge Borrow Area. The procedures used in this testing are described in Section 6.2.10.1. A detailed description of this evaluation is contained in Scientific Notebook SN-M&O-SCI-033-V1 (Wong 2002e, pages 1050-1601). The results from the dynamic testing of the 10 fill specimens are presented in the following section.

6.5.3.1 Measurements

Ten reconstituted specimens of the Fran Ridge borrow material were tested dynamically. These specimens were constructed from samples sent to UTACED by the USBR Laboratory (see Section 6.5.2). Each specimen was compacted using tamping. The initial properties of the specimens are presented in Table 29. The nominal specimen diameters were either 2.78 in (7.05 cm) or 1.38 in (3.51 cm) and the heights were about 2.0 to 2.3 times the diameters. The specimens were compacted to dry densities that ranged from 90 to 97% of the modified Proctor maximum dry density. The value of the modified Proctor maximum dry density is 114.5 pcf and the optimum water content is 11% (Section 6.5.2). Also, the specimens were compacted with "scalped" material such that the maximum particle size was no larger than 17% (1/6) of the specimen diameter.

Four of the specimens were tested in two stages. In stage 1, the specimens were dynamically tested at their molding water contents to evaluate the small- and large-strain properties. These four specimens are denoted as UTA-23-K ($w = 2.63\%$), UTA-23-L ($w = 2.77\%$), UTA-23-U ($w = 10.92\%$) and UTA-23-W ($w = 11.15\%$). Upon completion of stage 1 testing, the confining chamber and drive system were removed, and water was percolated through each specimen for one day using a vacuum assist of about 0.1 atmospheres on the downstream side of the specimen. Each specimen was then re-tested dynamically in this state of increased water content (stage 2), to investigate the impact on the dynamic properties of increasing the water content of the granular fill after placement. The specimens were renamed in stage 2 as UTA-23-M ($w = 13.47\%$), UTA-23-N ($w = 15.78\%$), UTA-23-V ($w = 13.50\%$) and UTA-23-Y ($w = 13.53\%$), respectively. Unfortunately, the heights and total unit weights of the four specimens were not measured in stage 2; hence, the dry unit weight from stage 1 was used for the dry unit weight in stage 2. The test pressures and types of tests performed on the Fran Ridge specimens are shown on Table 30.

6.5.3.2 Results

The variation of G_{\max} with σ_{cell} for the 10 Fran Ridge specimens is shown in Figure 218. The log G_{\max} - log σ relationship can be approximated by a linear relationship on a semilog plot, as expected (Hardin and Drnevich 1972, page 622). The value of G_{\max} generally increases with increasing dry unit weight and, for the denser specimens, decreases with increasing water content.

Table 29. Initial Properties of Reconstituted Specimens of the Fran Ridge Borrow Material

UTACED Designation	SMF Designation	Depth (ft)	SMF Classification	Height ^a (cm)	Diameter ^a (cm)	Total Mass ^a (grams)	Water Content ^a (%)	Dry Unit Weight (pcf)	Total Unit Weight ^a (pcf)	% of Modified Proctor ^{a,b}
UTA-23-K	65A-X613	N.A.	Granular Fill	14.26	7.05	944.1	2.63	103.1	105.8	90
UTA-23-M	65A-X613	N.A.	Granular Fill	14.26 ^c	7.05	-- ^c	13.47	103.1 ^c	117.0	90
UTA-23-L	65A-X613	N.A.	Granular Fill	7.20	3.48	116.5	2.77	103.1	105.9	90
UTA-23-N	65A-X613	N.A.	Granular Fill	7.20 ^c	3.48	-- ^c	15.78	103.1 ^c	119.3	90
UTA-23-O	65A-X613	N.A.	Granular Fill	14.13	7.04	962.1	4.72	104.2	109.1	91
UTA-23-P	65A-X613	N.A.	Granular Fill	7.15	3.50	119.4	4.55	103.5	108.2	90
UTA-23-U	65A-X613	N.A.	Granular Fill	7.70	3.80	172.8	10.92	111.1	123.3	97
UTA-23-V	65A-X613	N.A.	Granular Fill	7.70 ^c	3.80	-- ^c	13.50	111.1 ^c	126.2	97
UTA-23-W	65A-X613	N.A.	Granular Fill	16.00	7.12	1244.0	11.15	109.7	121.9	96
UTA-23-Y	65A-X613	N.A.	Granular Fill	16.00 ^c	7.12	-- ^c	13.53	109.7 ^c	124.5	96

Sources: DTN: MO0203DHRSSWHB.001, ^a Wong (2002e, Appendix 42, page 16)

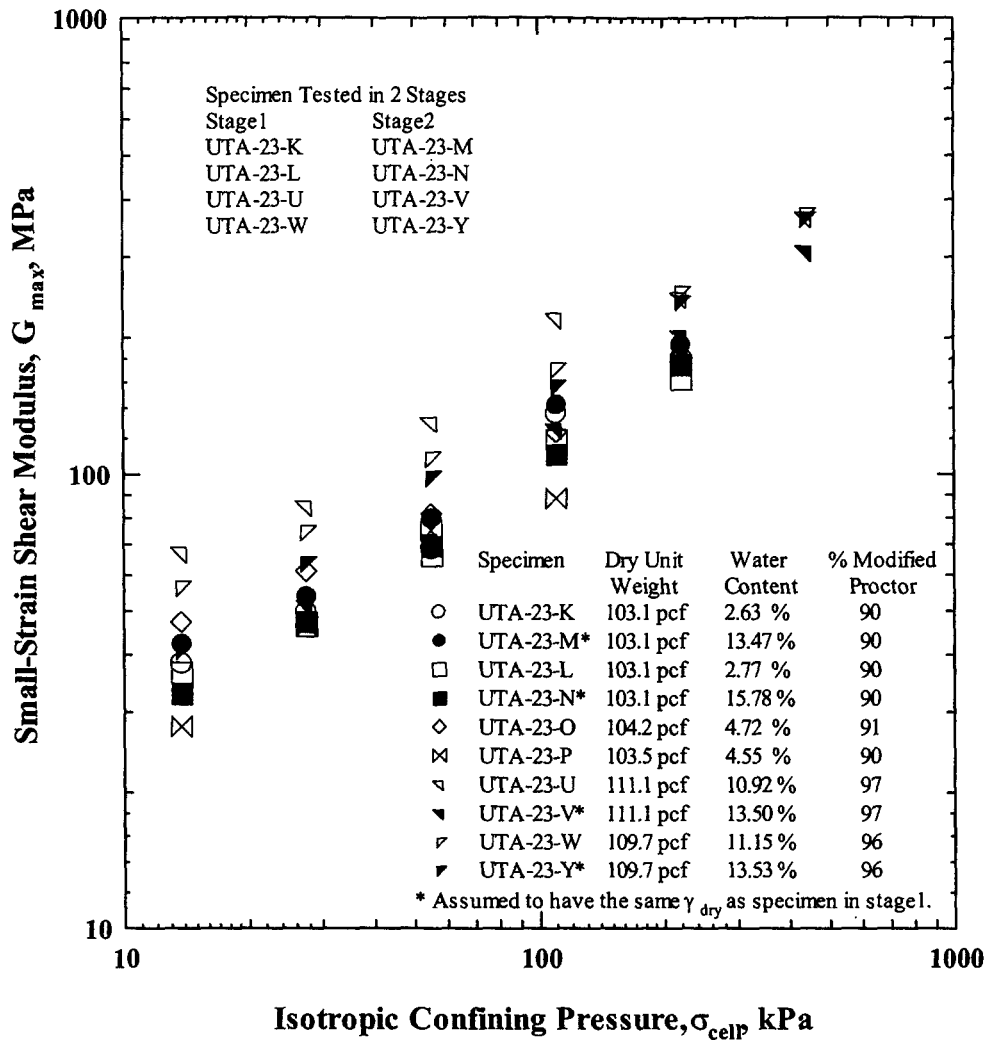
^b Based on Modified Proctor (ASTM D 1557) results (Figure 215).

^c Initial height and total unit weight of these specimens were inadvertently not measured in stage 2. The dry unit weight from stage 1 was used for the dry unit weight in stage 2.

Table 30. Confining Pressures at which RCTS Tests Were Performed on the Fran Ridge Borrow Material

UTACED Designation	SMF Designation	Depth (ft)	SMF Classification	Estimated Mean Total Stress (psi)	Low-Amplitude RC Test Pressures (psi)	High-Amplitude RC Test Pressures (psi)	Low- and High-Amplitude TS Test Pressures (psi)
UTA-23-K	65A-X613	N.A.	Granular Fill	8	2, 4, 8, 16, 32	8, 32	8, 32
UTA-23-L	65A-X613	N.A.	Granular Fill	8	2, 4, 8, 16, 32	8, 32	8, 32
UTA-23-M	65A-X613	N.A.	Granular Fill	8	2, 4, 8, 16, 32	8, 32	8, 32
UTA-23-N	65A-X613	N.A.	Granular Fill	8	2, 4, 8, 16, 32	8, 32	8, 32
UTA-23-O	65A-X613	N.A.	Granular Fill	8	2, 4, 8, 16, 32	8, 32	8, 32
UTA-23-P	65A-X613	N.A.	Granular Fill	8	2, 4, 8, 16, 32	8, 32	8, 32
UTA-23-U	65A-X613	N.A.	Granular Fill	8	2, 4, 8, 16, 32, 64	8, 32	8, 32
UTA-23-V	65A-X613	N.A.	Granular Fill	8	2, 4, 8, 16, 32, 64	8, 64	8, 64
UTA-23-W	65A-X613	N.A.	Granular Fill	8	2, 4, 8, 16, 32, 64	8, 32	8, 32
UTA-23-Y	65A-X613	N.A.	Granular Fill	8	2, 4, 8, 16, 32, 64	8, 32	8, 32

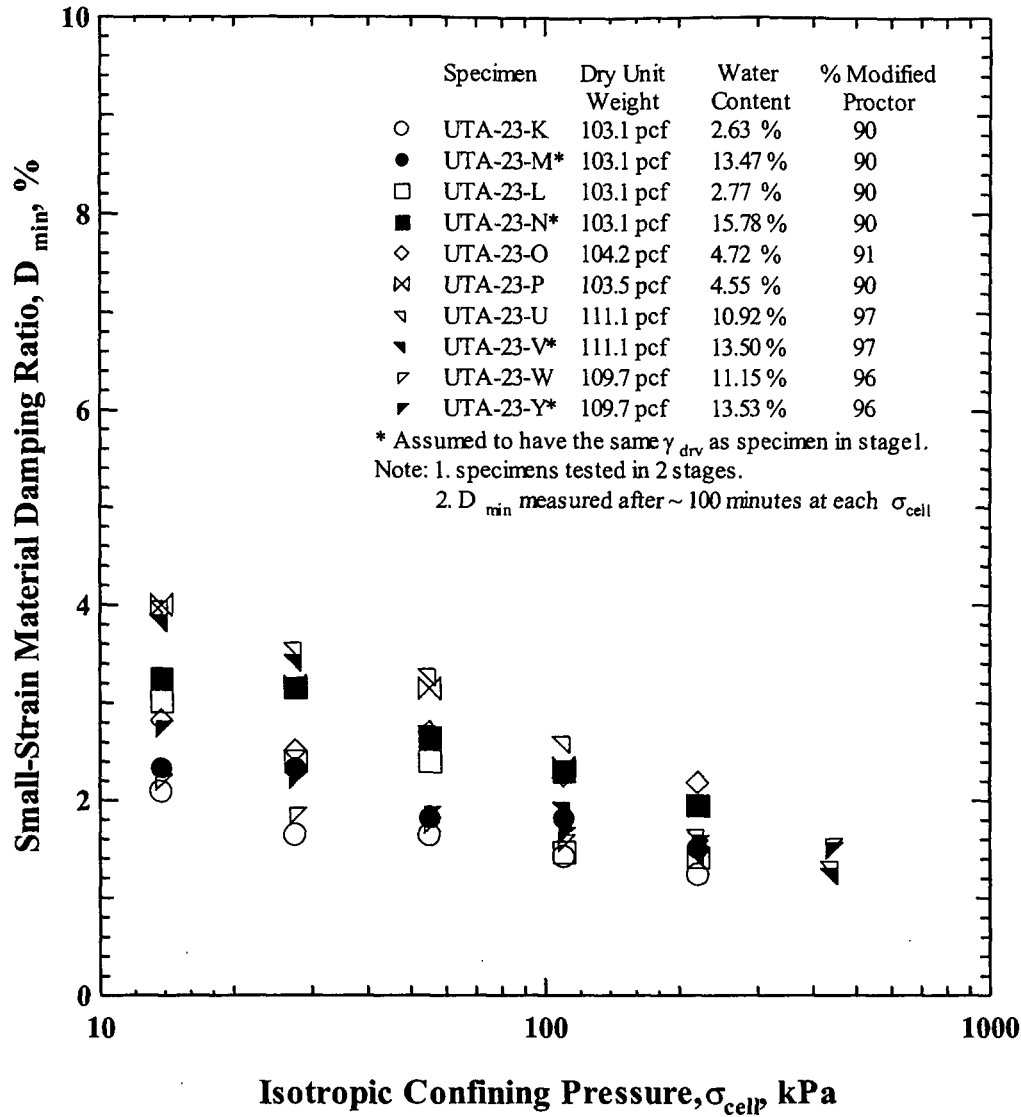
Source: Wong (2002e, Appendix 42, page 19)



Source: Wong (2002e, Appendix 42, page 49)

Figure 218. Variation in Small-Strain Shear Modulus with Isotropic Confining Pressure of Reconstituted Specimens from the Fran Ridge Borrow Area

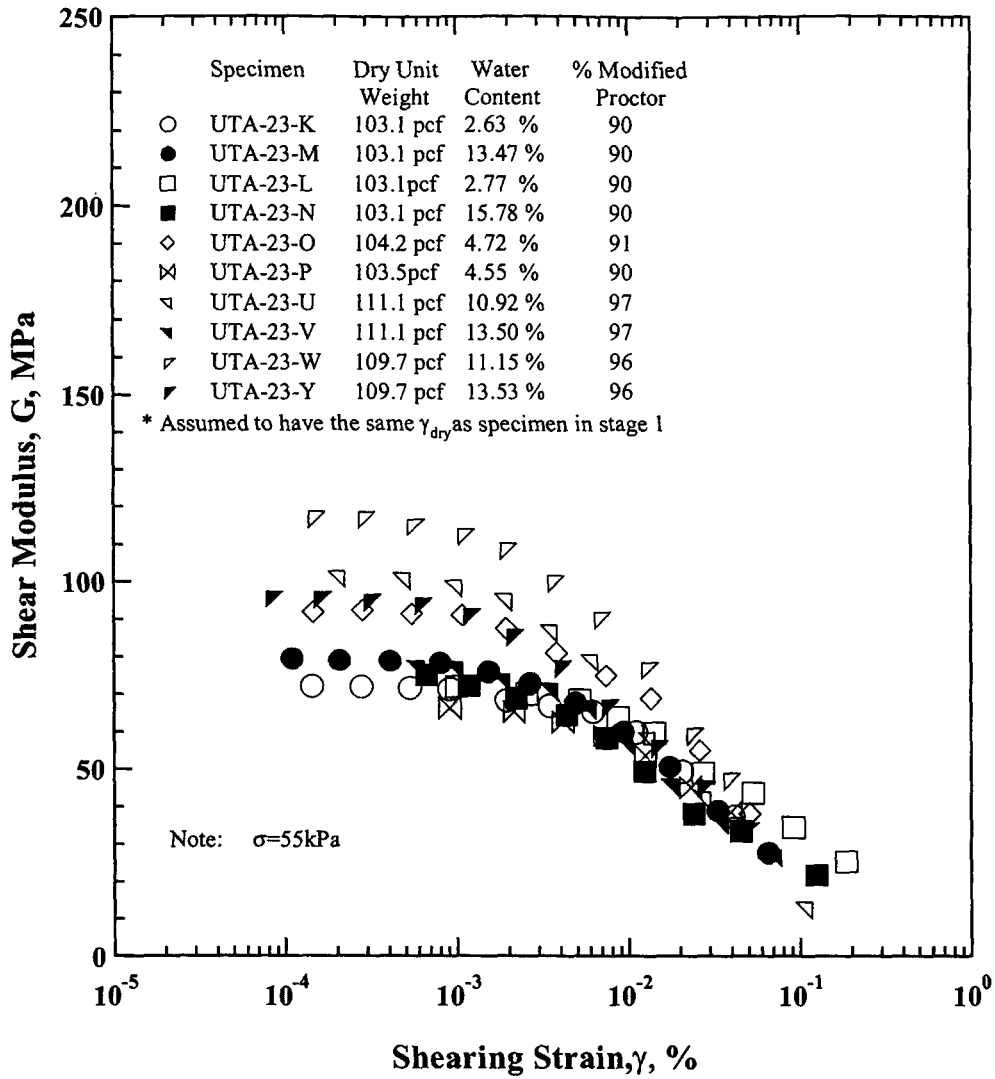
The variation of D_{min} with σ_{cell} for the ten specimens is shown in Figure 219. The value of D_{min} decreases as σ_{cell} increases as expected (Hardin and Drnevich 1972, page 622). The values of D_{min} at 1 atmosphere are above those predicted for sands by Seed et al. (1986, Figure 6) as seen by looking at the small-strain values shown in Figure 143. The effects of f on G_{max} and D_{min} are small and are shown in Figures XVII-11 and XVII-12, respectively.



Source: Wong (2002e, Appendix 42, page 50)

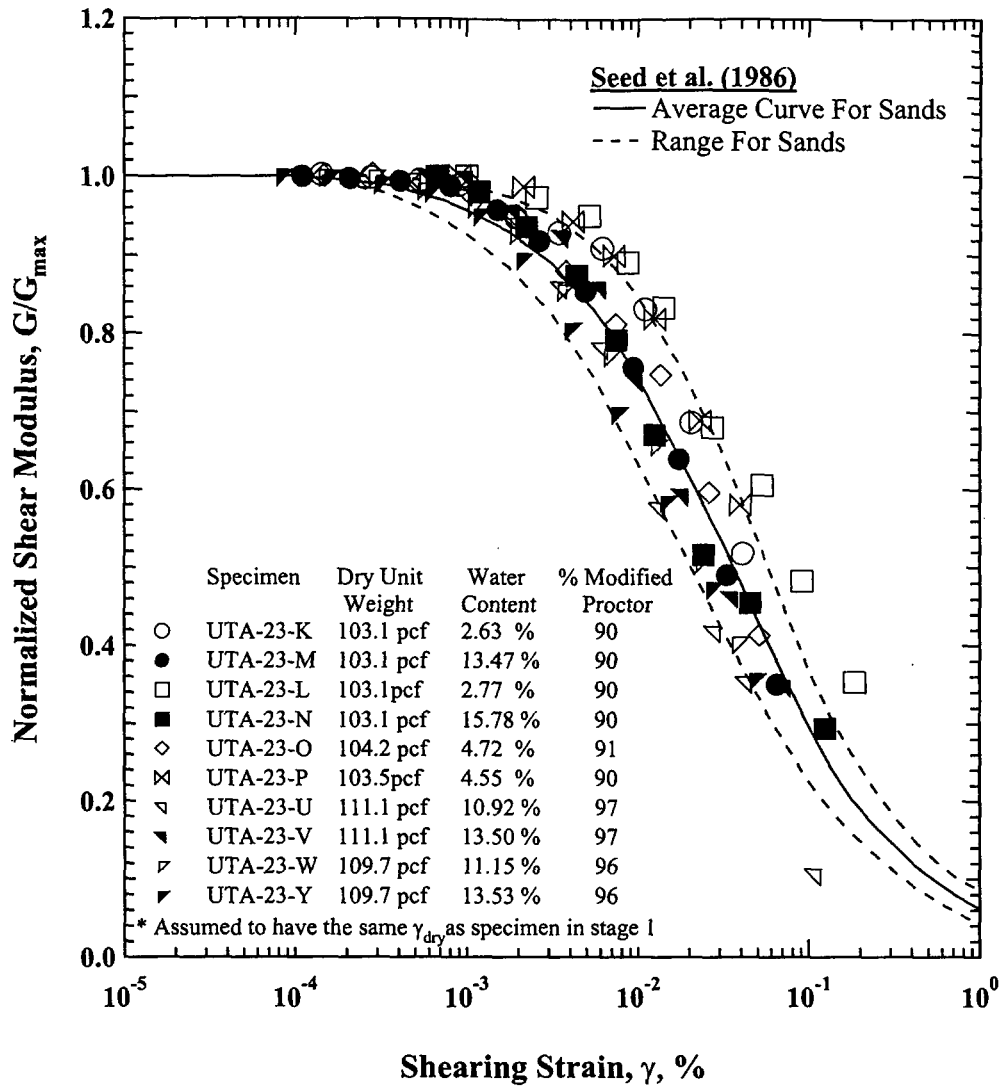
Figure 219. Variation in Small-Strain Material Damping Ratio with Isotropic Confining Pressure of Reconstituted Specimens from the Fran Ridge Borrow Area

The influence of γ on G , G/G_{max} , and D is shown in Figures 220 to 222, respectively. The specimens are behaving very much like a sandy soil, as seen by the comparisons in Figures 221 and 222 with the Seed et al. (1986, Figures 2 and 6) curves. The main difference is the higher values of D_{min} measured in the specimens.



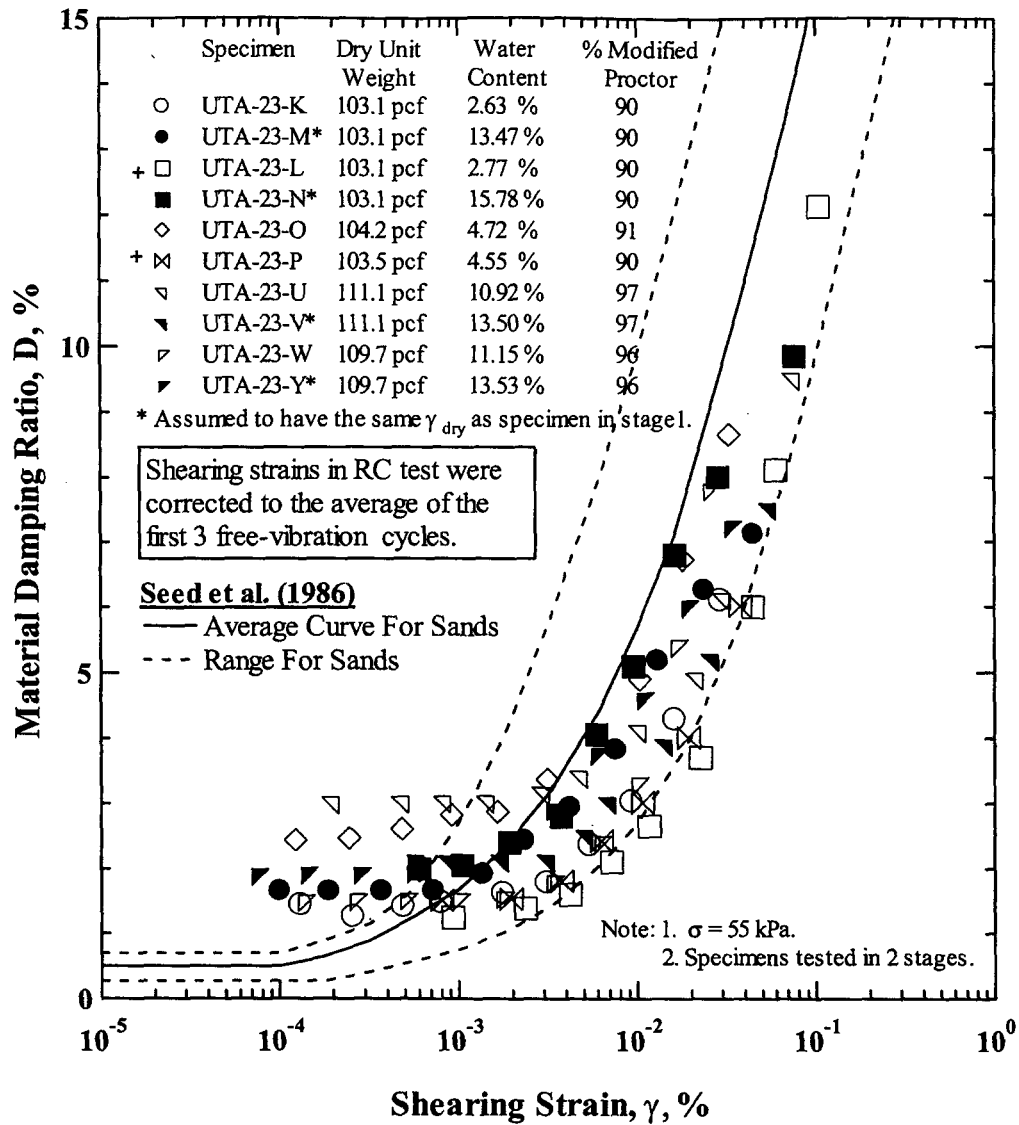
DTN: MO0203DHRSSWHB.001

Figure 220. Variation in Shear Modulus with Shearing Strain of Reconstituted Specimens from the Fran Ridge Borrow Area



DTN: MO0203DHRSSWHB.001

Figure 221. Variation in Normalized Shear Modulus with Shearing Strain of Reconstituted Specimens from the Fran Ridge Borrow Area



DTN: MO0203DHRSSWHB.001

Figure 222. Variation in Material Damping Ratio with Shearing Strain of Reconstituted Specimens from the Fran Ridge Borrow Area

6.6 GEOLOGIC CONDITIONS

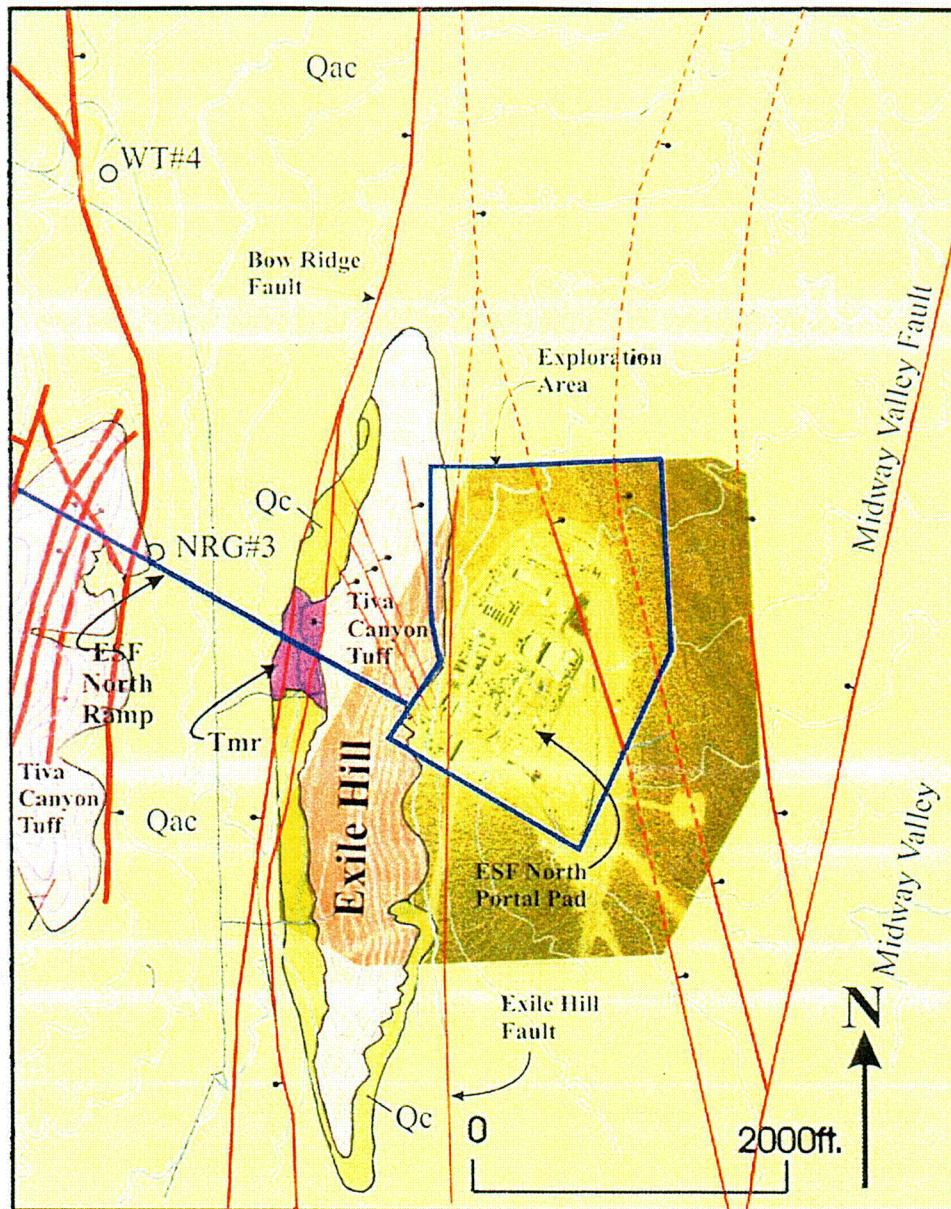
6.6.1 Regional Geologic and Topographic Conditions

Yucca Mountain and the WHB Area (Figure 1) lie within the central southern part of Nevada within the Great Basin, which is part of the Basin and Range structural/physiographic province. Pre-Tertiary rocks, consisting of a thick sequence of Proterozoic and Paleozoic sedimentary rocks, underlie approximately 1,000 to 3,000 meters of Miocene volcanic rock in the Yucca Mountain area (Gibson et al. 1990, page 3).

Units of the Paintbrush and Timber Mountain groups are included in the Miocene volcanic sequence exposed at Yucca Mountain (Sawyer et al. 1994, page 1314). The Claim Canyon caldera and environs, located approximately 6 km north of the study area, is the source of the 12.7 to 12.8 million-year old pyroclastic rock and lava comprising the Paintbrush Group (Byers et al. 1976, page 24; Sawyer et al. 1994, pages 1312-1314). Four formations of pyroclastic-flow and pyroclastic-fall deposits with interbedded lavas, dipping 5 to 10° to the east, form a homoclinal sequence included in the Paintbrush Group (Byers et al. 1976, page 24; Christiansen et al. 1977, page 951). Two of these formations, the Topopah Spring Tuff and Tiva Canyon Tuff, are voluminous, densely welded ignimbrites, grading upward from rhyolite to quartz latite composition (Lipman et al. 1966, page F7; Byers et al. 1976, page 25; Schuraytz et al. 1989, page 5925).

As shown on Figure 223, the WHB Area (Figure 1) is situated mainly in Midway Valley along the east side of Exile Hill, though a small part of the WHB Area laps onto Exile Hill. Exile Hill is a horst, bounded on its west side by the Bow Ridge fault and on its east side by the Exile Hill fault. Exile Hill consists of Tiva Canyon Tuff that is surrounded and partially covered by Quaternary alluvium/colluvium. The upper Tertiary and Quaternary sediments (identified by the symbol Qac) that fill Midway Valley consist mostly of alluvial deposits (fluvial and colluvial sediments) and some thin eolian deposits. Over most of the WHB Area the alluvium is covered by an artificial fill known as the North Portal pad or by the adjacent muck piles. The North Portal pad is a man-made fill constructed on the Midway Valley alluvium to support tunneling of the ESF.

Elevation of the ground surface in the region of the WHB Area ranges from about 3,000 feet southeast of the site, in the lower reaches of Forty Mile Wash, to over 6,000 feet about 4 miles to the north, in the area of the Timber Mountain caldera. The crest of Yucca Mountain, located about 2 miles to the west, is at an average elevation of about 4,900 feet. Near the site of the proposed WHB, relief is approximately 250 feet, ranging from about elevation 3,850 feet at the crest of Exile Hill, to the west, to about elevation 3,600 feet at the center of Midway Valley, to the east.



Modified from DTN: GS980608314221.002

Figure 223. Generalized Geologic Map of the WHB Area, including Exile Hill

CO4

6.6.2 Subsurface Geologic Conditions

Based on the drilling data discussed in Sections 6.2.2 and 6.2.3, an interpretation of subsurface geologic conditions has been developed for the WHB Area (Figure 224).⁸ The interpretation presumes that the thicknesses of lithostratigraphic units remain relatively constant across the WHB Area (Assumption 2), and that a northeast-striking, southeast-dipping volcanic sequence has been structurally disrupted by several northerly-trending, high-angle, primarily normal, faults.⁹ These faults are depicted as cutting the entire volcanic bedrock sequence, but not disrupting the overlying alluvium. The top of rock profile developed from drilling indicates a relatively even bedrock/alluvium contact. Therefore, the results of this program do not provide any evidence of structural displacement at the base of the alluvium. This is consistent with the findings of Swan et. al. (2001), who found no evidence of Quaternary faulting in trenches excavated in the area of the WHB.

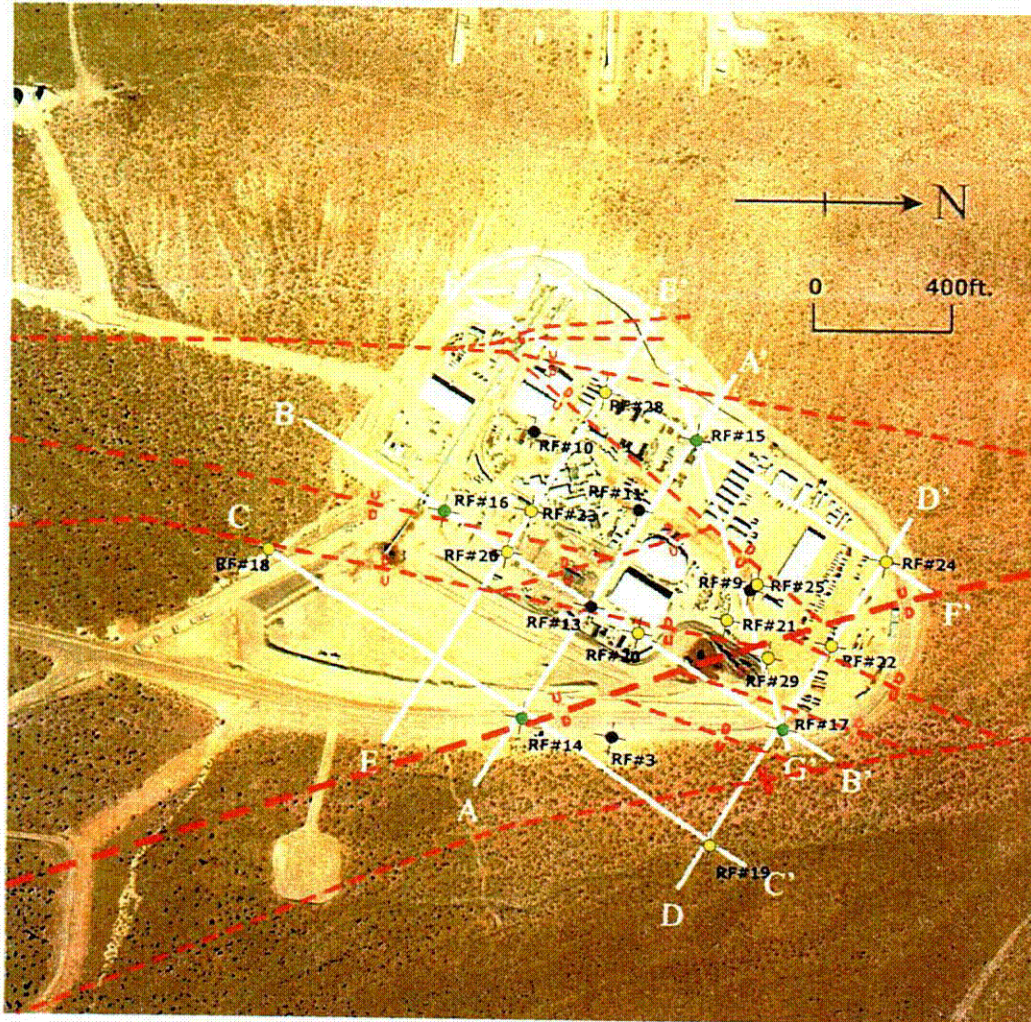
The subsurface depictions represent an interpretation of general geologic conditions beneath the WHB Area that is consistent with the available subsurface data. It is recognized, however, that the number and locations of faults are possibly different than shown, and other interpretations of the data are possible. In fact, most of the faults have been observed in only a single borehole or not at all. Faults shown on the cross sections are represented with a single line; however, elevation changes in contacts between boreholes could be the result of displacement along several parallel or imbricate faults.

Figure 224 is a plan view map showing the location of boreholes, interpreted geologic structures (faults), and cross sections. Seven cross sections, designated A-A' through G-G', are presented on Figures 225 through 231 and illustrate the subsurface geologic interpretation developed for the site. Sections A-A', D-D' and E-E' are cut approximately parallel to the dip of the volcanic stratigraphy. Sections B-B', C-C' and F-F' are cut approximately parallel to the strike of the volcanic stratigraphy. Section G-G' is cut normal to the strike of a normal fault that cuts across the northeast corner of the WHB Area, which will be referred to herein as the "Exile Hill fault splay." Figure 232 presents a map of interpreted contours of top-of-bedrock developed from the borehole data and bedrock outcrops on Exile Hill. The following paragraphs discuss the interpretive geologic features shown on the sections. Note that borehole RF#21 was not used in creating Figure 232.

In most of the WHB Area, the alluvium is covered by a man-made fill constructed on the Midway Valley alluvium to support tunneling of the ESF. The North Portal pad fill was constructed of colluvium and bedrock from shallow excavations at the toe of Exile Hill and for the north portal of the ESF, alluvium from distant borrow pits, and tunnel muck. The North Portal pad is about 800 to 1,200 feet by 600 to 700 feet in size and slopes roughly 2 percent to the east, from approximately elevation 3,683 at the base of Exile Hill to 3,670 feet.

⁸ This interpretation concerns the part of the WHB Area lying east of the Exile Hill fault. Different stratigraphic units and a different bedding strike and dip pertain west of the Exile Hill fault.

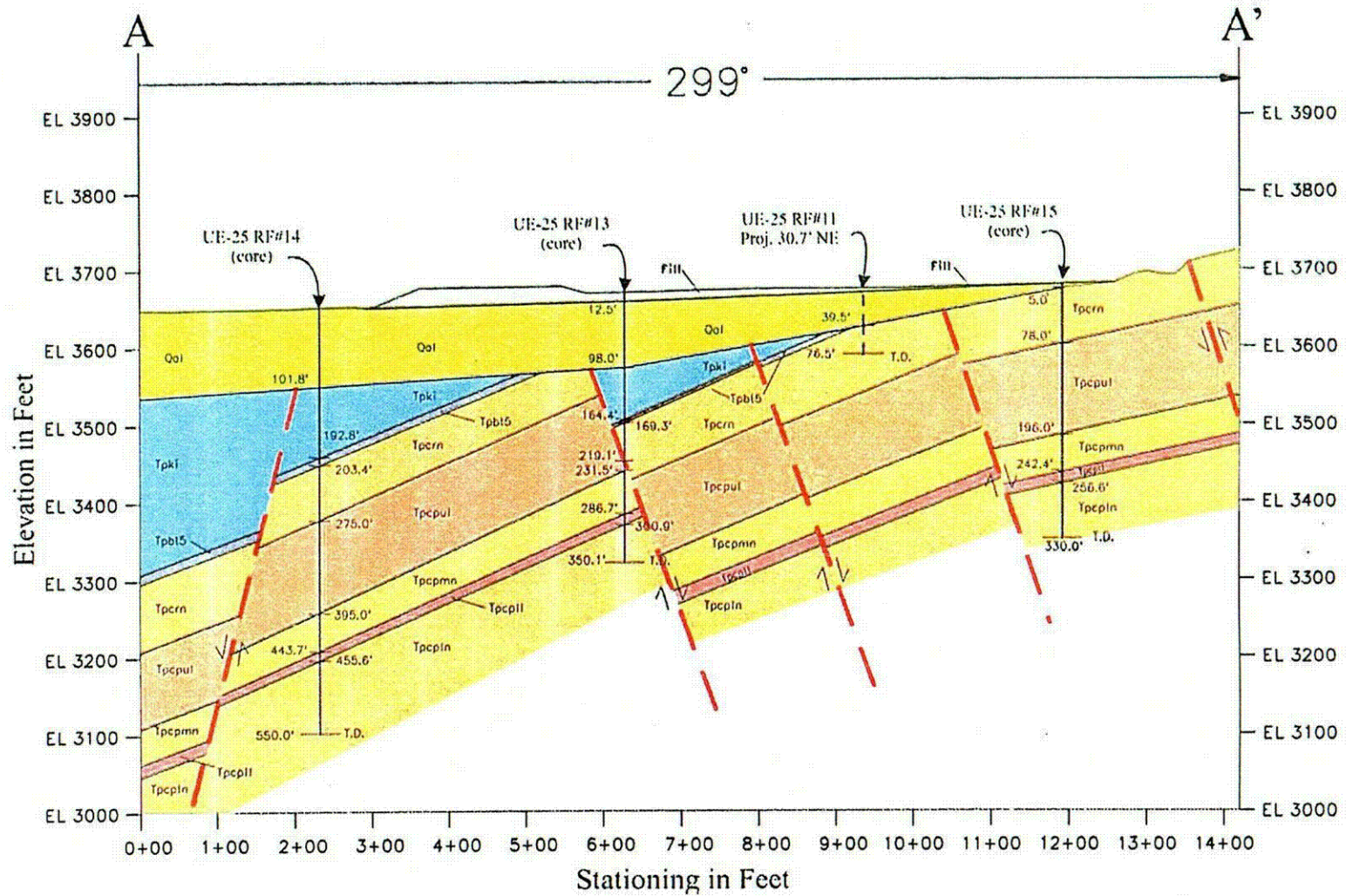
⁹ The welded and nonwelded tuffs encountered in the drilling program are deposited in various thicknesses over an unknown paleo-topography. Developing a geologic interpretation that takes paleo-topography into account is beyond the scope of this investigation; and any insight into this factor is limited by the use of mud rotary drilling techniques and widely spaced core holes. Surficial processes, such as erosion by wind and rain, could have easily developed highs and lows along the surface of bedrock units before subsequent deposition occurred.



DTNs: GS020383114233.003, MO0008GSC00286.000,
Assumption 6; YMP Photograph Number - BN 8811-50

Note: Boreholes in black are pre-existing holes, boreholes in yellow are mud rotary holes, and boreholes in green are core holes. Faults are projected from top-of-bedrock and are dashed where approximate.

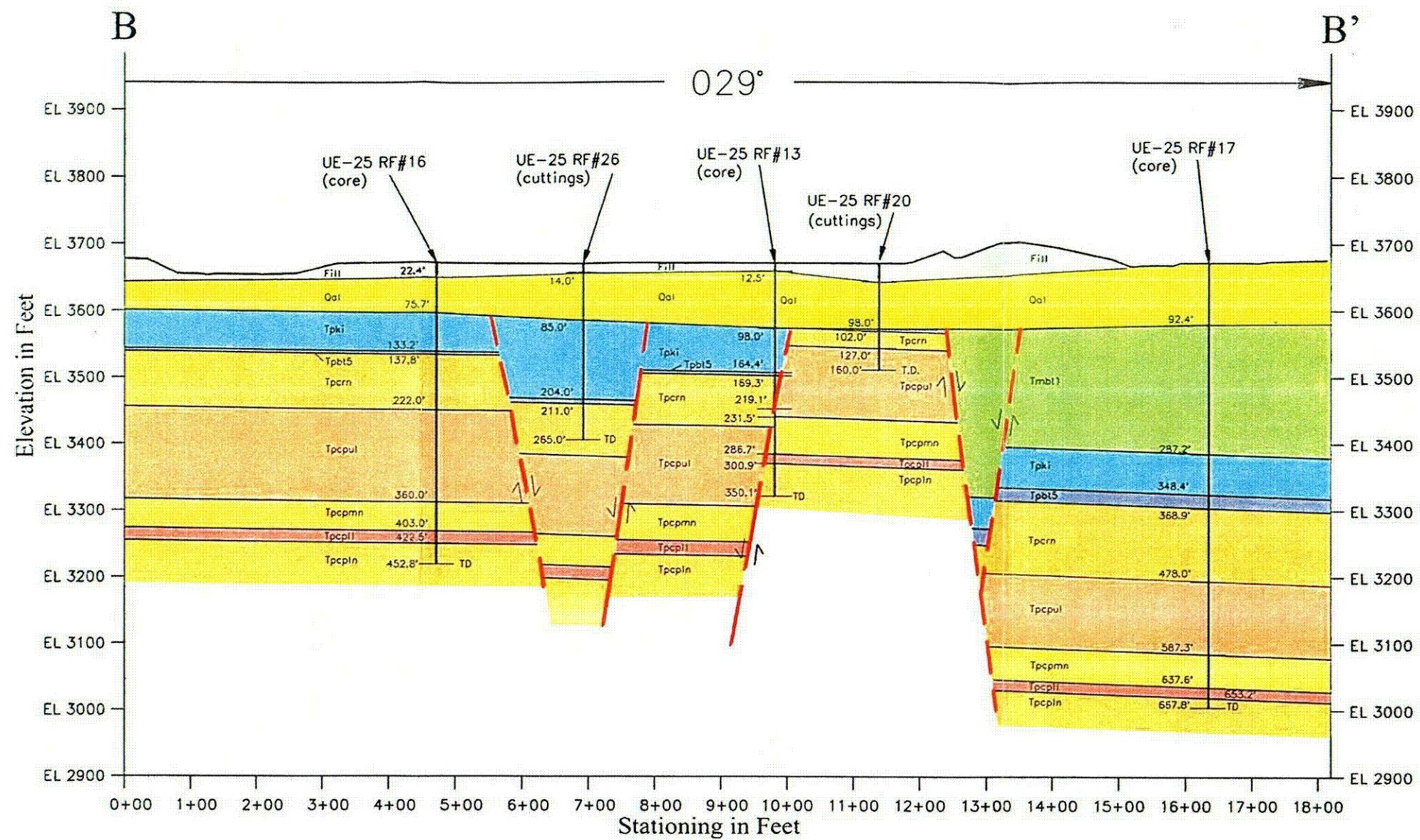
Figure 224. Locations of Cross Sections and Interpreted Faults through the WHB Area



DTNs: GS020383114233.003, MO0008GSC00286.000
and Assumption 6

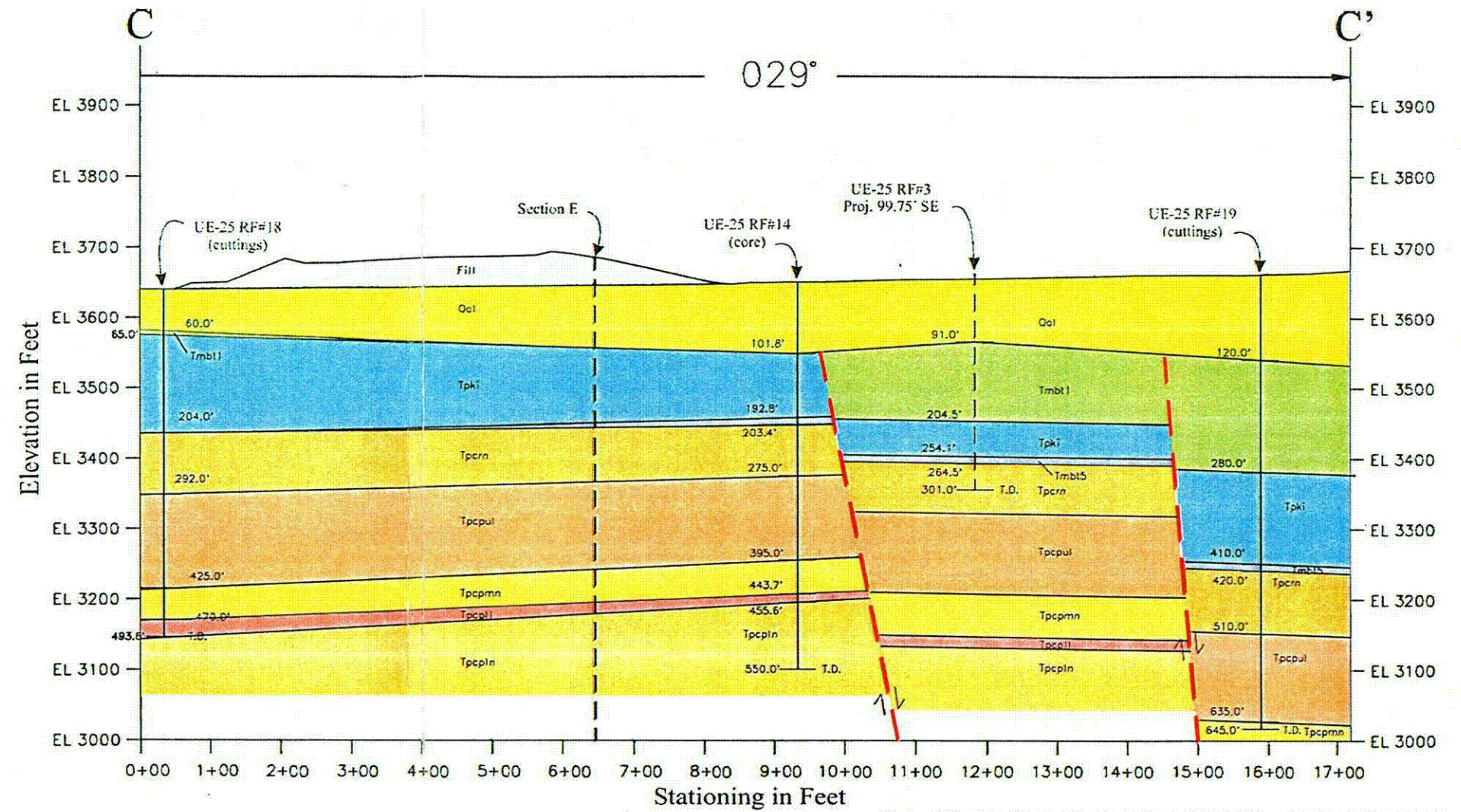
Figure 225. WHB Area Geologic Cross Section A-A', Looking South

COG



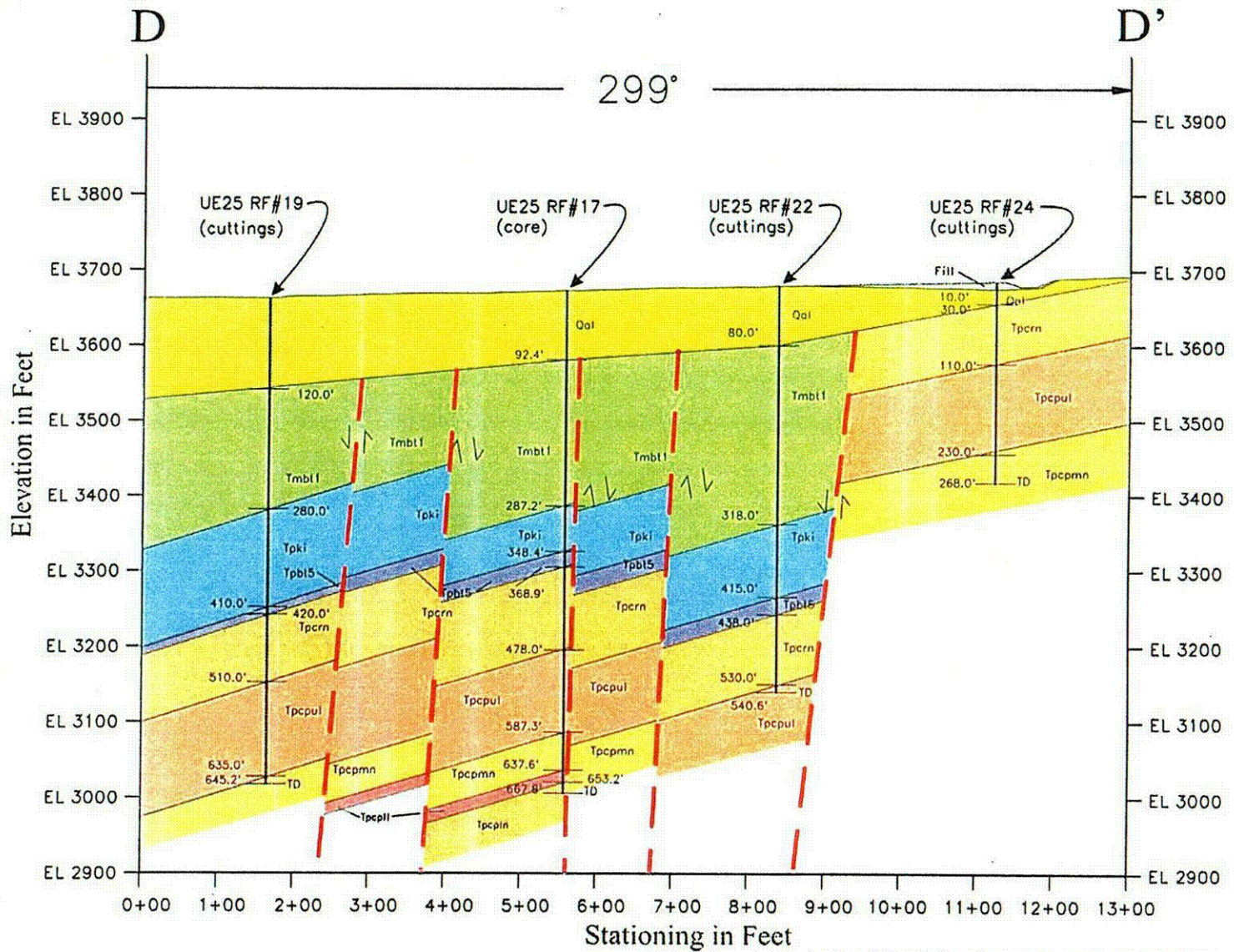
DTNs: GS020383114233.003, MO0008GSC00286.000

Figure 226. WHB Area Geologic Cross Section B-B', Looking West



DTNs: GS020383114233.003, MO0008GSC00286.000 and GS931008314211.036

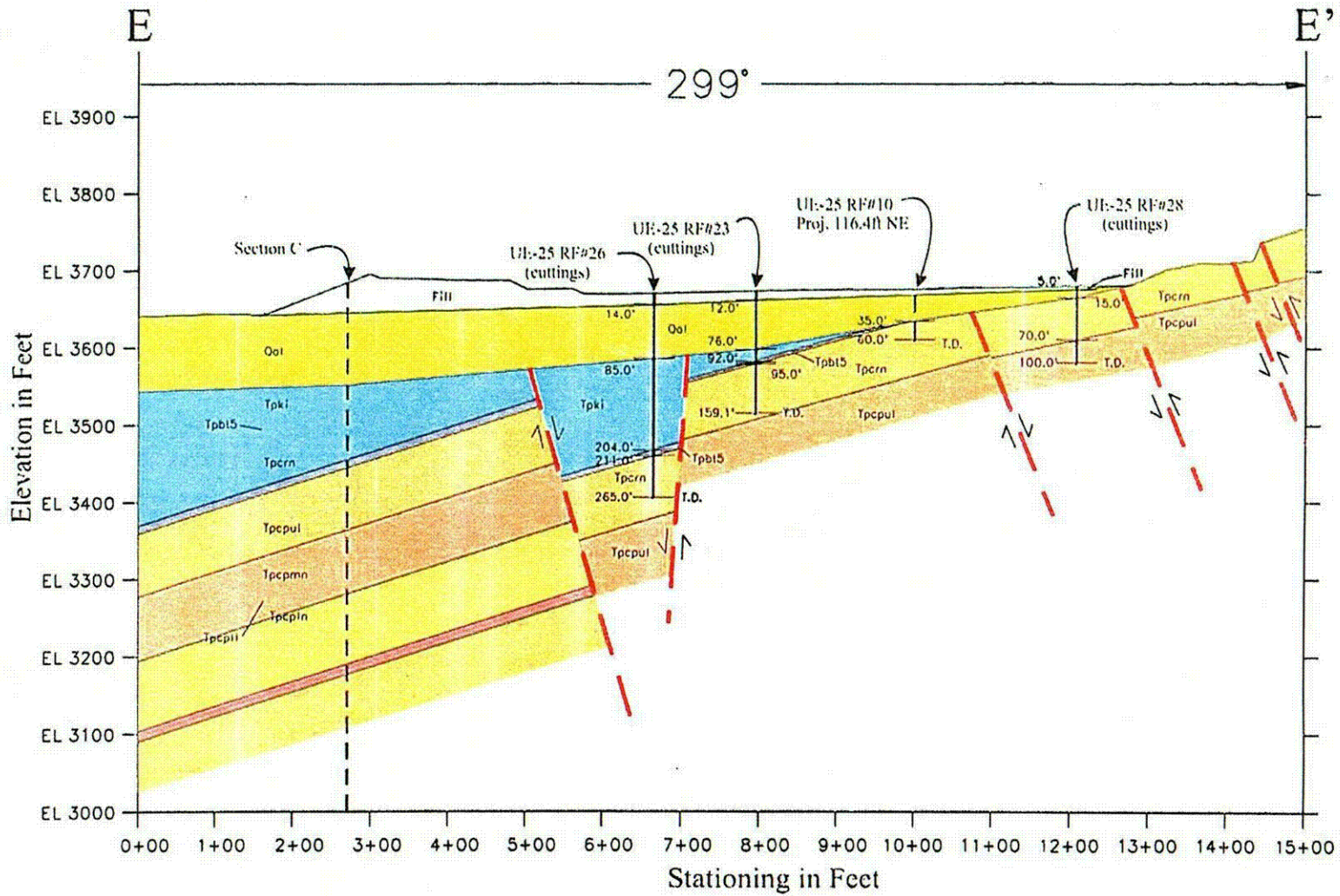
Figure 227. WHB Area Geologic Cross Section C-C', Looking West



DTNs: GS020383114233.003, MO0008GSC00286.000

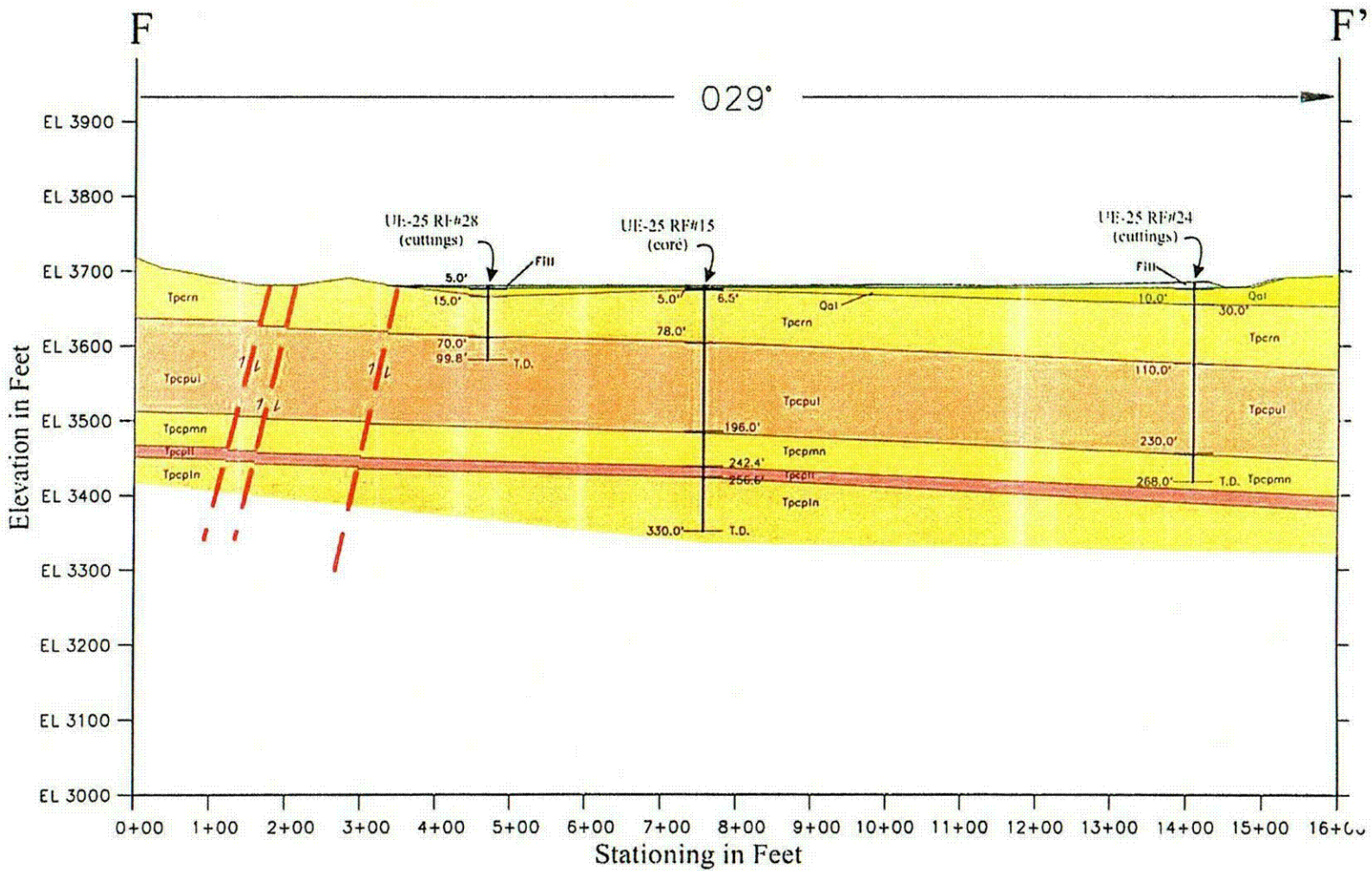
Figure 228. WHB Area Geologic Cross Section D-D', Looking South

009



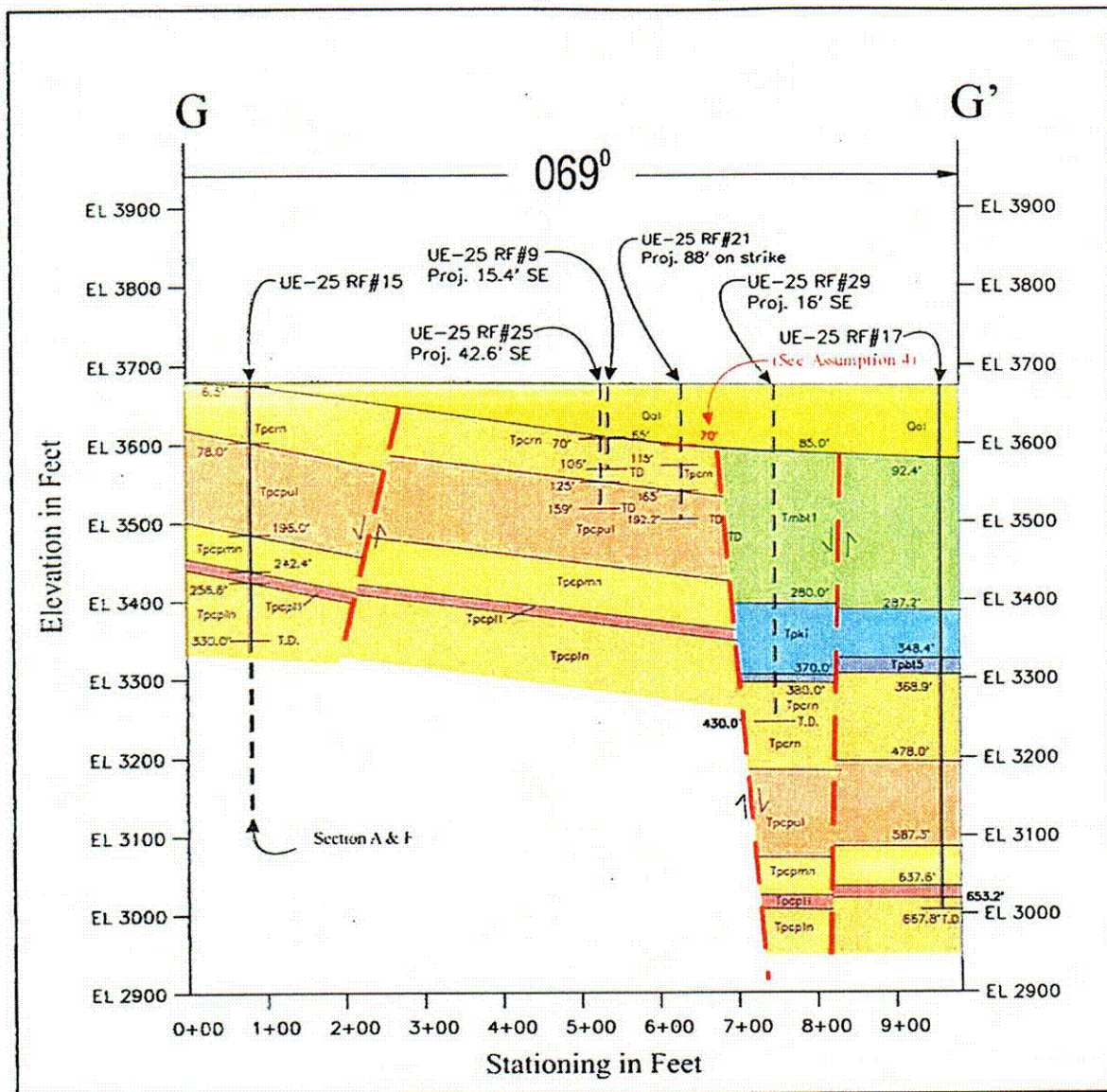
DTNs: GS020383114233.003, MO0008GSC00286.000
and Assumption 6

Figure 229. WHB Area Geologic Cross Section E-E', Looking South



DTNs: GS020383114233.003, MO0008GSC00286.000

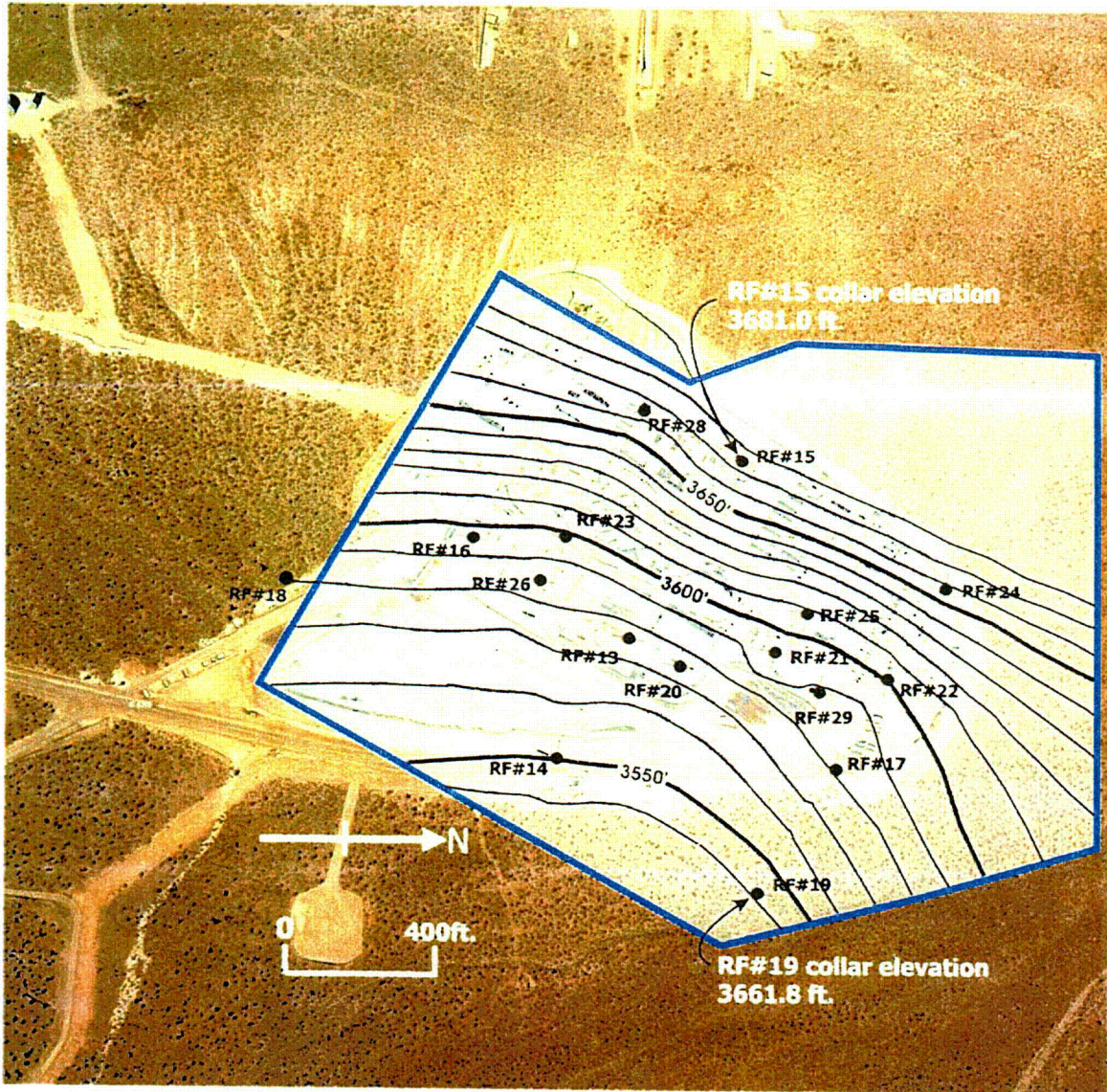
Figure 230. WHB Area Geologic Cross Section F-F', Looking West



DTN: GS020383114233.003 and Assumption 6

Figure 231. WHB Area Geologic Cross Section G-G', Looking Northwest

C12



DTN: GS020383114233.003

Note: Contours are of top-of-bedrock, including welded and nonwelded units (10-foot contour interval). In accordance with Assumption 4 (Section 5), data from borehole RF#21 was not used in creating these contours.

Figure 232. Elevation Contours for Top-of-Bedrock Encountered in Boreholes

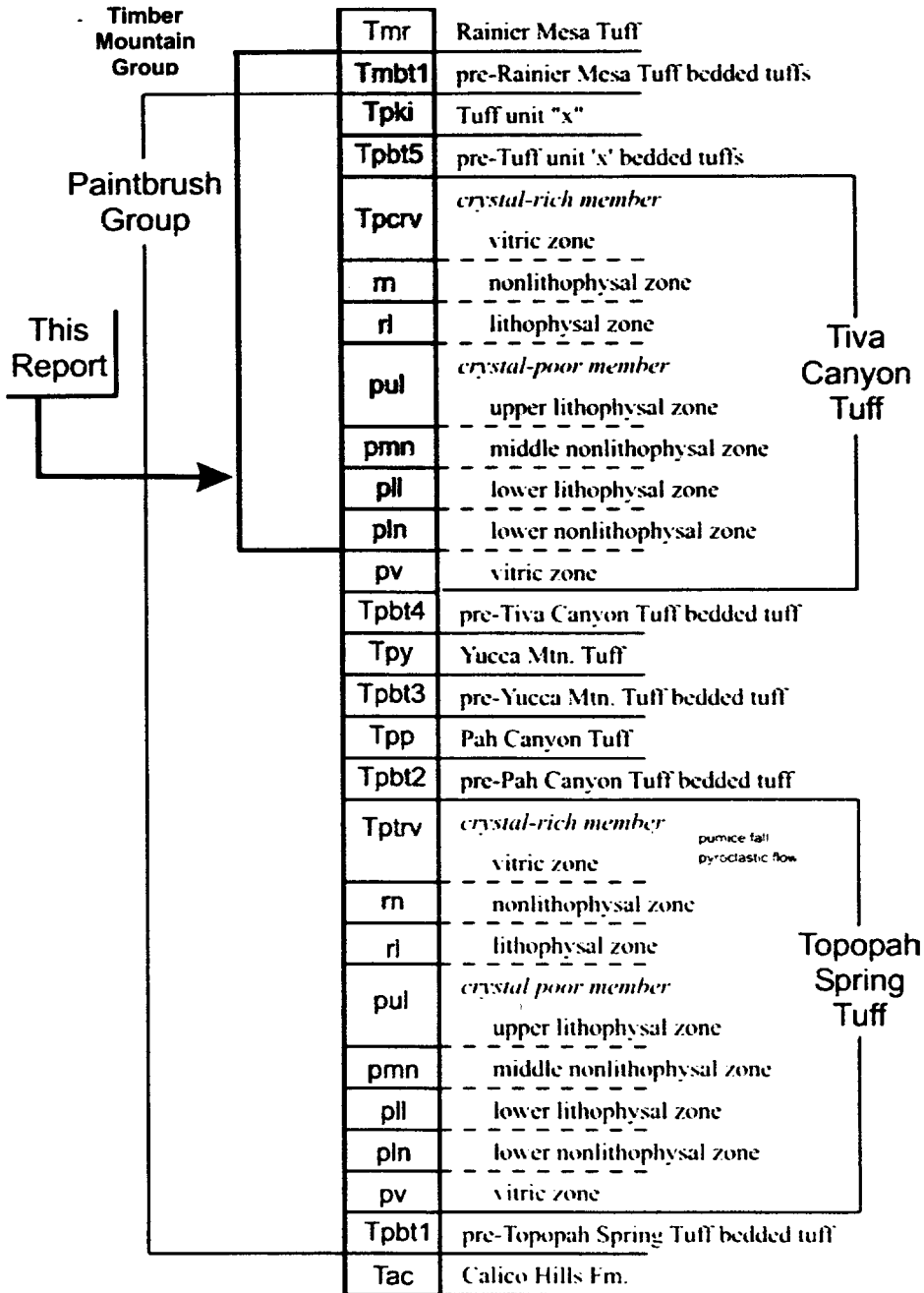
The alluvium varies in thickness from zero on the western edge of the WHB Area along the base of Exile Hill to over 100 feet in the part of the WHB Area located east of the muck pile. Alluvial materials in the WHB area consist of interbedded caliche-cemented and non-cemented, poorly sorted gravel with some fines, cobbles and boulders. For detailed descriptions of the alluvial material, refer to Section 6.2.4.

Under the alluvium are welded and nonwelded volcanic rock units of the Timber Mountain and Paintbrush groups. Figure 233 provides a lithostratigraphic column for relevant units of these groups. Nonwelded units beneath the site include the pre-Rainier Mesa Tuff bedded tuffs (Tmbt1) of the Timber Mountain Group, and the Tuff unit "x" (Tpki) and pre-Tuff unit "x" bedded tuffs (Tpbt5) of the Paintbrush Group. Beneath these nonwelded units is the Tiva Canyon Tuff, which is generally densely welded. The Tiva Canyon Tuff has been divided into two members; the younger crystal-rich member (Tpcr) and the older crystal-poor member (Tpcp). These members are further divided into zones, for example, the Tiva Canyon Tuff crystal-rich nonlithophysal zone (Tpcrn) (Buesch et al. 1996, pp. 22, 33-38). Detailed geologic descriptions of the various zones of Tiva Canyon Tuff encountered in the boreholes are presented in Attachments I and II. To simplify the distinction between the welded and nonwelded Tiva Canyon Tuff and the post-Tiva Canyon Tuff bedded tuffs, the vitric and lithophysal zones (Tpcrv and Tpcrl) of the crystal-rich member of the Tiva Canyon Tuff have been included with the crystal-rich nonlithophysal zone (Tpcrn) in this report. For the purposes of this report, subzones are not identified on the logs of boreholes RF#14 to RF#29.

The general orientation of bedding beneath the WHB Area is northeast-striking and southeast-dipping, which is slightly different than the orientation of bedding mapped on nearby Exile Hill. The *Plan View Geologic Map of the Drainage Channel and North Portal* (DTN: GS940408314224.004) shows the strike and dip of five contact observations in the North Portal cut, located west of the Exile Hill fault. Four of the contacts are in the upper lithophysal zone of the crystal-poor member of the Tiva Canyon Tuff (Tpcpul); their strikes ranged from N36°W to N8°W and their dips ranged from 14 to 22 degrees to the northeast. The remaining contact was in an intensely fractured zone in the lithophysal zone of the crystal-rich member of the Tiva Canyon Tuff (Tpcrl); its strike and dip were N40°E and 20°SE. Therefore, the bedding on Exile Hill is, in general, north-northwest-striking and east-northeast-dipping.

The following three-point problems were solved to interpret strike and dip of the bedrock stratigraphy beneath the WHB Area, based on the drilling data (Figure 224). These results are based on limited information from fault-bounded blocks within the WHB area. The elevations of the top of the Tpcpul in boreholes RF#18, RF#14, and RF#20 suggest that the bedding in this area is oriented N33°E, 23°SE. The elevations of the top of the Tpcpul in boreholes RF#13 (Tpcpul projected to 249ft.), RF#25, and RF#21 yield an orientation of N43°E and 18°SE.

General Lithostratigraphic Column at Yucca Mountain, Nevada



Source: Modified from Mongano et. al. (1999, Page 13).

Note: Gray-shaded areas indicate the units that are referred to in this report.

Figure 233. Generalized Lithostratigraphic Column Showing the Stratigraphic Interval Considered in this Scientific Analysis

However, given that boreholes RF#18, RF#20, RF#21, and RF#25 were mud rotary holes, the exact elevations of Tpcpul contacts are not known precisely. Therefore, the strikes and dips from these three-point problems are considered approximate. For example, if the top of the Tpcpul in borehole RF#21 is actually five feet¹⁰ higher, then the orientation derived from the elevations of the top of the Tpcpul in boreholes RF#13, RF#25, and RF#21 becomes N51°E, 17°SE.

For the purposes of this report, the strike and dip of the volcanic stratigraphy beneath the WHB Area are interpreted to be about N16°E and 25°SE. Various representations of the orientation of bedding in the WHB Area are shown on Figures 225 through 231. Regional mapping efforts (DTN: GS980608314221.002) demonstrate a large degree of variability in strike and dip of the Tiva Canyon Tuff, N16°E, 25°SE is within this variability and can be considered a reasonable representation of subsurface conditions.

The most prominent structural feature encountered during this exploration is a north-northwest-trending, east-northeast-dipping normal fault that cuts across the WHB Area, near boreholes RF#14 and RF#29. This fault, informally referred to in this report as the "Exile Hill fault splay," is shown as the bolder (wider) fault trace on Figure 224. A regional geologic map (DTN: GS980608314221.002) shows a down-to-the-east fault east of Exile Hill that terminates at the Midway Valley fault south of the WHB Area. The fault mapped in DTN: GS980608314221.002 can be represented by the Exile Hill fault splay by having the splay terminate into the Midway Valley fault further to the north than previously mapped. This relationship between the regional mapping and the Exile Hill fault splay is shown on a modified portion of the regional geologic map (Figure 223).

The largest displacement associated with the Exile Hill fault splay is on the northern edge of the WHB Area. Between boreholes RF#22 and RF#24 there is approximately 300 feet of down-to-the-northeast separation, dropping the nonwelded pre-Rainier Mesa Tuff bedded tuffs (Tmbt1) on the northeast against the densely welded Tiva Canyon Tuff on the southwest. This relatively substantial vertical displacement along the Exile Hill fault splay has, in effect, subdivided the WHB Area into two distinct domains. Southwest of this fault, the top of the welded Tiva Canyon Tuff is relatively near the surface, ranging from zero to a maximum of about 190 feet below natural grade. In contrast, on the northeast side of the Exile Hill fault splay, the top of the Tiva Canyon Tuff ranges from about 250 to 480 feet below natural grade. A substantially greater thickness of the post-Tiva Canyon Tuff nonwelded bedded tuffs (Tptb5, Tпки, Tmbt1) occurs beneath the alluvium on the northeast side of the Exile Hill fault splay relative to the southwest side. The offset diminishes to the southeast along the strike of the fault, with 65 feet of down-to-the-east separation near borehole RF#14.

In addition to the Exile Hill fault splay, the interpretation of subsurface conditions includes several other faults that cut the volcanic bedrock within the WHB Area. These other faults are shown on Figure 224 as the thinner fault traces on either side of the Exile Hill fault splay. As

¹⁰ The estimated accuracy of the contacts is plus or minus 5 feet for mud rotary boreholes and plus or minus 1 foot for core, relative to the designated contact depth. If some of the rock that is cored is not recovered, this introduces additional uncertainty. The contacts within the Tiva are also gradational, as the units are based on considerations such as differences in phenocryst content and percentage of lithophysae voids.

shown on Figure 224, most, but not all, of these faults strike north-northeasterly and exhibit down-to-the-east normal displacement. Thickening and thinning of units across the cross sections could be the result of strike slip movement along faults, however, given the dynamic environment of deposition and the limitations of the data set, no attempt has been made to demonstrate lateral movement on faults. Further discussion of these faults and the subsurface geology, with specific reference to each of the seven sections, is provided in the following paragraphs.

Section A-A' (Figure 225) cuts approximately parallel to the dip of bedding across the central part of the WHB Area. It shows an easterly dipping, homoclinal volcanic sequence consisting of Tiva Canyon Tuff (Tpc), pre-Tuff unit "x" bedded tuffs (Tptb5), and Tuff unit "x" (Tpki) that is unconformably overlain by an easterly thickening sequence of Quaternary alluvium and by North Portal pad fill/muck. The crystal-rich member of the Tiva Canyon Tuff (Tpcrn) outcrops along the west side of the section, on the east slope of Exile Hill and the alluvium thickens to the east, from zero near borehole RF#15 to about 120 feet near borehole RF#14.

The Exile Hill fault splay, which is east of borehole RF#14, shows about 75 feet of down-to-the-east separation. The fault intersected by borehole RF#13 is a northeast-trending, northwest-dipping normal fault that exhibits approximately 100 feet of down-to-the-west separation. The fault between boreholes RF#13 and RF#11 is a northwest-trending, northeast-dipping reverse fault that exhibits about 25 feet of up-to-the-west separation. The fault between boreholes RF#11 and RF#15 is a northeast-trending, northwest-dipping normal fault that shows about 25 feet of down-to-the-west separation. The Exile Hill fault, located west of borehole RF#15, has about 5 feet of up-to-the-west separation.

Section D-D' (Figure 228) cuts approximately parallel to the dip of bedding across the northern part of the WHB Area. It shows an easterly dipping volcanic sequence consisting of Tiva Canyon Tuff (Tpc), pre-Tuff unit "x" bedded tuffs (Tptb5), Tuff unit "x" (Tpki), and pre-Rainier Mesa Tuff bedded tuffs (Tmbt1), unconformably overlain by an easterly thickening sequence of Quaternary alluvium and by North Portal pad fill/muck. At the western edge of the section the alluvium is only a few feet thick, deepening to over 120 feet to the east of RF#19. Between boreholes RF#24 and RF#22 is the Exile Hill fault splay, with approximately 360 feet of down-to-the-northeast separation along this section. East of the Exile Hill fault splay, three northeast-trending, northwest-dipping normal faults drop the volcanic stratigraphy approximately 220 feet down to the northwest. The southeasternmost fault on Section D-D' is a northwest-trending, southwest-dipping reverse fault that has produced about 5 feet of up-to-the southwest separation along this section.

Section E-E' (Figure 229) cuts approximately parallel to the dip of bedding across the southern part of the WHB Area. It shows a southeasterly dipping volcanic sequence consisting of Tiva Canyon Tuff (Tpc), pre-Tuff unit "x" bedded tuffs (Tptb5), and Tuff unit "x" (Tpki), that is unconformably overlain by an easterly thickening sequence of Quaternary alluvium and by North Portal pad fill/muck. From west to east this section shows the alluvium thickening from zero near the base of Exile Hill to approximately 100 feet on the eastern edge of the section. It also shows the presence of a down-dropped block that accounts for the relatively thick section of Tuff unit "x" encountered in borehole RF#26, compared to that encountered in borehole RF#23. The fault along the eastern side of this down-dropped block is a northeast-trending, northwest-

dipping normal fault that has produced about 120 feet of down-to-the-west separation. The fault along the western side of this block is a northeast-trending, southeast-dipping normal fault that has produced about 90 feet of down-to-the-east separation. The fault between boreholes RF#28 and RF#10 is a northeast-trending, northwest-dipping normal fault that has produced minor down-to-the-west separation. The Exile Hill fault just west of borehole RF#28 has approximately 10 to 15 feet of up-to-the-west separation. The other faults west of borehole RF#28 are north- to northwest-trending, west-dipping reverse faults that have produced minor up-to-the-west separations.

Section B-B' (Figure 226) cuts approximately parallel to the strike of bedding across the central part of the WHB Area. It shows a volcanic sequence consisting of Tiva Canyon Tuff (Tpc), pre-Tuff unit "x" bedded tuffs (Tptb5), Tuff unit "x" (Tpki), and pre-Rainier Mesa Tuff bedded tuffs (Tmbt1) that is unconformably overlain by Quaternary alluvium. The alluvium is overlain in some areas by North Portal pad fill or muck.

The volcanic stratigraphy exhibits a slight (approximately 3°) northeasterly apparent dip and is disrupted by five normal faults. North of borehole RF#16, a graben brackets borehole RF#26. The northeast-trending, northwest-dipping normal fault along the south side of this graben has dropped the top of the Tiva Canyon Tuff about 70 feet. An uplifted block, or horst, centered on borehole RF#20 is bounded on the southwest by the fault encountered by borehole RF#13 and on the northeast by the Exile Hill fault splay. The northeast-trending, northwest-dipping normal fault encountered in borehole RF#13 exhibits about 120 feet of down-to-the-northwest separation, and the Exile Hill fault splay exhibits about 330 feet of down-to-the-northeast separation. Between the graben and the horst is an intermediate block that is bounded on the south by the fault shown immediately to the north of borehole RF#26. This northwest-trending, southwest-dipping normal fault exhibits about 50 feet of down-to-the-south separation between the graben and the intermediate block. The northernmost fault on this section is a northeast-trending, northwest-dipping normal fault that terminates at the Exile Hill fault splay. This fault exhibits about 90 feet of down-to-the-west separation.

Section C-C' (Figure 227) cuts approximately parallel to the strike of bedding across the southeastern edge of the WHB Area. It shows a volcanic sequence consisting of Tiva Canyon Tuff (Tpc), pre-Tuff unit "x" bedded tuffs (Tptb5), Tuff unit "x" (Tpki), and pre-Rainier Mesa Tuff bedded tuffs (Tmbt1) that is unconformably overlain by a northeasterly thickening sequence of Quaternary alluvium. Alluvium thickens to the north edge of the section to over 120 feet. The alluvium is overlain in some areas by muck. The Exile Hill fault splay exhibits about 50 feet of down-to-the-northeast separation just north of borehole RF#14. The fault immediately south of borehole RF#19 is a northwest trending, southwest-dipping normal fault that exhibits about 160 feet of up-to-the-south separation.

Section F-F' (Figure 230) cuts approximately parallel to the strike of bedding across the northwestern edge of the WHB Area, near the base of Exile Hill. This section shows the Tiva Canyon Tuff unconformably overlain by a thin veneer of alluvium and North Portal pad fill in some areas and cropping out on Exile Hill. The alluvium thickens to about 30 feet on the northern edge of the section. Three north- to northwest-trending, southwest-dipping reverse faults exhibit minor separation to the south of borehole RF#28.

Section G-G' (Figure 231) cuts normal to the strike of the Exile Hill fault splay across the northern portion of the WHB Area. It shows a volcanic sequence consisting of Tiva Canyon Tuff (Tpc), pre-Tuff unit "x" bedded tuffs (Tptb5), Tuff unit "x" (Tpki), and pre-Rainier Mesa Tuff bedded tuffs (Tmbt1) that is unconformably overlain by a northeasterly thickening sequence of Quaternary alluvium and North Portal pad fill (a surface profile of this section was not developed, therefore, the pad fill is not represented). The alluvium thickens to the northeast from zero at the southwest end to about 75 feet thick at the east-northeast end of the section. Along this section, the Exile Hill fault splay shows approximately 320 feet of down-to-the-northwest separation. The fault between RF#15 and RF#25 is a northeast-trending, northwest-dipping normal fault that shows about 75 feet of down-to-the-west separation. The fault to the southwest of RF#17 is a northeast-trending, northwest-dipping fault.

In summary, the WHB Area can be characterized as underlain by densely welded, rhyolitic, pyroclastic flows of the Tiva Canyon Tuff, nonwelded bedded tuffs of the post-Tiva Canyon Tuff and the pre-Rainier Mesa Tuff bedded tuffs and by Quaternary alluvium. The Quaternary alluvium thickens towards the east from zero along Exile Hill to over 120 feet thick on the eastern side of the area. Structurally, the area is crisscrossed with mostly high-angle normal faults of various displacements. A northwest-trending normal fault, cutting across the northeastern edge of the WHB site, informally referred to in this report as the Exile Hill fault splay, has produced significant down-to-the-northeast displacement of the volcanic stratigraphy. As a result, the area to the northeast of the Exile Hill fault splay is characterized by a significantly thicker sequence of nonwelded bedded tuffs overlying the Tiva Canyon Tuff, and the area to the southwest of the Exile Hill fault splay is typically characterized by no or a relatively thin sequence of nonwelded tuffs overlying the Tiva Canyon Tuff. The westernmost extent of the nonwelded bedded tuffs occurs midway across the WHB area. From this line, the nonwelded bedded tuffs generally thicken to the east. The exception to this trend is the result of an elongate graben that trends to the southeast beginning just north of borehole RF#26.

6.6.3 Groundwater Conditions

The WHB Area is located in a part of the Yucca Mountain area with about a 1270-foot thick unsaturated zone, where the water table slopes to the east-southeast (USGS 2001, Figure 6-1). There are no boreholes within the WHB Area that penetrate the water table and thus the depth to the water table is approximated based on nearby boreholes (see below). The water table elevation map developed for the Yucca Mountain Saturated Zone Site-Scale Flow and Transport Model (USGS 2001, Figure 6-1) indicates an area typically referred to as the large hydraulic gradient to the north of the WHB Area, but this feature is at least 8,500 feet north. USGS (2001, Table I-1, DTN: GS000508312332.001) list all borehole information in metric units; for this report, these metric values have been converted to feet.

The approximation of depth to and gradient of the water table beneath the center of the WHB Area is based on several boreholes (DTN: GS000508312332.001). The water table in borehole UE-25 WT#4 (Figure 223), which is 5,000 feet to the northwest of the WHB Area, is at an elevation of 2397.6 feet. There are four additional boreholes within about 8,500 feet of the WHB Area (UE-25 WT#18, UE-25 a#1, UE-25 b#1, and UE-25 WT#14,) that penetrate the water table at 2397.6, 2398.3, 2397.0, and 2394.0 feet, respectively. With respect to the WHB Area, borehole UE-25 WT#18 is located northwest, UE-25 a#1 and UE-25 b#1 are to the

west-southwest, and UE-25 WT#14 is to the southeast. The location of the boreholes and the elevation of the water table indicate an extremely small gradient that slopes to the east-southeast beneath the WHB Area. A typical elevation of the water table under the WHB Area is about 2400 feet, and the typical ground (fill pad) elevation for the WHB Area is about 3670 feet; therefore, the typical depth to the water table is about 1270 feet. Because both the water table and the ground elevation have little gradient in the WHB Area, a depth to the water table of 1270 feet is a reasonable value for the entire WHB Area. The elevations of the UE-25 RF# series of boreholes used in this investigation have elevations that vary from 3640.3 to 3680.8 feet and depths that vary from 100.0 to 667.8 feet (Table 3). These relations of ground elevation, total depth of the boreholes, and the elevation of the water table indicate that the water table is about twice as deep as the deepest borehole in the WHB Area; therefore, all boreholes are within the unsaturated zone.

6.7 EVALUATION OF SEISMIC VELOCITY DATA FROM WHB AREA

Section 6.7 compares the results obtained using various seismic methods. First, Section 6.7.1 reviews some comparison studies that have been published that substantiate that agreement can be obtained by the methods used: downhole seismic, suspension seismic and SASW. Section 6.7.2 then examines the data obtained at the WHB Area using these three methods.

6.7.1 Shear-Wave Velocities Determined by Various Seismic Methods at Other Sites

In-situ seismic methods (downhole, suspension, SASW) have been used to measure low-strain v_s and v_p , and laboratory test methods (resonant column, torsional shear) have been used to measure low-strain shear modulus. According to the theory of elasticity, low-strain shear modulus, G_{max} , is the product of the total density, ρ , and the square of the low-strain shear-wave velocity, v_s , so the values of G_{max} can be converted to v_s and vice versa by Eq. 14 (Section 6.2.5).

It is reasonable to ask if these different techniques can be expected to provide the same values of v_s or, equivalently, G_{max} . This section reviews some of the studies of this subject that have been published, while Section 6.7.2 focuses on comparing the data acquired and developed for the WHB. Although some attention is given to compression-wave velocities, the primary focus is on shear-wave velocity and G_{max} as being more important analysis parameters.

In the in-situ tests, it is very difficult to apply dynamic stresses that induce various strain levels, but the measurement of P and S wave velocity at low strain levels is quite easy. On the other hand, it is difficult in laboratory tests to measure v_s and v_p under actual stress conditions (which are often not known) and the test specimens are always disturbed to some degree. However, it is easier to carry out a laboratory test with various levels of strain under controlled stress conditions.

Geophysical methods have the advantage of testing a large volume of the geologic formation, including discontinuities and imperfections that typically are not represented in laboratory test specimens. The volume tested varies with the technique and the arrangement of source and receiver(s). The distances involved are relatively small in the typical suspension seismic setup, while in the downhole seismic and SASW technique, larger volumes of the formation are involved when the receiver(s) are placed farther from the source. Laboratory tests involve

relatively small specimens, and in some cases the sample tested may have been selected because it could be trimmed into a stable cylindrical specimen, that is, the material was not so weak that it would be damaged by the coring or other sampling procedure and it did not contain joints, shears or other types of discontinuities that would cause the specimen to separate into fragments during handling. In the case of granular soil, such as the alluvium at the site, the material is recompacted to the estimated in-situ density and water content, but the original soil fabric and other features (cementation, aging) cannot be reestablished.

Downhole seismic and SASW surveys are useful for evaluating the average seismic velocity of a layer with a relatively uniform seismic velocity. However, downhole seismic and SASW surveys are not generally relied upon to detect the presence of relatively thin¹¹ layers of high or low seismic velocity, although interval velocities between successive depths can be calculated from downhole seismic results.¹² Suspension seismic surveys, on the other hand, are useful for identifying the seismic velocity over relatively short intervals (typically 3.3 feet). In addition, the seismic energy in a downhole survey tends to lessen with depth due to material damping, leading to difficulties in interpreting the records from greater depths. Material damping does not affect the suspension seismic survey at deeper depths because the source and receivers that are lowered down the borehole are connected by tubes that maintain them at a constant spacing. Rather, suspension seismic measurements are affected by local material conditions that can result in unusually high signal attenuation.

Table 31 summarizes some of the main characteristics of the downhole seismic, suspension seismic, and SASW methods.

Several published studies compare the shear-wave velocities obtained by various seismic methods. EPRI (1993) contains shear-wave velocity comparisons for three sites with distinctly different subsurface conditions. The seismic methods used are summarized in Table 32.

EPRI (1993, Section 8) compared the seismic surveys performed at each of the sites and concluded "that velocities vary significantly with local geologic conditions, but that with a reasonable level of care in the interpretation of data, very similar values of velocity are obtained by the different investigators." However, it should be noted that the variability in the results obtained, when plotted as a function of depth, was sometimes wide, and sometimes exceeded 100 percent. Because the boreholes used were sometimes different, as well as the logger/interpreter and the seismic method being different, it is generally difficult to assess how much of the variability is due to subsurface conditions, method, logger technique, and interpreter decisions.

The crosshole data presented is particularly indicative of the variability that can result from subsurface conditions. For example, at Gilroy 2, compression-wave velocity was measured by the crosshole method using four boreholes drilled on a line at 15-foot spacings. The variability in interpreted velocity was as much as 70 percent at certain depths, although the method, logger

¹¹ Relatively thin, i.e., a few feet or less

¹² When it is desirable to obtain interval velocities with the downhole method, it is preferred to use multiple geophones in the borehole and compute the interval velocities from measurements made with a single source excitation.

technique and interpreter were all apparently constant, suggesting that variation of this magnitude can occur over short distances due to geologic variability.

Table 31. Comparison of Downhole Seismic, Suspension Seismic and SASW Methods

Characteristic	Suspension Seismic	Downhole Seismic	SASW
Energy source	Built-in solenoid hammer	Hammer on plank	Hammer at close source-receiver spacings; sledgehammer, dropped weight, bulldozer or vibroseis at longer spacings
Type of wave generated	P and S	P and S	Rayleigh or other surface wave
Ability to reverse polarity	Yes	Yes	No
Primary direction of wave motion	Upward, vertical	Downward, near vertical but becoming more inclined at shallow depth	Horizontal
Wave frequency, Hz	S wave 500 - 1,000 P wave 1,000 - 3,000	S wave 20 - 40 P wave 50 - 200	5 - 500 or more
Boreholes required	One	One	None
Borehole requirements	Liquid-filled; uncased generally preferred; plastic casing is acceptable	Dry preferred; casing optional	Not applicable
Maximum effective depth, ft	1,600	300 to 700	Up to 500
Resolution	Resolution constant with depth	Resolution decreasing with depth	Resolution decreasing with depth
Borehole drift survey	Not required	Not required	Not applicable
Space limitations	Can be performed wherever a borehole can be drilled	Can be performed wherever a borehole can be drilled	Line length is about 2 times the depth surveyed, so on-site and off-site constraints may limit survey depth
Type of wave interpreted	P and S _H	P and S _H	R, converted to S using theory and assumed Poisson's ratio
Interval velocity	Yes	Only with geophones at multiple depths	No
Average velocity	Yes, by accumulation of individual travel times	Yes	Yes

Table 32. Seismic Methods Used at EPRI Comparison Sites

Site	Seismic Surveys
Gilroy 2	P-S downhole; P-S suspension; P-S crosshole and damping; P-S crosshole and damping
Treasure Island	P-S downhole; P-S crosshole and damping; seismic cone
Lotung	P-S uphole and P-S crosshole; v_s refraction

Source: EPRI (1993, Tables 8-2, 8-4 and 8-6)

Ohya (1986) compared suspension seismic and downhole seismic measurements made in the same boreholes at five sites. Based on 144 measurement pairs, the $v_s(\text{suspension})$ to $v_s(\text{downhole})$ ratio averaged 1.028, indicating that the suspension values averaged 2.8 percent higher than the downhole values.

For the compression-wave velocities, even better agreement was obtained. Based on 137 measurement pairs, the $v_p(\text{suspension})$ to $v_p(\text{downhole})$ ratio averaged 1.014, indicating that the suspension values averaged 1.4 percent higher than the downhole values. The observed range of $v_s(\text{suspension})/v_s(\text{downhole})$ was from approximately 0.79 to 1.20, and $v_p(\text{suspension})/v_p(\text{downhole})$ from approximately 0.90 to 1.49. Given that the suspension method yields an interval velocity, while the downhole method yields an average velocity, the agreement is very good.

Ohya (1986, page 1229) also compared suspension seismic and crosshole seismic measurements made at three sites. For this comparison, different boreholes are necessarily used, since the suspension method uses a sole borehole while the crosshole uses three or more boreholes. Based on 36 measurement pairs, $v_s(\text{suspension})/v_s(\text{crosshole})$ averaged 1.133 and $v_p(\text{suspension})/v_p(\text{crosshole})$ averaged 1.06. Because the subsurface conditions at these sites were not uniform, many factors may be responsible for the divergences. In addition, the shear wave measured by suspension is a upwardly propagating wave with particle motion in the horizontal plane, while cross hole measures a horizontally propagating wave with particle motion in the vertical plane.

Ohya (1986, page 1234) concluded that:

- If subsurface conditions are uniform, the suspension, downhole and crosshole methods will produce the same values of P and S wave velocity.
- If subsurface conditions are not uniform, the three methods will produce the different values of P and S wave velocity as follows:
 - ▶ the downhole method will produce an average velocity for the layers
 - ▶ the suspension method will provide more detailed, accurate velocity information, reflecting the changes in velocity from layer to layer
 - ▶ the crosshole method may produce false velocity measurements.

- Deformation or failure of the ground may be significantly influenced by the properties of a weak layer. To this end, it is important to obtain velocity information for a weak layer accurately, even if the weak layer is thin. Suspension logging is suited to this application.

Brown (1998) conducted SASW measurements at nine strong-motion station sites where borehole seismic measurements were previously conducted. The team performing the SASW measurements collected their data and made their interpretations without recourse to the available borehole logs or borehole seismic profiles. Brown (1998) presents detailed results for the nine sites. In addition to the traditional comparison of v_s versus depth, quarter-wavelength amplification ratios and predicted dispersion curves from the downhole profiles were calculated.

Based on his interpretation of the SASW data and subsequent comparison with the other available data (downhole seismic at all sites and suspension seismic at some sites), Brown concluded that:

At five of the nine sites, agreement between the SASW and borehole v_s profiles was very good; at four of the nine sites the SASW and borehole v_s profiles had significant differences.

Some of the differences between the SASW and borehole v_s profiles are due to lateral variability and the difference between the "point" borehole measurements and the global SASW measurements.

The lateral variability in the subsurface, as measured by differences in surface-wave dispersion curves and SASW v_s profiles, were generally low at the test sites with multiple arrays. The differences were greatest near the ground surface and decreased with depth. This trend is due in part to the larger volume of material that is sampled as the sampling depth increases, so that the velocities at depths of several hundred feet represent the average properties over lateral distances of several hundred feet.

Because so much dispersion data is collected in the near-surface and there is little ambiguity in interpreting shorter wavelength data, the accuracy of the SASW method is considered greater near the ground surface than at depth. The SASW models have low resolution at depth.

At several sites the largest relative difference between the downhole and SASW v_s profiles occurred in the upper 10 feet, with the SASW v_s typically being lower than the downhole v_s . At two sites this was likely due to the borehole having been advanced through well-compacted fill while the SASW profile was located in softer surficial ground conditions beyond the fill. At several sites, however, the SASW profile appeared to be in visually similar material and a discrepancy was still observed. In these cases, different moisture conditions (and hence different effective stress conditions) may have contributed to a change in v_s values.

The discrepancies between SASW and downhole profiles near the surface may also be because the downhole velocities are averaged over greater depths and are therefore higher. The downhole method also samples a smaller volume of material than the SASW method and may

not be representative of average or global properties at the site.¹³ If the subsurface is non-uniform, the downhole shear-wave travel path may not follow the straight line path used in the interpretation. In the downhole method, identification of the shear wave arrivals is difficult because the compression wave is usually still present at the onset of the shear wave, obscuring the shear wave.¹⁴

The SASW interpretations were made with one exception using an adopted value of Poisson's ratio of 0.25. However, based on the borehole seismic measurements and groundwater level, a higher value of Poisson's ratio would have been appropriate. At most of the sites the groundwater table is situated between 20 and 50 feet bgs, and Poisson's ratio is in the range of 0.4 to 0.49 below the water table. If the SASW interpreter had had knowledge of the depth to groundwater, he would have chosen a higher value of Poisson's ratio and would have achieved better agreement with the borehole seismic results. This indicates the value of considering all available data when making SASW interpretations relative to "blind" interpretations.

At sites where v_s increases gradually with depth, the v_s increase may be difficult to interpret, making the profile less reliable. Depending on the profiles should be accurate. In this case, layer boundaries are somewhat arbitrary, but the trend of increasing v_s with depth is well defined. The v_s profile is fairly well resolved to a depth of one-half to one-third or the maximum wavelength in the dispersion curve.

SASW measurements from sites with a sudden large v_s increase may be difficult to interpret, making the profile less reliable. Depending on the velocity contrast, the profile may only be resolved to one-fifth the maximum wavelength in the dispersion curve or less.

Brown et al. (2000) present further discussion of the studies presented by Brown (1998) and focus primarily on the results obtained at one site, the Rinaldi Receiving Station, as a typical and uncomplicated example of the nine study sites .

Based on their interpretation of the SASW data and subsequent comparison with the other available data (downhole seismic and suspension seismic at Rinaldi), the authors concluded that:

- The shear-wave velocity profiles from the downhole seismic and SASW methods compare well in general.
- In many situations the SASW can provide profiles suitable for site response predictions.
- SASW measurements are inherently different than borehole measurements as they involve a much larger volume of material. Lateral variations and non-homogeneities in

¹³ Note: However, when collecting the near-surface SASW data, the source and receivers are closer together and therefore sample a smaller volume of material. Thus, the SASW data at shallow depths may not be representative of the average or global properties of the site, so data for shallow depths should be collected at several locations.

¹⁴ The potential for refraction along a nonlinear travel path would be particularly great near the surface where the geophone depth is less than the source offset from the borehole, as well as at sites with non-horizontal velocity layering, as could result from faults with vertical offset and dipping beds.

the materials may cause differences in the shear-wave velocity profiles interpreted from the two methods.

In summary, the various seismic geophysical methods appear to provide good agreement in many cases. However, even when practiced at the same location, each method is measuring properties of a different volume of soil and in a different manner. Thus, the resulting velocity profiles may be different, but it is not evident that one of these profiles may be "correct" while the others are "incorrect".

Laboratory tests are generally used to obtain the modulus reduction and damping ratio curves, but the low-strain shear modulus is taken from in-situ measurements. In cases where the in-situ material is a fill that has not yet been constructed, in-situ measurements are not possible and the results of laboratory tests on laboratory-compacted samples must be used. However, v_s and G_{max} are affected very significantly by factors such as aging, which may not be properly represented in laboratory-compacted samples.

6.7.2 Comparison of Shear-Wave Velocities from Borehole Seismic Methods

The traditional method of comparing several shear-wave velocity profiles (v_s as a function of depth) is to plot the profiles on a common graph and make a visual comparison. For this purpose, the downhole and SASW profiles are the interpreted average layer velocities, and for suspension, the interpreted interval velocities. This type of comparison between downhole and suspension shear-wave velocities is made on Figures VII-1 to VII-16. This comparison method may be appropriate if the absolute values of velocity over a particular range of depth are important. The drawback to this method is that the comparison is often subjective and qualitative. Where velocity is high, absolute differences in velocity may stand out, while larger relative differences in lower velocity layers near the surface may not stand out. Further, the suspension velocity measured over a short interval may be highly variable and difficult to visually compare with averaged velocities from downhole or SASW surveys.

In terms of site response to ground motion, travel time is a more fundamental parameter than is velocity. Travel time can be calculated by (Brown 1998, equation 3.1 on page 39):

$$tt_s(z) = \sum_1^j \frac{h_i}{v_{s,i}} \quad (\text{Eq. 40})$$

where $tt_s(z)$ is the shear-wave travel time to depth z below ground surface; h_i is the thickness of the i^{th} layer, where layers range from 1 at the surface to j at depth z ; and $v_{s,i}$ is the shear-wave velocity of the i^{th} layer (for the bottom layer, layer j , only the part of the layer above depth z is considered in determining h_j). For SASW velocity profiles, the above equation is used. For suspension, the travel times from individual measurements must be accumulated with depth. In addition, the travel time from the ground surface to the shallowest measurement must be assigned arbitrarily. For downhole surveys, travel times have been interpreted from the measured data and subsequently further interpreted to yield a velocity profile. Either the interpreted travel times or the interpreted velocity profiles could be used: in this report, the interpreted velocity profile is used as the basis for comparisons because these are the

interpretations that would actually be used in ground motion analyses. Plots of accumulated shear-wave travel time versus depth are shown on Figures VIII-1 to VIII-16.

A plot of \bar{v}_s , the average shear-wave velocity from the ground surface to a given depth z , also emphasizes differences in travel times between two profiles. Equation 41 (Brown 1998, equation 3.2 on page 40) can be used to calculate \bar{v}_s :

$$\bar{v}_s = \frac{z}{tt_s(z)} \quad (\text{Eq. 41})$$

where $tt_s(z)$ is as defined by Eq. 40. The information contained in the travel time versus depth and \bar{v}_s versus depth plots is similar. Plots of \bar{v}_s versus depth for the deeper profiles are presented on Figures VIII-17a through VIII-23a.

Although the \bar{v}_s versus depth comparison provides a better understanding of the potential effect of alternative profiles on a ground motion analysis, its interpretation is still subjective. A better understanding can be achieved by the quarter-wavelength amplification ratio (Boore and Brown 1998). This technique derives from the quarter-wavelength amplification approximation introduced by Joyner et al. (1981, pages 1346-1347). The quarter-wavelength amplification approximation states that, for a particular frequency, the amplification, A , of shear waves propagating vertically towards the surface can be approximated by the square root of the ratio of the seismic impedance (product of shear-wave velocity and density) averaged over a depth corresponding to a quarter wavelength and the seismic impedance at the depth of the source. The approximation is relatively insensitive to discontinuities in seismic velocity and does not produce the peaks and valleys resulting from the interference of reflected waves. Thus, a smoothed amplification function is obtained. Then, the quarter-wavelength amplification ratio, A_2/A_{dh} , is the ratio of the quarter-wavelength amplifications for two different velocity profiles, and is calculated by Eq. 42 (Brown 1998, equation 3.6 on page 42):

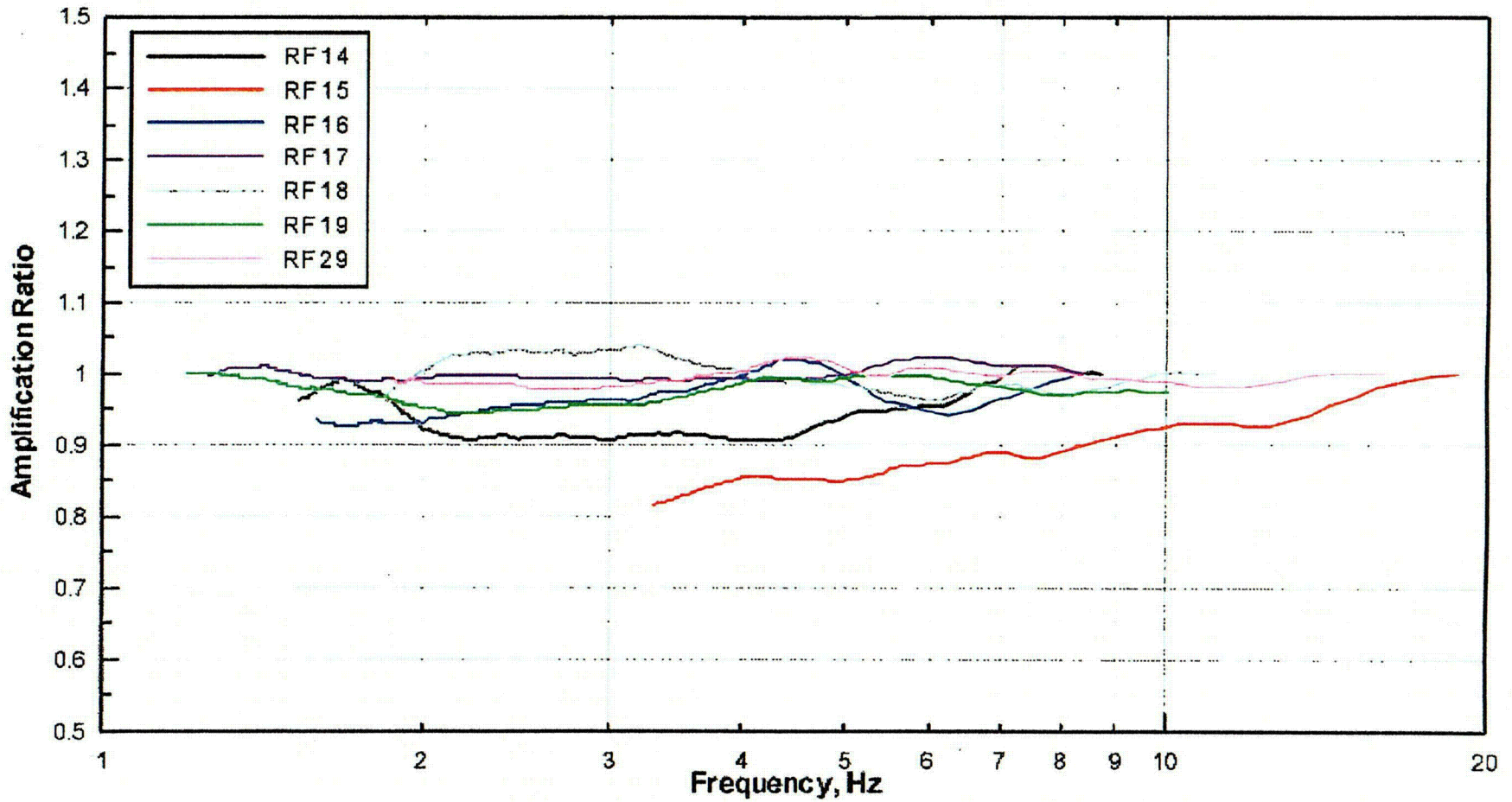
$$\frac{A_2}{A_{dh}} = \sqrt{\frac{\bar{v}_{s,dh}}{\bar{v}_{s,2}}} \quad (\text{Eq. 42})$$

where the subscript 2 represents an alternative velocity profile and the subscript dh represents the reference profile, which, in this report, is always taken as the downhole velocity profile. As implied by earlier discussion, calculation of the quarter-wavelength amplification ratio for suspension results requires making an assumption (Assumption 5 in Section 5) about the part of the profile above the shallowest data. In this report, the suspension profile is assumed to be the same as the downhole profile at shallow depths where there are no suspension data. This assumption causes the ratio to equal unity at the highest frequency (shallowest depth). Plots of amplification ratio versus depth for the deeper profiles are presented on Figures VIII-17b through VIII-23b. Figure 234 presents all the suspension to downhole profile comparisons on a single figure. The remainder of this section provides some comments about these various comparative figures.

Velocity is used frequently in this section, and abbreviations are adopted as follows:

- v_s is shear-wave velocity
- v_p is compression-wave velocity
- v_{sdh} , v_{pdh} are downhole seismic shear-wave velocity and compression-wave velocity
- v_{sRR} , v_{pRR} are suspension seismic (based on receiver-to-receiver data) shear-wave velocity and compression-wave velocity
- v_{sSR} , v_{pSR} are suspension seismic (based on source-to-receiver data) shear-wave velocity and compression-wave velocity

Borehole RF#13 was advanced in 1998 using compressed air as the drilling fluid to lift drill cuttings from the borehole. Observations of borehole wall conditions made in that borehole led to the decision to advance boreholes RF#14 to RF#29 using other methods (rotary wash and diamond core barrel). These same conditions may have had some impact on the suspension seismic measurements and so are summarized here.



DTN: MO0205SWDQRTWF.000

NOTE: Method based on Quarter-Wavelength Amplification Ratio (Joyner, et. al., 1981, pp. 1346-1347, Brown 1998, pp. 41-42)

Figure 234. Amplification Ratio Comparing Shear-Wave Velocity from Downhole and Suspension Logging Surveys

C14

A downhole video camera was used to record borehole conditions after the borehole had been advanced to a depth of approximately 185 feet bgs (YMP 1998). The recording made in the portion of the boring below the surface casing (i.e., from 95 to 185 feet bgs) showed an enlarged hole immediately below the surface casing (from approximately 95 to 97 feet bgs) of as much as three to four times the 6¼-inch nominal drill bit diameter and is consistent with an observed abnormally high grout volume used in that interval to backfill the annular space between the casing and borehole wall. Additional zones of erosion were observed from 118 to 121, 134 to 159, 166 to 173, and 184 to 185 feet bgs. Much of the borehole wall did not appear to have a smooth surface; rather, coarse particles (gravel?) could be observed protruding out of the borehole wall. These observations were key to the decision to advance later boreholes using water as the drilling fluid.

As mentioned above, the video log was made when the borehole had been advanced to a depth of approximately 185 feet bgs. After the video log was made, the borehole was advanced to a total depth of 350 feet bgs. In view of the nature of materials and operation, it is likely that additional erosion of the borehole walls occurred in the interval that was video-logged after the video logging had been completed. Erosion may also have occurred below a depth of 185 feet bgs, but there is no video log of this deeper interval.

Because of the enlargement of the borehole due to erosion by compressed air, when the PVC casing was grouted in place for use in taking downhole seismic and suspension seismic measurements, either a larger annulus of grout was created or voids were left between the casing and the surrounding tuff, or both. Either of these possible conditions can affect the suspension seismic measurements at the borehole, but should have little effect on the downhole seismic or SASW measurements.

The suspension seismic method measures the waves that travel from the source through the material in close proximity to the borehole wall to the two closely spaced receivers (Figure 29). Under normal conditions, the grout annulus surrounding the casing is too thin to act as a wave carrier that affects the velocities. However, if the grout annulus is sufficiently large, the waves may be transmitted through grout, which may have a higher or lower shear-wave velocity than the native bedrock, in which case the observed arrival time would not be correct. The grout used to fill the annulus around the casing likely had a higher shear-wave velocity than the material at the borehole site above about 245 feet bgs.

A suspension seismic measurement is more affected than a downhole seismic measurement by the thickness of the grout-filled annulus between the casing and the borehole wall. Because of the close spacing of suspension receivers, the measured shear wave necessarily travels parallel to and relatively close to the boring. Depending on the wavelength, a thin grouted zone should be transparent to the shear waves. However, thicker grout zones could act as wave-guides, resulting in the measurement of the shear-wave velocity of the grout rather than that of the rock. Downhole measurements are not as affected by the thicker grout zones because most of the waves' travelpaths before arriving at the receiver is within the in-situ subsurface material.

Figure VII-1 indicates that the suspension shear-wave velocity profile in borehole RF#13 generally agrees with the downhole shear-wave velocity profile, except for the interval between about 100 feet and 140 feet bgs, approximately corresponding to the tuff unit "x" (Tpki). The

difference at this interval is likely due to the effects of erosion of the borehole walls (by the compressed air used to lift drill cuttings from the borehole) on the suspension seismic measurements.

As expected, the suspension shear-wave interval velocities plotted on Figure VII-1 indicate considerably more variation than does the downhole profile due to the shorter suspension sampling length (1 meter). For the purposes of ground motion analysis, these localized variations from the trend value do not appear to be significant. Based on the average suspension velocities derived from the accumulated time curve and shown on Figure VII-1, the suspension average velocities are about 10 to 15 percent greater than the downhole velocities to about 250 feet bgs. However, the suspension shear-wave interval velocities are clearly higher than the downhole average velocity between about 100 and 140 feet, where the downhole seismic is judged to better reflect the shear-wave velocity of the rock materials. Below about 250 feet bgs the receiver-to-receiver average shear-wave velocity (v_{sRR}) agrees well with the shear-wave velocity profiles from the 1998 and 2000-1 downhole surveys, while the shear-wave velocity from the 2000-2 downhole survey is about 10 percent higher than the v_{sRR} . The SASW-1 profile agrees well with the downhole seismic surveys and the suspension seismic survey at shallow depths, but yields a much higher velocity below 69 feet bgs.

Figure VIII-1 shows that the downhole shear-wave travel times from the 2000-1 survey are unchanged from 265 to 275 feet and increase at an abnormally low rate from 275 to 290 feet. The downhole travel times appear to indicate that the travel path in the downhole survey is not a simple straight line path from source to receiver; thus, the suspension and downhole methods may be measuring the velocities of different rock, which could explain why the velocities are somewhat different. Figure VIII-1 indicates remarkable agreement between the three downhole v_p surveys, both in general and in detail. Of the three v_s surveys, the 1998 and 2000-1 surveys agree well except between 265 and 315 feet, where the 2000-1 data show some unusual travel times, which differ from the 1998 survey. The 2000-2 v_s survey shows faster travel times than the 1998 and 2000-1 v_s surveys, but agrees very well with the suspension v_s survey down to about 215 feet. At that depth, the 2000-2 downhole v_s survey shows an unusual decrease in travel time and, below that depth, shows a value of v_s that is almost identical to the velocity interpreted below 246 feet in the 1998 survey.

At borehole RF#14 (Figure VII-2), the suspension v_s are somewhat higher than the v_{sdh} to a depth of about 305 feet. Below that depth, a single average value of v_{sdh} was interpreted, while the suspension survey indicates the existence of four source-to-receiver and five receiver-to-receiver intervals of vastly different v_s . As shown on Figure VIII-2, the downhole shear-wave travel times are unusual from about 335 to 340 feet bgs. Two values of travel time were interpreted at depths of 335 and 340 feet, and a gap of 13 ms separates the record above and below 335/340 feet (Section 6.2.5). Because this gap was ignored in developing the downhole v_s profile, the suspension profile agrees better with the downhole profile than with the actual downhole data.

Figure VIII-17a shows that the average v_s from the downhole and suspension methods does not agree very well above 380 feet bgs in borehole RF#14, but the two methods agree well below 380 feet. This figure also shows that the average v_s from the downhole profile agrees well with

the actual downhole travel times down to 335 feet, but poorly below that depth. This finding was expected due to the unusual offset in the travel times discussed above.

Figure VIII-17b shows that the amplification expected at borehole RF#14 from the suspension profile is less than or approximately the same as the amplification expected from the downhole profile. Also, the amplification expected from the actual downhole travel times is greater than the amplification expected from the downhole profile at low frequencies.

Figure VII-18 shows that the v_{pRR} , v_{pSR} at borehole RF#14 are higher than v_{pdh} from about 50 to 220 feet and from about 440 to 520 feet, and are somewhat lower from about 220 to 330 feet and from 380 to 420 feet. However, a major difference in the v_{pSR} and the v_{pdh} values occurs between about 332 and 381 feet, where the suspension data indicates a major reduction in the v_{pSR} in the Tiva Canyon Tuff crystal-poor upper lithophysal zone (Tpcpul) unit. Sheet 3 of the log of borehole RF#14 (Attachment I) indicates that there are zones of nonwelded fracture fill from 334 to 359 feet and from 369 to 395 feet; these zones are described as reworked and variously bedded clay/silt sized tuffaceous material. Based on this description, the material traversed by the borehole is more of a soil than a rock; consequently, it is expected that the velocity would be lower compared to depth intervals where competent Tpcpul was encountered. However, this does not imply that the downhole data needs to be reinterpreted because the seismic waves undoubtedly reached the geophone emplacement by traveling a nonlinear path through solid rock over most of their path and only briefly crossing through the fracture fill. The suspension seismic waves, on the other hand, travel a relatively short distance from source to receivers and have less potential for "straying" from the material immediately adjacent to the borehole walls.

At borehole RF#15 (Figure VII-3), the suspension v_s are somewhat higher than the v_{sdh} . Figure VIII-18a shows that the average v_s from the suspension survey is greater than that from the downhole profile at all depths, while the average v_s from nearby SASW survey 10+37 is greater than that from the downhole profile at depths greater than about 45 feet, but less at shallower depths. As a result, the amplification expected from the SASW profile is greater than that expected from the downhole profile at frequencies greater than about 11 Hz, and less at smaller frequencies (Figure VIII-18b).

Figure VII-19 shows that the v_{pRR} and v_{pSR} at borehole RF#15 are higher than the v_{pdh} to a depth of about 133 feet and are somewhat lower below that depth.

At borehole RF#16 (Figure VII-4), the suspension v_s are somewhat higher than the v_{sdh} to a depth of about 376 feet. Below that depth, the downhole travel times exhibit a marked increase in slope (Figure VIII-4), indicating a higher shear-wave velocity, whereas the suspension travel times show little change in trend. The trend of compression-wave travel times below 376 feet is about the same as above 376 feet for both suspension and downhole surveys (Figure VIII-4). The v_p/v_s ratio from the downhole interpretation implies that Poisson's ratio is near zero. Below 376 feet, the suspension interpretation appears more credible than the downhole interpretation. The suspension v_p are somewhat higher than the v_{pdh} .

Figure VIII-19a shows that the average v_s from the suspension survey in borehole RF#16 is greater than that from the downhole profile at depths greater than about 110 feet. The

amplification expected from the suspension profile is somewhat less than that expected from the downhole profile (Figure VIII-19b).

Figure VII-20 shows that the v_{pRR} and v_{pSR} at borehole RF#16 are higher than the v_{pdh} from about 30 to 280 feet bgs, are nearly identical from about 280 to 376 feet bgs and are significantly lower below about 376 feet bgs. As shown on Figure VII-36, the Poisson's ratio from the downhole interpretation is only about 0.02 below a depth of about 376 feet, while the Poisson's ratio values from the suspension survey have values of about 0.25 to 0.28, which are more typical for the rock at the site.

At borehole RF#17 (Figure VII-5), the suspension and downhole v_s agree well at all depths. Figure VIII-20a shows that the average v_s values from the suspension survey are nearly identical to those from the downhole profile and, as a result, the amplification ratio is nearly equal to one (Figure VIII-20b). The average v_s values from nearby SASW survey 34+36 are quite different from the downhole and suspension profiles at all depths. As a result, the amplification expected from the SASW profile is less than that expected from the downhole profile at frequencies above approximately 4.7 Hz and greater at lower frequencies (Figure VIII-19b).

Figure VII-21 shows that v_{pSR} at borehole RF#17 are higher than v_{pdh} from about 55 to 400 feet bgs, though only slightly so from about 100 to 280 feet bgs. The v_{pSR} and v_{pdh} are nearly identical from about 400 to 500 feet bgs. From about 500 to 620 feet bgs, v_{pdh} are higher than v_{pSR} , though only slightly so below about 560 feet.

At borehole RF#18 (Figure VII-6), the suspension and downhole v_s agree well except from 170 to 220 feet and below 350 feet. In the interval from 170 to 220 feet the layer of lower v_s rock detected in the suspension survey was not interpreted from the downhole data. Below 350 feet the suspension interval v_s (Figure VII-6) is highly variable, as are the downhole travel times (Figure VIII-6). The shear-wave travel times on Figure VIII-6 indicate better agreement between the downhole and suspension than does Figure VII-6. The average v_s shown on Figure VIII-21a indicates excellent agreement above about 170 feet bgs, and fair agreement below that. The amplification ratio (Figure VIII-21b) is close to unity. If Figure VIII-21b were based on the actual downhole travel times rather than the downhole profile, the agreement would likely be even better. At this borehole, the basic data agrees very well, but the profiles have been developed somewhat differently, and accentuate differences.

As for the compression wave data in borehole RF#18, Figure VIII-6 indicates that the compression-wave travel time in the downhole survey becomes progressively greater than that in the suspension survey. This is reflected on Figure VII-22 by v_{pSR} that are significantly higher than v_{pdh} .

At borehole RF#19 (Figure VII-7), the suspension and downhole v_s agree well at all depths. The downhole v_s is somewhat less than the suspension v_s from about 105 to 282 feet, but is somewhat greater from about 282 to 550 feet. This leads to the divergence in the average v_s curves on Figure VIII-22a between about 130 and 575 feet. However, the amplification ratio is close to unity.

The average v_s values from nearby SASW survey 34+36 are quite different from the downhole profile at borehole RF#19 at depths above about 210 feet, though they agree well below that depth. As a result, the amplification expected from the SASW profile is less than that expected from the downhole profile at frequencies above approximately 3 Hz and is about the same at lower frequencies (Figure VIII-22b).

As for the compression wave data at borehole RF#19, Figure VIII-7 indicates that the compression-wave travel time in the downhole survey becomes progressively greater than that in the suspension survey. This is reflected on Figure VII-23 by v_{pSR} that are somewhat to significantly higher than v_{pdh} at all depths below about 95 feet.

At borehole RF#20 (Figure VII-8), the suspension v_s are about 10 to 20 percent higher than the v_{sdh} .

As for the compression wave data at borehole RF#20, Figure VIII-8 indicates that the compression-wave travel time in the downhole survey becomes progressively greater than that in the suspension survey. This is reflected on Figure VII-24 by v_{pSR} that are somewhat higher than v_{pdh} at all depths.

At borehole RF#21 (Figure VII-9), the suspension and downhole v_s agree well at all depths except from about 84 to 118 feet. Between 90 and 110 feet, the downhole shear-wave travel times (Figure VIII-9) form an unusual pattern that make the downhole difficult to interpret. The same pattern does not repeat itself in the downhole compression-wave travel times. Thus, in the interval from 84 to 118 feet, the suspension interpretation appears more credible than the downhole interpretation.

Figure VII-25 shows that v_{pSR} at borehole RF#21 are higher than v_{pdh} from about 20 to 91 feet. The v_{pSR} and v_{pdh} are nearly identical from about 91 to 116 feet bgs and from about 120 to 183 feet bgs.

At borehole RF#22 (Figure VII-10), the suspension and downhole v_s agree well at all depths where data are available for both methods. Figures VIII-10 and VII-26 indicate that the v_{pSR} at borehole RF#21 are somewhat higher than v_{pdh} .

At borehole RF#23 (Figure VII-11), the suspension v_s are about 30 percent lower than the v_{sdh} from 20 to about 54 feet bgs, and about 20 higher from 120 to 150 feet. The methods agree well from 9 to 21 feet and from 70 to 110 feet bgs. Some of the discrepancy between the methods can be explained by the differences in layer interface depths that the investigators selected as part of their interpretation.

Figure VIII-11 indicates that the suspension and downhole compression-wave travel times at borehole RF#23 are fairly similar down to about 120 feet and below 120 feet the suspension travel times are faster than the downhole travel times. However, an unusual time offset occurs in the downhole record between 12 and 15 feet bgs. Figure VII-27 does not appear to reflect the similarities in travel times above about 70 feet bgs, probably due to differences in where the velocity layers were picked by the different investigators. This is probably also due in part to the time jump in the downhole travel times that occurs between the measurements at 12 and 15 feet bgs.

At borehole RF#24 (Figure VII-12), the suspension v_s are generally higher than (often near double) the v_{sdh} at all depths where suspension data is available. The suspension interval velocities indicate that v_s is highly variable from 25 feet to 260 feet, while the downhole travel times on Figure VIII-12 indicate that v_s is relatively uniform in this interval, though there is significant scatter about the trendline. The downhole and suspension shear-wave travel times on Figure VIII-12 diverge markedly while the compression wave travel times agree rather well.

Figure VIII-12 indicates that the suspension and downhole compression wave travel times at borehole RF#24 are fairly similar overall, but that the suspension times exhibit more variation from a constant slope (constant velocity). Figure VII-28 reflects this situation in that a single downhole velocity has been assigned to the rock below about 30 feet bgs, while several layer velocities have been assigned to the suspension results.

At borehole RF#25 (Figure VII-13), the suspension and downhole v_s agree well at all depths where data is available for both methods. Figures VIII-13 and VII-29 indicate that the v_{pdh} are generally higher than the v_{pSR} and v_{pRR} .

At borehole RF#26 (Figure VII-14), the suspension and downhole v_s agree well at all depths where data is available for both methods, though there is some variation in selection of the number of velocity layers and thus in layer interface depths.

Figure VIII-14 indicates that the suspension and downhole compression-wave travel times at borehole RF#26 are fairly similar overall. Figure VII-30 reflects this situation in that the v_{pdh} are sometimes higher and sometimes lower than the v_{pSR} and v_{pRR} .

At borehole RF#28 (Figure VII-15), the suspension and downhole v_s are difficult to compare due to differences in layer interface depths. The shear-wave travel times on Figure VIII-15 suggest that the two sets of data agree well. As for the v_p , a meaningful comparison on Figure VII-31 is hampered by the differences in velocity-layer boundaries. The small divergence in the compression-wave travel times on Figure VIII-15 indicates that the v_{pSR} and v_{pRR} are slightly higher than the v_{pdh} .

At borehole RF#29 (Figure VII-16), the suspension and downhole v_s agree well except from about 120 to 138 feet bgs, although v_{sSR} and v_{sRR} are about 10 percent higher than the v_{sdh} from about 138 to 230 feet bgs. The downhole shear-wave travel times shown on Figure VIII-16 are somewhat nonlinear from about 105 to 130 feet, making it possible to make alternative interpretations, which might yield better agreement between the downhole and the suspension v_s in the interval from 120 to 138 feet. The downhole shear-wave travel times on Figure VIII-16 show some unusual travel time changes from about 340 feet to the measurement at 405 feet, which coincide with a "cycle" of extreme variation of the suspension seismic shear-wave interval velocities over the same depth interval, as shown on Figure VII-16.

Figure VIII-16 indicates that the shear-wave travel times for the downhole and suspension surveys agree well, while Figure VIII-23a indicates that the average v_s for both methods are fairly close at all depths. As a result, the amplification ratio is close to unity (Figure VIII-23b).

The steady and significant divergence in the compression-wave travel times on Figure VIII-16 indicates that the v_{pSR} are higher than the v_{pdh} at borehole RF#29. This is reflected on

Figure VII-32 by higher v_{pSR} than v_{pDH} at all depths except from about 75 to 127 feet bgs, where the difference is only slight.

The agreement between downhole and suspension results at individual boreholes is sometimes very good and sometimes only fair. The reasons for this variable agreement can probably be attributed to geologic conditions, although a detailed analysis of the correlation of velocity to geologic conditions has not been undertaken. Some of the geologic factors that may be influential include:

- As discussed in Section 6.2.2, several zones of “fracture fill material” were identified in some of the cored boreholes. These fractures are believed to be vertical and have been infilled with detrital volcanic material consisting primarily of clay and fine-grained sediment. Due to the short measurement interval and the limited potential for refraction, in the suspension method, the typically low density, non-cemented clayey fill could result in spurious suspension velocity values in what is otherwise high-velocity rock. The velocities from the downhole and SASW methods, which involve much longer travel paths and have much greater potential for refraction, would not be greatly affected by the fractures.
- As discussed in Section 6.2.2, the densely welded pyroclastic flows of Yucca Mountain contain zones within the flows that are characterized by having an abundance of lithophysae. Lithophysal zones occur where vapor concentrates in the densely welded part of ignimbrites to form lithophysal cavities. The WHB drilling encountered the upper and lower lithophysal zone of the Tiva Canyon Tuff (Tpcpul and Tpcpll respectively). As noted, grout can fill in these voids during casing installation. The grout may have greater or lesser velocity than the surrounding rock. Due to the short measurement interval and the limited potential for refraction, in the suspension method, the grout-filled voids could result in spurious suspension velocity values. The velocities from the downhole and SASW methods, which involve much longer travel paths and have much greater potential for refraction, would not be greatly affected by the grout-filled voids located only adjacent to the borehole.

It can also be observed that some of the differences in velocities obtained from the different methods could be reduced by considering alternative interpretations, that is, selecting different layer boundaries than have been reported here in recognition of what information can be obtained by considering information external to that furnished by the individual seismic method alone.

6.8 PREVIOUS DATA

6.8.1 Overview

In addition to previously acquired data discussed above (mainly related to borehole RF#13 and general geologic data), there are additional geotechnical data that may be useful to the current objectives. These include the results of qualified geotechnical laboratory tests performed on core specimens from boreholes UE-25 NRG#2, UE-25 NRG#2a, UE-25 NRG#2b, UE-25 NRG#3,

USW NRG-6, USW NRG-7/7a, USW SD-9 and USW SD-12¹⁵ (discussed in Section 6.8.2) and a few in-place and laboratory measurements of the density of alluvium (discussed in Section 6.8.3).

6.8.2 Previous Geotechnical Testing on Core Samples

CRWMS M&O (1997, Section 5.1) presented a statistical summary of physical and mechanical properties of bedrock for the YMP. A similar analysis was performed for this scientific analysis because (1) some of the lithostratigraphic contacts changed since the previous analysis was performed, (2) the previous statistical summary had no data tracking number associated with it, and (3) the details of statistical analysis could not be traced to source information.

Table 33 summarizes the depth at which the tops of the lithostratigraphic zones or subzones of interest were encountered in boreholes NRG#2, NRG#2a, NRG#2b, NRG#3, NRG-6, NRG-7a, SD-9 and SD-12. Only Tpbt4 and younger units have been considered because the older units are located at depths beyond those investigated for this report.

Table 34 summarizes statistical values of dry density, saturated density, particle density and porosity derived from the laboratory data in DTNs: SNL01A05059301.005 and SNL02030193001.001 through SNL02030193001.027, excluding SNL02030193001.025 (superseded). The total densities and water contents of the specimens were not measured and are unknown. The porosity values represent the total porosity, n , defined by:

$$n = \frac{\rho_s - \rho_d}{\rho_s} \quad (\text{Eq. 43})$$

where: ρ_s = grain density (i.e., the density of the solid particles in the soil or rock mass)
 ρ_d = dry density.

Table 35 shows values of porosity, void ratio, and saturation water content that were calculated from the mean values of specific gravity and dry density values in Table 34. Void ratio equals the ratio of the porosity to the quantity one minus the porosity. Saturation water content is the water content when the rock is saturated, which equals the ratio of the void ratio to the specific gravity. Note that the values of porosity computed from the mean values are slightly different than the mean of the reported porosity values given in Table 34. This may be due to not having a particle density value for every dry density value.

The magnitude of the saturation water content, as well as the difference between the values of dry density and saturated density, indicates that a wide range of values of total density is possible for tuff unit "x" (Tpki), the bedded tuffs (Tmbt1 and Tpbt4), and the nonwelded to partially welded Tpcpv1 subzone. The smaller values of saturation water content for the welded zones of the Tiva Canyon Tuff bedrock limit the range of possible values for water content and total density.

¹⁵ These boreholes will be referred to herein by the abbreviated designations NRG#2, NRG#2a, NRG#2b, NRG#3, NRG-6, NRG-7, SD-9 and SD-12.

DTN: MO9905LABDYNRS.000 reports water content measurements on three specimens of unwelded tuff (Tpki) acquired in borehole RF#13 between 138.3- and 142.0-foot depth; the values range from 3.0 to 3.2 percent (Table 36). Water content measurements on three specimens of welded tuff (Tpcpmn) acquired in borehole RF#13 between 254.6- and 257.3-foot depth

Table 33. Depths in Feet to Tops of Selected Lithostratigraphic Units by Borehole

Lithostratigraphic unit ⁽¹⁾	Symbol	UE-25 NRG#2	UE-25 NRG#2a	UE-25 NRG#2b	UE-25 NRG#3	USW NRG-6	USW NRG-7a	USW SD-9	USW SD-12
Not described	--						0.0	0.0	0.0
alluvium/ colluvium	Qal		0.0	0.0					
Rainier Mesa Tuff	Tmr	0.0		2.2					
pre-Rainier Mesa Tuff bedded tuff	Tmbt1	138.6		119.4					
Tuff unit "x"	Tpki	⁽²⁾	80.6	157.3					
Post-Tiva Canyon Tuff bedded tuff	Tpbt5		151.0	⁽³⁾					
Tiva Canyon Tuff crystal rich, vitric, non to partially welded	Tpcrv3		165.9						
Tiva Canyon Tuff crystal rich vitric, moderately welded subzone	Tpcrv2		168.0						
Tiva Canyon Tuff crystal rich, vitric, vitrophyre subzone	Tpcrv1		170.2						
Tiva Canyon Tuff crystal rich, nonlithophysal	Tpcrn		172.0		0.0				
Tiva Canyon Tuff crystal poor upper lithophysal	Tpcpul		261.5		100.0				
Tiva Canyon Tuff crystal poor middle nonlithophysal	Tpcpmn				206.7				5.3
Tiva Canyon Tuff crystal poor lower lithophysal	Tpcpll				268.2	0.0			93.4
Tiva Canyon Tuff crystal poor lower nonlithophysal	Tpcpln	169.8				55.0	17.0	53.6	129.5
Tiva Canyon Tuff, crystal-poor vitric densely welded subzone	Tpcpv3								
Tiva Canyon Tuff crystal-poor vitric moderately welded subzone	Tpcpv2	276.3				135.3	69.7	57.2	239.5
Tiva Canyon Tuff crystal-poor vitric nonwelded to partially welded subzone	Tpcpv1	282.8				151.8	79.2	76.5	256.0
pre-Tiva Canyon Tuff bedded tuff	Tpbt4			265.2		158.6	102.0	91.5	263.7
Total depth of borehole, if borehole terminated above the top of Tpbt4		294	265.7		330.0				

DTNs: GS941108314211.052 for SD-9, GS940908314211.045 for SD-12, GS940708314211.032 for NRG-7a, and GS940308314211.009 for the other boreholes

Notes:

- (1) Units older than Tpbt4 are not shown.
- (2) Bow Ridge Fault Zone penetrated from 164.6-169.8 ft in NRG#2.
- (3) Bow Ridge Fault Zone penetrated from 232.3-265.2 (?) ft in NRG#2b. No Tiva Canyon Tuff below 232.3 ft.
- (4) Shading in cells indicates that the zone was not encountered.

INTENTIONALLY LEFT BLANK

Table 34. Statistics by Lithostratigraphic Unit

Properties	Statistic	Borehole	Lithostratigraphic Unit														
			Tmr	Tmbt1	Tpki	Tpbt5	Tpcrv3	Tpcrn	Tpcpul	Tpcpmn	Tpcpll	Tpcplin	Tpcpv2	Tpcpv1	Tpbt4		
Saturated Density (lbm/ft ³)	Count	NRG#2			13				19				17				
		NRG#2a															
		NRG#2b	8														
		NRG#3							14	9	18	4					
		NRG#6									19	11	4	1			
		NRG#7										14	5	5	2		
		SD-9												1			
		SD-12												9	1		2
	All	8		13				33	9	22	23	51	10	7	4		
	Mean	NRG#2											150.1				
		NRG#2a			103.5												
		NRG#2b	109.0														
		NRG#3							134.3	139.5	147.4	144.8					
		NRG#6										149.8	146.2	118.8	110.5		
		NRG#7											146.0	122.7	112.0	95.5	
		SD-9													111.7		
		SD-12									147.0			150.4	127.2		111.7
	All	109.0		103.5				132.6	139.5	147.3	149.0	148.2	121.6	111.7	103.6		
	Coefficient of Variation	NRG#2											0.40				
		NRG#2a			3.25					5.69							
		NRG#2b	3.58														
NRG#3								4.74	2.76	1.67	3.71						
NRG#6											0.95	1.71	6.13				
NRG#7												2.87	3.05	2.29	3.74		
SD-12										0.62		0.62				6.05	
All		3.58		3.25				5.33	2.76	1.52	2.06	2.18	4.62	1.93	9.96		
Dry Density (lbm/ft ³)	Count	NRG#2		3									17				
		NRG#2a			13												
		NRG#2b	10														
		NRG#3							14	9	18	4					
		NRG#6										19	12	4	2	4	
		NRG#7											14	6	6	2	
		All	10	3	13				33	9	18	23	43	10	8	6	
	Mean	NRG#2		104.9									146.1				
		NRG#2a			76.3												
		NRG#2b	83.3														
		NRG#3							120.6	131.1	142.3	139.2					
		NRG#6										146.5	140.9	101.1	82.7	80.5	
		NRG#7											140.0	105.7	86.6	62.9	
	All	83.3	104.9	76.3				117.8	131.1	142.3	145.2	142.7	103.8	85.6	74.7		
	Coefficient of Variation	NRG#2		3.36									0.62				
		NRG#2a			5.80					11.67							
		NRG#2b	7.88														
		NRG#3							9.01	3.69	2.62	4.25					
		NRG#6										1.36	2.84	14.18	1.60	18.40	
		NRG#7											4.82	5.33	3.54	0.42	
	All	7.88	3.36	5.80				10.61	3.69	2.62	2.76	3.61	9.22	3.73	19.65		

Table 34. Statistics by Lithostratigraphic Unit
(continued)

Properties	Statistic	Borehole	Lithostratigraphic Unit													
			Tmr	Tmbt1	Tpki	Tpbt5	Tpcrv3	Tpcrn	Tpcpul	Tpcpmn	Tpcpll	Tpcpln	Tpcpv2	Tpcpv1	Tpbt4	
Particle Density (lbm/ft ³)	Count	NRG#2		3								17				
		NRG#2a			10	1	1	13								
		NRG#2b	8													
		NRG#3							9	7	7	3				
		NRG#6										5	4	3	1	4
		NRG#7											7	2	3	2
		SD-9												1	4	
		SD-12												1	1	2
	All	8	3	10	1	1	22	7	13	10	40	7	9	8		
	Mean	NRG#2		152.5								157.9				
		NRG#2a			145.6	149.3	149.4	159.9								
		NRG#2b	145.9													
		NRG#3						159.8	157.2	156.9	157.0					
		NRG#6									155.9	155.9	151.9	149.8	152.9	
		NRG#7										155.9	154.2	145.0	149.1	
		SD-9											151.5	148.3		
		SD-12									153.8	155.1	155.7	150.5	143.7	146.9
	All	145.9	152.5	145.6	149.3	149.4	159.8	157.2	155.5	156.1	156.7	152.3	146.9	150.4		
	Coefficient of Variation	NRG#2		0.48								0.25				
		NRG#2a			1.04			1.00								
		NRG#2b	0.86													
		NRG#3						1.14	0.64	0.18	0.40				1.58	
		NRG#6									0.21	0.16	0.60			
		NRG#7										0.39	0.17	1.95	2.72	
SD-9													0.20			
SD-12									0.38	0.28	0.34			0.33		
All	0.86	0.48	1.04			1.03	0.64	1.05	0.53	0.72	0.98	1.76	2.33			
Porosity (%)	Count	NRG#2		3								17				
		NRG#2a			14	2	3	20								
		NRG#2b	10													
		NRG#3						14	9	18	4					
		NRG#6									22	15	6	5		
		NRG#7										12	4	4	2	
		SD-9												1		
		All	10	3	14	2	3	34	9	18	26	44	10	5	7	
	Mean	NRG#2		31.3								7.5				
		NRG#2a			47.4	45.6	30.8	27.5								
		NRG#2b	42.9													
		NRG#3						24.5	16.5	9.2	11.5					
		NRG#6									6.0	9.5	31.5	47.9		
		NRG#7										11.1	32.2	39.1	51.8	
		SD-9												42.5		
		All	42.9	31.3	47.4	45.6	30.8	26.2	16.5	9.2	6.9	9.1	31.8	39.8	49.0	
	Coefficient of Variation	NRG#2		8.13								8.80				
		NRG#2a			5.45	2.02	9.74	32.49								
		NRG#2b	10.10													
		NRG#3						31.04	18.09	26.80	34.28					
		NRG#6									23.95	31.49	32.62	16.98		
		NRG#7										45.62	14.12	4.01	14.47	
		SD-9														
		All	10.10	8.13	5.46	2.02	9.74	32.08	18.09	26.80	40.19	37.75	25.49	5.14	15.42	

DTN: MO0202GEOSOILP.000

Table 35. Porosity, Void Ratio, and Saturation Water Content by Lithostratigraphic Unit

Lithostratigraphic Unit	Saturated Density, lbs/ft ³	Dry Density, lbs/ft ³	Particle Density, lbs/ft ³	Porosity %	Porosity *	Void Ratio *	Saturation Water Content *, %
Tmr	109.0	83.3	145.9	42.9	42.9	75.2	51.5
Tmbt1	-	104.9	152.5	31.3	31.2	45.4	29.8
Tpki	103.5	76.3	145.6	47.4	47.6	90.8	62.4
Tpbt5	-	-	149.3	45.6	-	-	-
Tpcrv3	-	-	149.4	30.8	-	-	-
Tpcrn	132.6	117.8	159.8	26.2	26.3	35.6	22.3
Tpcpul	139.5	131.1	157.2	16.5	16.6	19.9	12.6
Tpcpmn	147.3	142.3	155.5	9.2	8.5	9.2	5.9
Tpcpll	149.0	145.2	156.1	6.9	7.0	7.5	4.8
Tpcplin	148.2	142.7	156.7	9.1	8.9	9.8	6.3
Tpcpv2	121.6	103.8	152.3	31.8	31.8	46.7	30.6
Tpcpv1	111.7	85.6	146.9	39.8	41.7	71.5	48.7
Tpbt4	103.6	74.7	150.4	49.0	50.4	101.5	67.5

DTN: MO0204SEPSOILP.000

* Porosity, n, in percent may be calculated using $n = 100(1 - \gamma_d / \gamma_s)$, where γ_d and γ_s are the mean values of dry density and particle density in Table 34, respectively. Void ratio, e, in percent may be calculated using $e = 100(\gamma_s / \gamma_d - 1)$. Saturation water content, w_{sat} , may be calculated as $w_{sat} = (e / G)$, where G is the specific gravity. Specific gravity equals the particle density divided by the density of water (62.427961 lbm/ft³, density of water under standard conditions was used).

Table 36. Moist and Dry Density Results for Borehole RF#13

Depth feet	Lithostratigraphic Unit	Total Density		Water Content, %	Dry Density	
		lbs/ft ³	g/cm ³		lbs/ft ³	g/cm ³
138.3	tuff unit "x" (Tpki)	80.1	1.28	3.0	77.8	1.25
141.5		79.9	1.28	3.2	77.4	1.24
142.0		79.9	1.28	3.0	77.6	1.24
254.6	middle nonlithophysal zone of the crystal-poor member of the Tiva Canyon Tuff (Tpcpmn)	144.6	2.316	0.5	143.9	2.305
255.5		148.1	2.372	0.4	147.5	2.363
257.3		147.8	2.368	0.5	147.1	2.356

DTN: MO9905LABDYNRS.000. Values given in source in *Système International* units were converted to American units using 1 g/cm³ = 62.428 lbm/ft³.

ranged from 0.4 to 0.5 percent (Table 36) (DTN: MO9905LABDYNRS.000). Unfortunately, the core samples were not stored using specific measures to maintain the field water content. Thus, these values of water content are likely less than the actual values, and the same would be true of the total density values. The same is true for the water content values in Tables 14 through 16.

Figure 235 compares the mean values of total density from the gamma-gamma surveys (Table 12) with those from the RCTS tests (Tables 14, 15, 16 and 36) and from previous laboratory measurements on NRG and SD borehole samples (Table 34). Although the RCTS samples may have lost some moisture, their mean total density exceeds that from the gamma-gamma measurements in the Tiva Canyon Tuff, but is less in the nonwelded tuff unit "x". The differences in the mean values are large in the Tpki and Tpcpul. However, the number of RCTS results (the "count" shown on Figure 235) is too low to provide a reliable mean value. The values of dry and saturated density from the previous NRG and SD boreholes are not directly comparable with the total density for the gamma-gamma or RCTS measurements. However, the total density of a material must be between its dry density and saturated density, so these values should bracket the total density values. However, this relationship seems to hold only for units Tpki and Tpcpmn. It does not seem to be the case for Tpcpll and Tpcpln, and the situation is marginal for Tpcrn and Tpcpul.

At this time, it is reasonable to use the standard deviation values for the dry density measurements in bedrock in Table 33 as an approximation of the variability of the bedrock units.

6.8.3 Alluvium

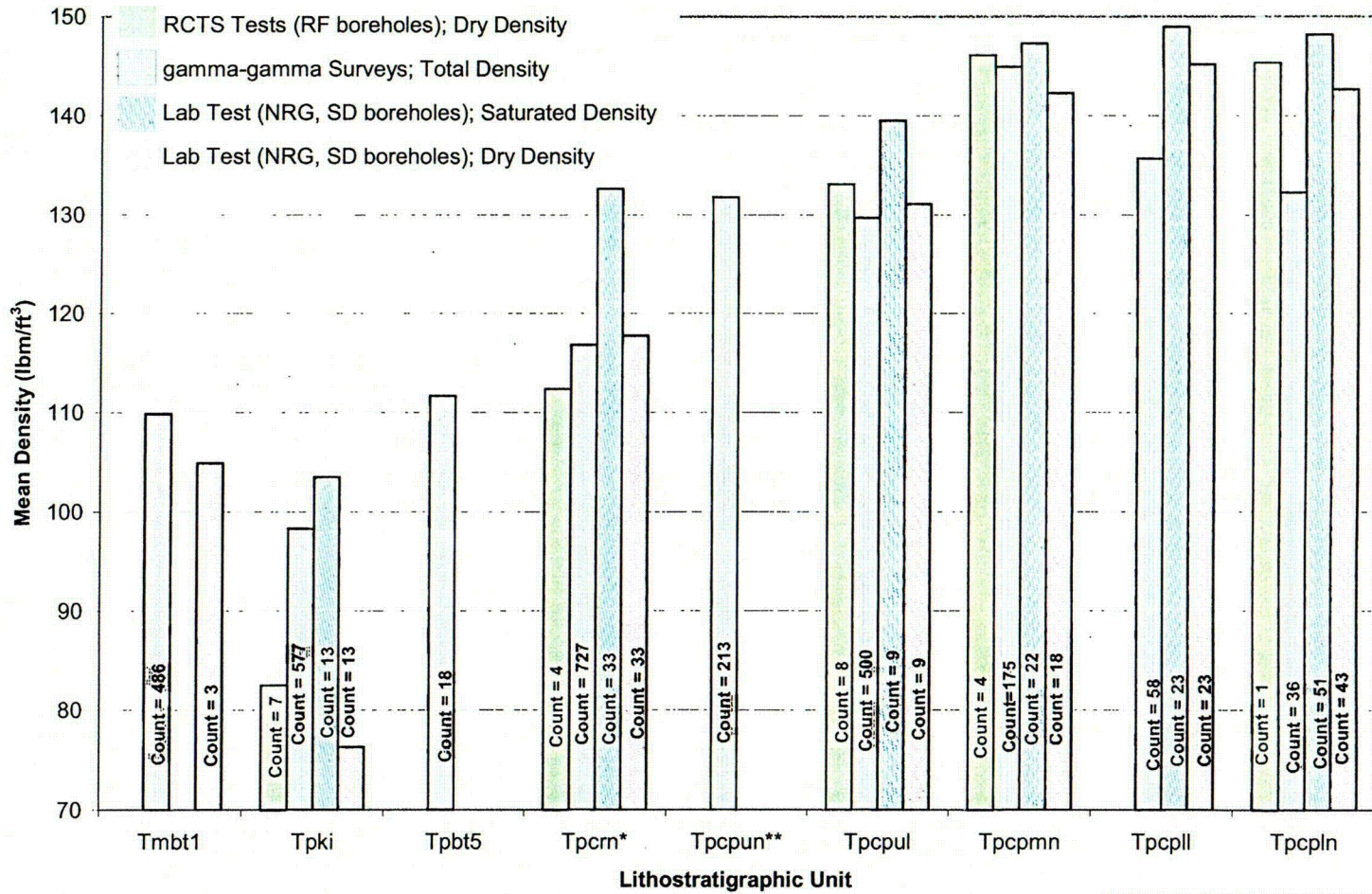
In addition to the in-place density tests performed in alluvium in test pits TP-WHB-1 through -4 (Section 6.2.4), a few other measurements of alluvium density have been made in-situ or in the laboratory by previous investigators. Density of the alluvium/colluvium in the WHB Area was measured by:

- Water replacement tests in alluvium/colluvium (QTac) encountered in some of the NRSF-TP series (also known as the NRG-TP series) of test pits (DTN: GS920983114220.001).
- Laboratory tests on drive-tube samples¹⁶ of alluvium/ colluvium (QTac) from borehole UE-25 RF#3b (DTN: SNSAND85081500.000, Table 3).¹⁷
- Sand-cone and nuclear tests¹⁸ in alluvium encountered in test pit SFS-3 (Ho et al. 1986, pp. 6, 7, 14, 22, and 54).

¹⁶ DTN: SNSAND85081500.000 does not state the dimensions of the drive tube sampler and other details.

¹⁷ One problem with the data should be noted. For the sample from a depth of 22.0 feet, the various values reported in Table 3 of DTN: SNSAND85081500.000 are inconsistent. Based on a review of the data, it appears that the reported values of total density and water content are correct, and the reported value of dry density is incorrect and should be 1.460 g/cm³ or 92.2 lbs/ft³. The reported porosity is also incorrect and should be 41.8 percent.

¹⁸ Ho et al. (1986) do not state the dimensions of the sand cone or the source penetration for the nuclear gage tests.



Note: * Tpcrn includes Tpcrv, Tpcrl and Tpcrm.

** Tpcpun is logged as a subunit in DTN: MO0101SEPBGLOG.000

DTNs: MO0204DENBROCK.000,
MO0202GEOSOLP.000, MO0204SEPGAMDM.000

Figure 235. Comparison of Density from gamma-gamma Surveys, RCTS tests and Previous Laboratory Data

C15

The test pit SFS-3 data reported by Ho et al. (1986) is ambiguous. Dry density and water content results are reported in three places (Ho et al. 1986, pages 14, 22 and 54). The measured total density is never reported. Unfortunately, the dry density is not measured directly, but is calculated using the total density and water content. The values of water content reported on page 22 differ from those reported on pages 14 and 54, although the values of dry density are the same in all cases, which would seem impossible because it implies that the total density (a measured quantity) changes depending on a quantity that is calculated from it. Two possible explanations are: (1) transcription errors were made at some time, or (2) the water content was measured by two different methods. Assuming the latter as the more likely case, it is not known which of the two values was used to compute the dry density, which makes it impossible to know how to compute the total density, which, as mentioned above, is not reported in Ho et al. (1986). For this report, the values on page 14 were arbitrarily used to calculate total density.

Figure 236 shows this previous data and, for comparison, the data presented in Sections 6.2.4 and 6.2.8.

The densities reported for the drive tube samples (DTN: SNSAND85081500.000, Table 3) appear to be significantly lower than the in-situ densities measured at similar depths. It is a common observation that the density of a dense granular material decreases significantly because of sampling, so the discrepancy between laboratory and in-situ densities is in line with expectations (see, for example, Marcuson 1978, p. 338). At best, the laboratory density values can be used as a guide to the trend of densities at depths greater than those at which in-situ tests were performed. Given the coarse nature of the alluvial/colluvial material, the water replacement tests should provide more reliable estimates of density than the sand-cone and nuclear tests because the former involves a much larger volume of material. In addition, the personnel performing the sand-cone and nuclear tests avoided testing coarser soil because of limitations in the methods they used (Ho et al. 1986, p. 6).

It should be emphasized that the number of density values is small, and the data quality is questionable in some cases (preferential sampling of finer-grained materials, driven samples). Consequently, significant variations from the recommended values are possible.

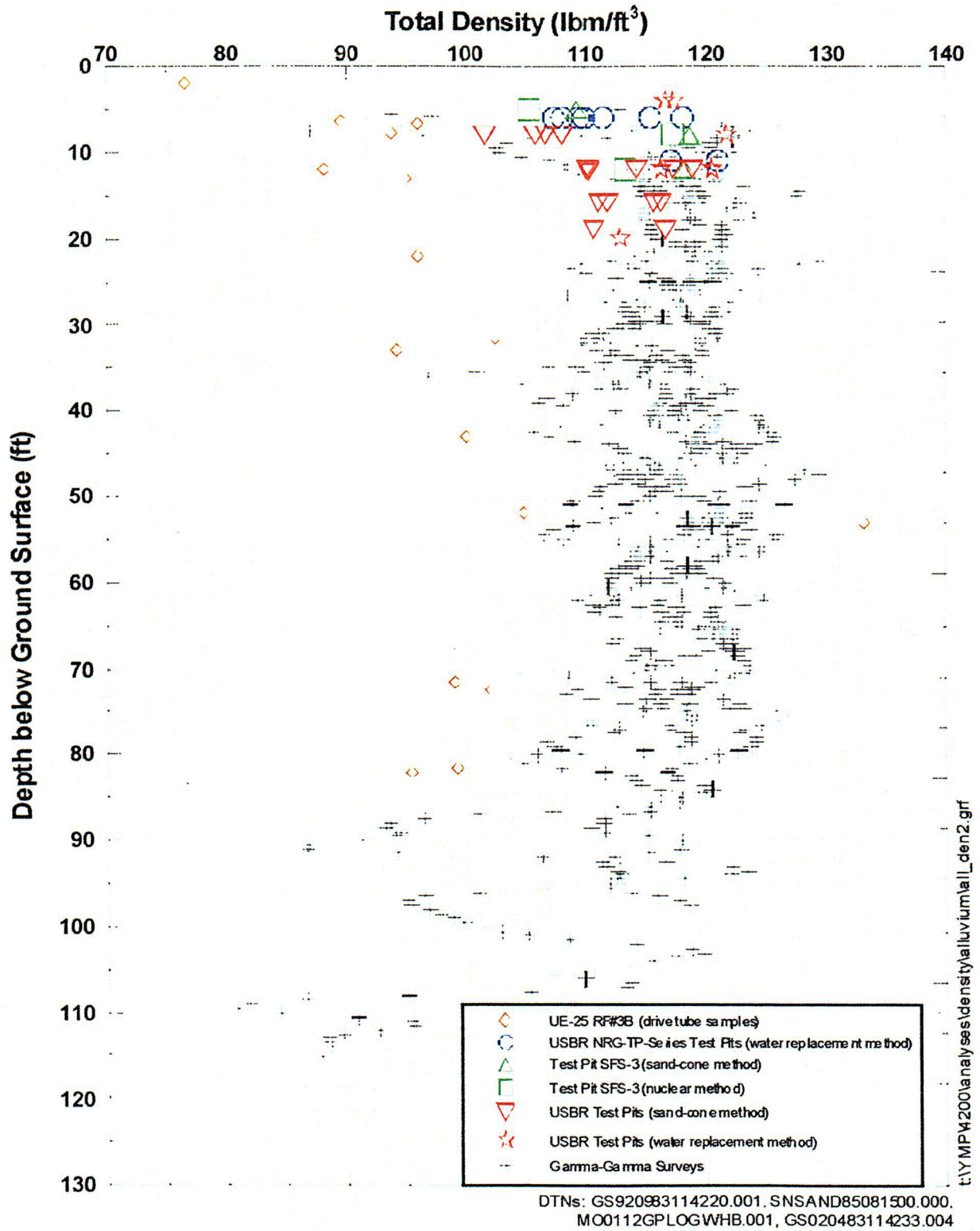


Figure 236. Total Density of Alluvium

7. CONCLUSION

This scientific analysis presents data that were acquired for use in preliminary geotechnical analyses for the WHB foundations and in the development of seismic design input ground motions for the WHB and the repository. The types of data considered herein are shear-wave velocity profile, compression-wave velocity profile, low-strain Poisson's ratio, low-strain shear modulus, modulus reduction, damping ratio, and total density. In addition, basic geotechnical data were acquired for borrow material that could potentially be used to construct an engineered fill pad at the WHB. The interpretations, findings, and recommendations in this scientific analysis supersede any conflicting interpretations, findings, and recommendations presented in CRWMS M&O (1999b).

7.1 SUMMARY

Field and geotechnical laboratory data are presented for three distinct geographic areas:

- The WHB Area
- The North Ramp and Main Drift of the ESF
- The crest of Yucca Mountain.

In addition, geotechnical laboratory data are presented for a composite sample of material from the Fran Ridge Borrow Area.

Data Acquired at the WHB Area

Section 6.2 summarizes the results of the explorations and tests performed in 2000 and 2001 in the WHB Area for the WHB and laboratory tests performed on samples from these explorations. The type of exploration or test and the scientific analysis section where the results are presented are as follows:

- 6.2.2 - Boreholes RF#14 through RF#29
- 6.2.3 - Revision of RF#13 borehole log
- 6.2.4 - Test pits TP-WHB-1 through TP-WHB-4
- 6.2.5 - Downhole seismic surveys in boreholes RF#13 through RF#29
- 6.2.6 - Suspension seismic surveys in boreholes RF#13 through RF#29
- 6.2.7 - SASW surveys SASW-1 through SASW-37 and D-12
- 6.2.8 - Borehole caliper and gamma-gamma in boreholes RF#16, RF#18, RF#20, RF#21, RF#22, RF#24, and RF#28
- 6.2.9 - Geotechnical laboratory static testing
- 6.2.10 - Geotechnical laboratory dynamic testing.

Data Acquired at the North Ramp and Main Drift of the ESF

Section 6.3 summarizes the results of geophysical surveys performed in 2001 along the Main Drift of the ESF and of laboratory tests performed on samples taken along the North Ramp. The type of exploration or test and the scientific analysis section where the results are presented are as follows:

- 6.3.2 - Shear-wave velocity profiles from SASW surveys T-1 to T-5.
- 6.3.3 - RCTS test results for samples of bedrock taken in the ESF North Ramp.

Data Acquired at the Crest of Yucca Mountain

Section 6.4 summarizes the results of the explorations and tests performed in 2000 and 2001 at or near the crest of Yucca Mountain. The type of exploration or test and the scientific analysis section where the results are presented are as follows:

- 6.4.2 - SASW surveys C-1 to C-7, S-1 to S-12, D-1 to D-11, and R-1 to R-3.
- 6.4.3 - Downhole seismic surveys using eight existing boreholes.

Data Acquired for Material from the Fran Ridge Borrow Area

Section 6.5 summarizes the results of geotechnical laboratory tests that were performed in 2000 and 2001 on a composite sample from the Fran Ridge Borrow Area. The type of tests and the scientific analysis section where the results are presented are as follows:

- 6.5.2 - Static tests.
- 6.5.3 - Dynamic tests.

The remainder of Section 6 presents analysis and discussions of the data as follows:

- 6.6 - Interpreted geologic conditions (stratigraphy, structure and groundwater) at the WHB Area.
- 6.7 - Evaluation of seismic velocity data for the WHB Area.
- 6.8 - Comparison with previous data.

7.2 RESTRICTIONS

The data in this report are valid for the specific sites investigated, i.e., the WHB Area shown on Figure 1, the emplacement area shown on Figure 157, and the Fran Ridge Borrow Area shown on Figure 213. The data in this report should be used only for the intended purposes, which were discussed in Section 1, and may not be adequate for other purposes.

7.3 UNCERTAINTIES AND LIMITATIONS

7.3.1 Sufficiency of Geotechnical Data for Fran Ridge Borrow Area

Currently, only four surface samples from the Fran Ridge Borrow Area have been taken, and only the composite of these four samples has been subjected to limited static and dynamic testing. Consequently, there is significant, high uncertainty concerning the materials in this borrow area and their geotechnical properties.

7.3.2 Sufficiency of Seismic Data for Emplacement Area

At the time that the data collection activities in this study were planned and conducted, the proposed emplacement area represented the base case repository layout that was evaluated as

part of site recommendation analyses (DOE 2001, Section 2.3.1.1). More recently, concepts regarding the repository layout have evolved, with the objectives of reducing uncertainties in a License Application and supporting a flexible design with respect to waste types and receipt. The current layout includes additional area to the east and north of the base case layout (Board et al. 2002, Figure 3-1). Thus, the velocity data collected to date does not sample some of these areas. Also, velocity surveys were limited in their depth penetration beneath the crest of Yucca Mountain. Measurements are lacking in the depth range from about 700 to 1000 feet bgs.

7.3.3 Sufficiency of Seismic Data in the WHB Area

With regards to the development of seismic design input ground motions, there are areas within the WHB Area where no velocity measurements have been made. In particular, there are areas outside of the existing pad in the northern part of the WHB Area where no surveys were performed based on environmental restrictions and the likelihood that all structures would be sited in the current pad/muck pile area. The lack of sampling can be adequately accounted for by incorporating a greater degree of variability in the velocity profiles used in the ground motion calculations. This would, however, result in more conservative design ground motions.

7.3.4 Accuracy of Contacts

Each of the lithostratigraphic units in the WHB area has distinctive characteristics that enable identification of the unit and the bounding contacts; therefore, there is very small uncertainty in the identification of lithostratigraphic units. The contacts are formed from depositional, welding, or crystallization processes and can be sharp or gradational. For gradational contacts, even though the features are gradational across 3 to 10 ft, the criteria for identification of the contact typically permits identification within a few feet. In boreholes with core, the accuracy of the contact is typically plus or minus 1 foot; however, where recovery of core is poor, the accuracy of contact identification is increased. In mud rotary boreholes, the accuracy is dependent on the sampling interval and the drilling and sampling techniques. In the WHB mud-rotary boreholes, the sampling interval is 5 ft and the minimum accuracy plus or minus 5 ft. Borehole geophysical logs and the trends in lithostratigraphic thickness can be used in many of the boreholes to help resolve the depth to lithostratigraphic contacts and minimize the uncertainty of the contact to the estimated accuracy of plus or minus 5 ft.

7.3.5 Strike and Dip of Bedding

The strike and dip of the stratigraphic beds were not directly measured in any of the qualified explorations in the WHB Area, but were calculated based on lithostratigraphic contact elevations in various boreholes in areas where it is thought that no fault disrupts the bedding (Section 6.6.2). Based on this approach, the bedding beneath the WHB Area appears to be northeast-striking and southeast-dipping, which is different than the orientation of bedding mapped on Exile Hill near the North Portal, where it tends to strike from N36°W to N8°W and dip from 14 to 22 degrees to the northeast. Therefore, the bedding on Exile Hill is, in general, north to northwest-striking and east to northeast-dipping. Because of the limited number of data sets that could be used to calculate the strike and dip, there is significant, high uncertainty concerning the distribution of strike and dip across the WHB Area. The absence of direct measurements of strike and dip and the discordance with measurements on nearby Exile Hill

introduce uncertainty in the structural interpretation (locations of faults) and the geologic cross sections.

7.3.6 Fault Locations

When the tops of stratigraphic units are connected between boreholes, there were often apparent discrepancies between calculated bedding dip and the dip anticipated on the basis of the assumed strike and dip of bedding. To account for this discrepancy, several faults have been interpreted as crisscrossing the WHB Area. In some cases, a point on the interpreted fault plane and the fault dip are known because the fault was observed in the borehole core; this helps constrain the potential location of the fault. In other cases, the fault was not directly observed, but is only inferred as being somewhere between boreholes. In addition, whenever faulting was invoked to explain an apparent stratigraphic offset, a single fault was introduced – however, multiple faults with lesser separation could also explain these situations. Thus, there is a moderate degree of uncertainty regarding the fault locations.

7.3.7 Dynamic Properties at High Shear Strain

The dynamic laboratory measurements of material properties were limited to strains of about 0.1% in this study because the emphasis was placed on the preclosure seismic design (hazard levels defined at annual exceedance probabilities of 10^{-3} and 10^{-4}). Consequently, data are lacking at higher strain levels, and the behavior at higher strain levels must be based on results published in the literature for other sites. Thus, there is a high degree of uncertainty regarding the dynamic material properties at high strain levels.

7.3.8 Uncertainty Concerning Borrow Area

At the time that this investigation was planned, exploration had been approved at only one potential borrow area for engineered fill material. Other potential borrow areas exist closer to the North Portal. If other borrow areas are considered, the data in this report for the Fran Ridge borrow area will not be pertinent.

8. INPUTS AND REFERENCES

8.1 DOCUMENTS CITED

Barr, D.L.; Moyer, T.C.; Singleton, W.L.; Albin, A.L.; Lung, R.C.; Lee, A.C.; Beason, S.C.; and Eatman, G.L.W. 1996. *Geology of the North Ramp — Stations 4+00 to 28+00, Exploratory Studies Facility, Yucca Mountain Project, Yucca Mountain, Nevada*. Denver, Colorado: U.S. Geological Survey. ACC: MOL.19970106.0496.

Beason, S.C.; Turlington, G.A.; Lung, R.C.; Eatman, G.L.W.; Ryter, D.; and Barr, D.L. 1996. *Geology of the North Ramp - Station 0+60 to 4+00, Exploratory Studies Facility, Yucca Mountain Project, Yucca Mountain, Nevada*. Denver, Colorado: U.S. Geological Survey. ACC: MOL.19970106.0449.

Blout, D.O.; Hammermeister, D.P.; Loskot, C.L.; and Chornack, M.P. 1994. *Geohydrologic Data Collected from Shallow Neutron-Access Boreholes and Resultant-Preliminary Geohydrologic Evaluations, Yucca Mountain Area, Nye County, Nevada*. Open-File Report 92-657. Denver, Colorado: U.S. Geologic Survey. ACC: NNA.19940228.0027.

Board, M.; Linden, A.; and Zhu, M. 2002. *Design Evolution Study-Underground Layout*. TDR-MGR-MG-000003 REV 00. Las Vegas, Nevada: Bechtel SAIC Company. ACC: MOL.20020429.0023.

Boore, D.M. and Brown, L.T. 1998. "Comparing Shear-Wave Velocity Profiles from Inversion of Surface-Wave Phase Velocities with Downhole Measurements: Systematic Differences Between the CXW Method and Downhole Measurements at Six USC Strong-Motion Sites." *Seismological Research Letters*, 69 (3), 222-229. El Cerrito, California: Seismological Society of America. TIC: 251417.

Brown, L.T. 1998. *Comparison of Vs Profiles from SASW and Borehole Measurements at Strong Motion Sites in Southern California*. Master's thesis. Austin, Texas: University of Texas, Austin. TIC: 251296.

Brown, L.T.; Boore, D.M.; and Stokoe, K.H., II. 2000. "Comparison of Shear-Wave Velocity Profiles from SASW and Downhole Seismic Tests at a Strong-Motion Site." Paper 2202 of *12WCEE 2000, 12th World Conference on Earthquake Engineering, Auckland, New Zealand, Sunday 30 January - Friday 4 February 2000*. Upper Hut, New Zealand: New Zealand Society for Earthquake Engineering. TIC: 251263.

BSC (Bechtel SAIC Company) 2001. *Technical Work Plan for: Testing and Monitoring*. TWP-MGR-MD-000018 REV 00. Las Vegas, Nevada: Bechtel SAIC Company. ACC: MOL.20011015.0022.

Buesch, D.C.; Dickerson, R.P.; Drake, R.M.; and Spengler, R.W. 1994. "Integrated Geology and Preliminary Cross Section Along the North Ramp of the Exploratory Studies Facility, Yucca Mountain." *High Level Radioactive Waste Management, Proceedings of the Fifth Annual International Conference, Las Vegas, Nevada, May 22-26, 1994*. 2, 1055-1065. La Grange Park, Illinois: American Nuclear Society. TIC: 210984.

- Buesch, D.C.; Spengler, R.W.; Moyer, T.C.; and Geslin, J.K. 1996. *Proposed Stratigraphic Nomenclature and Macroscopic Identification of Lithostratigraphic Units of the Paintbrush Group Exposed at Yucca Mountain, Nevada*. Open File Report 94-469. Denver, Colorado: U.S. Geological Survey. ACC: MOL.19970205.0061.
- Byers, F.M. Jr.; Carr, W.J.; Orkild, P.P.; Quinlivan, W.D.; and Sargent, K.A. 1976. *Volcanic Suites and Related Cauldrons of Timber Mountain-Oasis Valley Caldera Complex, Southern Nevada*. Professional Paper 919. Washington, D.C.: U.S. Geological Survey. TIC: 201146.
- Chen, A.T.F. and Stokoe, K.H., II. 1979. *Interpretation of Strain-Dependent Modulus and Damping from Torsional Soil Tests*. USGS-GD-79-002. Menlo Park, California: U.S. Geological Survey. TIC: 251943.
- Christiansen, R.L.; Lipman, P.W.; Carr, W.J.; Byers, F.M., Jr.; Orkild, P.P.; and Sargent, K.A. 1977. "The Timber Mountain-Oasis Valley Caldera Complex of Southern Nevada." *Geological Society of America Bulletin*, 88 (7), 943-959. [Boulder, Colorado]: Geological Society of America. TIC: 201802.
- Craig, R. 1997. "Completion of Milestone SPG391M4, Re-Evaluation of Subsurface Lithostratigraphic Contacts." E-mail from R. Craig to M. Tynan, October 1, 1997, with an attachment. ACC: MOL.19980513.0181; MOL.19980513.0182.
- CRWMS M&O 1997. *Yucca Mountain Site Geotechnical Report*. B00000000-01717-5705-00043 REV 01. Las Vegas, Nevada: CRWMS M&O. ACC: MOL.19980212.0354.
- CRWMS M&O 1999a. *Monitored Geologic Repository Site Layout System Description Document*. BCB000000-01717-1705-00007 REV 00. Two volumes. Las Vegas, Nevada: CRWMS M&O. ACC: MOL.19990512.0159.
- CRWMS M&O 1999b. *Preliminary Geotechnical Investigation for Waste Handling Building, Yucca Mountain Site Characterization Project*. BCB000000-01717-5705-00016 REV 00. Las Vegas, Nevada: CRWMS M&O. ACC: MOL.19990625.0182.
- Daley, T.M., Majer, E.L., and Karageorgi, E. 1994. *Combined Analysis of Surface Reflection Imaging and Vertical Seismic Profiling at Yucca Mountain, Nevada*. LBL-36467. Berkeley, California: Lawrence Berkeley National Laboratory. TIC: 247870.
- Day, W.C.; Potter, C.J.; Sweetkind, D.S.; Dickerson, R.P.; and San Juan, C.A. 1998. *Bedrock Geologic Map of the Central Block Area, Yucca Mountain, Nye County, Nevada*. Miscellaneous Investigations Series Map I-2601. [Washington, D.C.]: U.S. Geological Survey. ACC: MOL.19980611.0339.
- DOE (U.S. Department of Energy) 2001. *Yucca Mountain Science and Engineering Report*. DOE/RW-0539. [Washington, D.C.]: U.S. Department of Energy, Office of Civilian Radioactive Waste Management. ACC: MOL.20010524.0272.

EPRI (Electric Power Research Institute) 1993. *Method and Guidelines for Estimating Earthquake Ground Motion*. Volume 1 of *Guidelines for Determining Design Basis Ground Motions in Eastern North America*. EPRI TR-102293. Palo Alto, California: Electric Power Research Institute. TIC: 226495.

Foinquinos Mera, R. 1991. *Analytical Study and Inversion for the Spectral Analysis of Surface Waves Method*. Master's thesis. Austin, Texas: University of Texas, Austin. TIC: 252162.

Geslin, J.K.; Moyer, T.C.; and Buesch, D.C. 1995. *Summary of Lithologic Logging of New and Existing Boreholes at Yucca Mountain, Nevada, August 1993 to February 1994*. Open-File Report 94-342. Denver, Colorado: U.S. Geological Survey. ACC: MOL.19940810.0011.

Gibson, J.D.; Shephard, L.E.; Swan, F.H.; Wesling, J.R.; and Kerl, F.A. 1990. "Synthesis of Studies for the Potential of Fault Rupture at the Proposed Surface Facilities, Yucca Mountain, Nevada." *High Level Radioactive Waste Management, Proceedings of the International Topical Meeting, Las Vegas, Nevada, April 8-12, 1990, 1*, 109-116. La Grange Park, Illinois: American Nuclear Society. TIC: 202058.

Hardin, B.O. and Drnevich, V.P. 1972. "Shear Modulus and Damping in Soils: Measurement and Parameter Effects." *Journal of The Soil Mechanics and Foundations Division*, 98, (SM6), 603-624. New York, New York: American Society of Civil Engineers. TIC: 251418.

Ho, D.M.; Sayre, R.L.; and Wu, C.L. 1986. *Suitability of Natural Soils for Foundations for Surface Facilities at the Prospective Yucca Mountain Nuclear Waste Repository*. SAND85-7107. Albuquerque, New Mexico: Sandia National Laboratories. ACC: NNA.19890327.0053.

Joh, S.-H. 1996. *Advances in the Data Interpretation Technique for Spectral-Analysis-of-Surface-Waves (SASW) Measurements*. Ph.D. dissertation. Austin, Texas: University of Texas at Austin. TIC: 252117.

Joyner, W.B.; Warrick, R.E.; and Fumal, T.E. 1981. "The Effect of Quaternary Alluvium on Strong Ground Motion in the Coyote Lake, California, Earthquake of 1979." *Bulletin of the Seismological Society of America*, 71 (4), 1333-1349. Berkeley, California: Seismological Society of America. TIC: 251490.

Kausel, E. and Roesset, J.M. 1981. "Stiffness Matrices for Layered Soils." *Bulletin of the Seismological Society of America*, 71 (6), 1743-1761. Berkeley, California: Seismological Society of America. TIC: 251419.

Kim, D.-S. 1991. *Deformational Characteristics of Soils at Small to Intermediate Strains from Cyclic Tests*. Ph.D. dissertation. Austin, Texas: University of Texas at Austin. TIC: 252163.

Kim, D.-S. and Stokoe, K.H., II 1994. "Torsional Motion Monitoring System for Small-Strain (10^{-5} to $10^{-3}\%$) Soil Testing" *Geotechnical Testing Journal*, 17, (1), 17-26. Philadelphia, Pennsylvania: American Society for Testing and Materials. TIC: 251420.

Ladd, R.S. 1978. "Preparing Test Specimens Using Undercompaction." *Geotechnical Testing Journal*, 1 (1), 16-23. New York, New York: American Society for Testing and Materials. TIC: 243278.

Lipman, P.W.; Christiansen, R.L.; and O'Connor, J.T. 1966. *A Compositionally Zoned Ash-Flow Sheet in Southern Nevada*. Professional Paper 524-F. Washington, D.C.: U.S. Geological Survey. TIC: 219972.

Lodde, P.F. 1982. *Dynamic Response of San Francisco Bay Mud*. Ph.D. dissertation. Austin, Texas: University of Texas at Austin, Civil Engineering Department. TIC: 252236.

Luebbers M.J. 2000. Waste Handling Building - Revised Shear Wave Velocity Model. Scientific Notebook SN-M&O-SCI-015-V1. ACC: MOL.20000718.0213.

Luebbers, M.J. 2002a. Borehole Suspension Seismic Component of Geotechnical Investigation for a Potential Waste Handling Building. Scientific Notebook SN-M&O-SCI-024-V1. ACC: MOL.20020509.0127, MOL.20020509.0129, MOL.20020509.0130, MOL.20020509.0132.

Luebbers, M.J. 2002b. Borehole Suspension Seismic Component of Geotechnical Investigation for a Potential Waste Handling Building. Scientific Notebook SN-M&O-SCI-024-V2. ACC: MOL.20020509.0128, MOL.20020509.0130, MOL.20020509.0131, MOL.20020509.0132, MOL.20020509.0133.

Luebbers, M.J. 2002c. Downhole Seismic Component of Geotechnical Investigation for a Potential Waste Handling Building. Scientific Notebook SN-M&O-SCI-025-V1. ACC: MOL.20020228.0297.

Marcuson, W.F., III. 1978. "Determination of In Situ Density of Sands." *Dynamic Geotechnical Testing, A Symposium Sponsored by ASTM Committee D-18 on Soil and Rock for Engineering Purposes, American Society for Testing and Materials, Denver, Colorado, 28 June 1977*. ASTM STP 654. Pages 318-340. Philadelphia, Pennsylvania: American Society for Testing and Materials. TIC: 210237.

Mongano, G.S.; Singleton, W.L.; Moyer, T.C.; Beason, S.C.; Eatman, G.L.W.; Albin, A.L.; and Lung, R.C. 1999. *Geology of the ECRB Cross Drift - Exploratory Studies Facility, Yucca Mountain Project, Yucca Mountain, Nevada*. [Deliverable SPG42GM3]. Denver, Colorado: U.S. Geological Survey, ACC: MOL.20000324.0614.

Ohya, S. 1986. "In Situ P and S Wave Velocity Measurement." *Use of In Situ Tests in Geotechnical Engineering, Proceedings of In Situ '86, a Specialty Conference Sponsored by the Geotechnical Engineering Division of the American Society of Civil Engineers, Blacksburg, Virginia, June 23-25, 1986*. Geotechnical Special Publication No. 6. Clemence, S.P., ed. Pages 1218-1235. New York, New York: American Society of Civil Engineers. TIC: 250977.

Redpath, B. 2002. Downhole Seismic Logging at Yucca Mountain Crest. Scientific Notebook SN-M&O-SCI-039-V1. ACC: MOL.20020429.0150, MOL.20020429.0151, MOL.20020429.0152, MOL.20020429.0154.

Richart, F.E., Jr.; Woods, R.D.; and Hall, J.R., Jr. 1970. *Vibrations of Soils and Foundations*. Englewood Cliffs, New Jersey: Prentice Hall. TIC: 240470.

Roesset, J.M.; Chang D.-W.; and Stokoe, K.H., II. 1991. "Comparison of 2-D and 3-D Models for Analysis of Surface Wave Tests." *Soil Dynamics and Earthquake Engineering V, Fifth International Conference on Soil Dynamics and Earthquake Engineering, SDEE 91, Karlsruhe, Germany, September 23-26, 1991*. Pages 111-126. Boston, [Massachusetts]: Computational Mechanics Publications. TIC: 251643.

Ross, C.S. and Smith, R.L. 1961. *Ash Flow Tuffs: Their Origin, Geologic Relations, and Identification*. Professional Paper 366. Reston, Virginia: U.S. Geological Survey. TIC: 216668.

Sawyer, D.A.; Fleck, R.J.; Lanphere, M.A.; Warren, R.G.; Broxton, D.E.; and Hudson, M.R. 1994. "Episodic Caldera Volcanism in the Miocene Southwestern Nevada Volcanic Field: Revised Stratigraphic Framework, 40Ar/39Ar Geochronology, and Implications for Magmatism and Extension." *Geological Society of America Bulletin*, 106, (10), 1304-1318. Boulder, Colorado: Geological Society of America. TIC: 222523.

Schlumberger Educational Services 1987. *Log Interpretation Principles/Applications*. Houston, Texas: Schlumberger Educational Services. TIC: 236275.

Schuraytz, B.C.; Vogel, T.A.; and Younker, L.W. 1989. "Evidence for Dynamic Withdrawal from a Layered Magma Body: The Topopah Spring Tuff, Southwestern Nevada." *Journal of Geophysical Research*, 94, (B5), 5925-5942. Washington, D.C.: American Geophysical Union. TIC: 225936.

Seed, H.B.; Wong, R.T.; Idriss, I.M.; and Tokimatsu, K. 1986. "Moduli and Damping Factors for Dynamic Analyses of Cohesionless Soils." *Journal of Geotechnical Engineering*, 112 (11), 1016-1033. New York, New York: American Society of Civil Engineers. TIC: 243355.

Stokoe, K.H., II; Hwang, S.-K.; Roesset, J.M.; and Sun, C.W. 1994. "Laboratory Measurement of Small-Strain Material Damping of Soil Using a Free-Free Resonant Column." *Earthquake Resistant Construction and Design, Proceedings of the Second International Conference on Earthquake Resistant Construction and Design, Berlin, 15-17 June 1994*. Savidis, S.A., ed. Pages 195-202. Rotterdam, The Netherlands: A.A. Balkema. TIC: 251641.

Stokoe, K.H., II; Wright, S.G.; Bay, J.A.; and Roesset, J.M. 1994. "Characterization of Geotechnical Sites by SASW Method." *Volume Prepared by ISSMFE Technical Committee #10 for XIII ICSMFE, 1994, New Delhi, India*. Woods, R.D., ed. New York, New York: International Science Publisher. TIC: 251421.

USGS (U.S. Geological Survey) 2001. *Water-Level Data Analysis for the Saturated Zone Site-Scale Flow and Transport Model*. ANL-NBS-HS-000034 REV 01. Denver, Colorado: U.S. Geological Survey. ACC: MOL.20020209.0058.

Wahl, J.S.; Tittman, J.; Johnstone, C.W.; and Alger, R.P. 1964. "The Dual Spacing Formation Density Log." *Journal of Petroleum Technology*, [16], ([12]), 1411-1416. Dallas, Texas: Society of Petroleum Engineers of AIME. TIC: 250964.

Wilson, R.C.; Warrick, R.E.; and Bennett, M.J. [1978]. "Seismic Velocities of San Francisco Bayshore Sediments." [*Earthquake Engineering and Soil Dynamics, Proceeding of the ASCE Geotechnical Engineering Division Specialty Conference, June 19-21, 1978, Pasadena, CA.*] [3], 1007-1023. [New York, New York: American Society of Civil Engineers]. TIC: 252168.

Wong, I.G. 2001. Crosshole Seismic Velocity Measurements in the North Ramp of the Exploratory Studies Facility [Initial Entry - Notebook Cancelled]. Scientific Notebook SN-M&O-SCI-020-V1. ACC: MOL.20010827.0034.

Wong, I.G. 2002a. SASW Measurements Near the Top of Yucca Mountain and in the Potential Repository Block. Scientific Notebook SN-M&O-SCI-040-V1. ACC: MOL.20020619.0461, MOL.20020619.0462.

Wong, I.G. 2002b. Downhole Seismic Measurements at the Potential Waste Handling Building Site. Scientific Notebook SN-M&O-SCI-030-V1. ACC: MOL.20020227.0168.

Wong, I.G. 2002c. SASW Measurements at Waste Handling Building Site. Scientific Notebook SN-M&O-SCI-022-V1. ACC: MOL.20020520.0222; MOL.20020520.0223; MOL.20020520.0225; MOL.20020520.0226.

Wong, I.G. 2002d. SASW Measurements at the Top of Yucca Mountain. Scientific Notebook SN-M&O-SCI-023-V1. ACC: MOL.20020607.0198, MOL.20020607.0201, MOL.20020607.0202.

Wong, I.G. 2002e. Laboratory Dynamic Testing of Rock and Soil Specimens for the Potential Waste Handling Building Site. Scientific Notebook SN-M&O-SCI-033-V1. ACC: MOL.20020508.0336; MOL.20020508.0392; MOL.20020508.0337; MOL.20020508.0394.

Wong, I.; Kelson, K.; Olig, S.; Kolbe, T.; Hemphill-Haley, M.; Bott, J.; Green, R.; Kanakari, H.; Sawyer, J.; Silva, W.; Stark, C.; Haraden, C.; Fenton, C.; Unruh, J.; Gardner, J.; Reneau, S.; and House, L. 1995. *Seismic Hazards Evaluation of the Los Alamos National Laboratory*. Volume 1. Oakland, California: Woodward-Clyde Federal Services. TIC: 247191.

YMP (Yucca Mountain Site Characterization Project) 1998. Borehole Video for Geotechnical Hole UE-25 RF#13. LA-EES-7-LV-NBK-98-001, 41V. [Las Vegas, Nevada: Yucca Mountain Site Characterization Office]. ACC: MOL.19990914.0122.

YMP (Yucca Mountain Site Characterization Project) 2001. *Q-List*. YMP/90-55Q, Rev. 7. Las Vegas, Nevada: Yucca Mountain Site Characterization Office. ACC: MOL.20010409.0366.

8.2 STANDARDS AND PROCEDURES

10 CFR 63. 2002. *Energy: Disposal of High-Level Radioactive Wastes in a Geologic Repository at Yucca Mountain, Nevada*. Readily available.

AP-2.21Q, Rev. 1, BSCN 1. *Quality Determinations and Planning for Scientific, Engineering, and Regulatory Compliance Activities*. Las Vegas, Nevada: CRWMS M&O.
ACC: MOL.20010212.0018.

AP-2.22Q, Rev. 0. *Classification Criteria and Maintenance of the Monitored Geologic Repository Q-List*. Las Vegas, Nevada: CRWMS M&O. ACC: MOL.20020314.0046.

AP-SI.1Q, Rev. 3, ICN 4. *Software Management*. Las Vegas, Nevada: CRWMS M&O.
ACC: MOL.20020520.0283.

AP-SIII.5, Rev. 0. *Yucca Mountain Site Characterization Project Field Verification of Geophysical Operations*. Las Vegas, Nevada: CRWMS M&O. ACC: MOL.20010604.0219.

AP-SIII.6Q, Rev. 0. *Geophysical Logging Programs for Surface-Based Testing Program Boreholes*. Las Vegas, Nevada: CRWMS M&O. ACC: MOL.20010604.0045.

AP-SV.1Q, Rev 0, ICN 2. *Control of the Electronic Management of Information*.
Las Vegas, Nevada: CRWMS M&O. MOL.20000831.0065.

ASTM C 136-96a. 1996. *Standard Test Method for Sieve Analysis of Fine and Coarse Aggregates*. West Conshohocken, Pennsylvania: American Society for Testing and Materials.
TIC: 241447.

ASTM D 653-97. 1997. *Standard Terminology Relating to Soil, Rock, and Contained Fluids*.
West Conshohocken, Pennsylvania: American Society for Testing and Materials. TIC: 248967.

ASTM D 1557-91. 1998. *Standard Test Method for Laboratory Compaction Characteristics of Soil Using Modified Effort (56,000 ft-lbf/ft³ (2,700 kN-m/m³))*. West Conshohocken,
Pennsylvania: American Society for Testing and Materials. TIC: 242992.

LP-GEO-001Q-M&O, Rev. 0, ICN 0. *Laboratory Geotechnical Testing of Soil, Rock and Aggregate Samples*. Washington, D.C.: U.S. Department of Energy, Office of Civilian
Radioactive Waste Management. ACC: MOL.20001215.0254.

LP-GEO-002Q-BSC, Rev. 0, ICN 1. *Laboratory Dynamic Rock/Soil Testing*.
Washington, D.C.: U.S. Department of Energy, Office of Civilian Radioactive Waste
Management. ACC: MOL.20010406.0165.

NWI-SPO-004Q, Rev. 0. *Laboratory Dynamic Rock/Soil Testing*.
Las Vegas, Nevada: CRWMS M&O. ACC: MOL.19990317.0325.

PBRCTS-1, Rev. 4. *Technical Procedures for Resonant Column and Torsional Shear (RCTS) Testing of Soil and Rock Samples*. Austin, Texas: Geotechnical Engineering Center, University of Texas, Austin. TIC: 252682.

USBR 5000-86. *Procedure for Determining Unified Soil Classification (Laboratory Method)*. Denver, Colorado: U.S. Department of the Interior, Bureau of Reclamation. TIC: 232041.

USBR 5005-86. *Procedure for Determining Unified Soil Classification (Visual Method)*. Denver, Colorado: U.S. Department of the Interior, Bureau of Reclamation. TIC: 232041.

USBR 5205-89. *Procedure for Preparing Soil Samples by Splitting or Quartering*. Denver, Colorado: U.S. Department of the Interior, Bureau of Reclamation. TIC: 232041.

USBR 5300-89. *Procedure for Determining Moisture Content of Soil and Rock by the Oven Method*. Denver, Colorado: U.S. Department of the Interior, Bureau of Reclamation. TIC: 232041.

USBR 5320-89. *Procedure for Determining Specific Gravity of Soils*. Denver, Colorado: U.S. Department of the Interior, Bureau of Reclamation. TIC: 232041.

USBR 5325-89. *Procedure for Performing Gradation Analysis of Gravel Size Fraction of Soils*. Denver, Colorado: U.S. Department of the Interior, Bureau of Reclamation. TIC: 232041.

USBR 5330-89. *Procedure for Performing Gradation Analysis of Fines and Sand Size Fraction of Soils, Including Hydrometer Analysis*. Denver, Colorado: U.S. Department of the Interior, Bureau of Reclamation. TIC: 232041.

USBR 5335-89. *Procedure for Performing Gradation Analysis of Soils Without Hydrometer – Wet Sieve*. Denver, Colorado: U.S. Department of the Interior, Bureau of Reclamation. TIC: 232041.

USBR 5350-89. *Procedure for Determining the Liquid Limit of Soils by the One-Point Method*. Denver, Colorado: U.S. Department of the Interior, Bureau of Reclamation. TIC: 232041.

USBR 5360-89. *Procedure for Determining the Plastic Limit and Plasticity Index of Soils*. Denver, Colorado: U.S. Department of the Interior, Bureau of Reclamation. TIC: 232041.

USBR 5525-89. *Procedure for Determining the Minimum Index Unit Weight of Cohesionless Soils*. Denver, Colorado: U.S. Department of the Interior, Bureau of Reclamation. TIC: 232041.

USBR 5530-89. *Procedure for Determining the Maximum Index Unit Weight of Cohesionless Soils*. Denver, Colorado: U.S. Department of the Interior, Bureau of Reclamation. TIC: 232041.

USBR 7205-89. *Procedure for Determining Unit Weight of Soils In-Place by the Sand-Cone Method*. Denver, Colorado: U.S. Department of the Interior, Bureau of Reclamation. TIC: 232041.

USBR 7221-89. *Procedure for Determining Unit Weight of Soils In-Place by the Water Replacement Method in a Test Pit*. Denver, Colorado: U.S. Department of the Interior, Bureau of Reclamation. TIC: 232041.

8.3 SOURCE DATA, LISTED BY DATA TRACKING NUMBER (DTN)

GS000508312332.001. Water-Level Data Analysis for the Saturated Zone Site-Scale Flow and Transport Model. Submittal date: 06/01/2000.

GS020383114233.001. Waste Handling Building Test Pit Logs With Photomosaic Test Pit Maps. TDIF: 312887. Submittal date: 03/28/2002.

GS020383114233.003. Geotechnical Borehole Logs for the Waste Handling Building, Yucca Mountain Project, Nevada Test Site, Nevada. Submittal date: 03/28/2002.

GS020483114233.004. Geotechnical Field and Laboratory Test Results from Waste Handling Building Foundation Investigation. Submittal date: 04/15/2002.

GS020783114233.005. Gradation Analysis Test Results and Graphical Plots from Tests Performed on Materials Excavated from In-Situ Density Test Locations in Test Pits from the Waste Handling Building Foundation Investigations. Submittal date: 07/23/2002.

GS920983114220.001. Log of Test Pit or Auger Hole, Physical Properties Summary, Gradation Test, and Summary of Physical Properties Test Results for Hole Numbers NRSF-TP-11, TP-19, TP-21, TP-25, TP-28, TP-29, and TP-30. Submittal date: 09/03/1992.

GS931008314211.036. Graphical Lithologic Log of Borehole RF-3 (UE-25 RF#3), Version 1.0. Submittal date: 10/07/1993.

GS940208314211.004. Table of Contacts in Borehole USW UZ-N27. Submittal date: 02/10/1994.

GS940208314211.006. Table of Contacts in Boreholes USW UZ-N33 AND USW UZ-N34. Submittal date: 02/10/1994.

GS940308314211.009. Summary of Lithologic Logging of New and Existing Boreholes at Yucca Mountain, Nevada: August 1993 to February 1994. Submittal date: 03/01/1994.

GS940408314224.004. Plan View Geologic Map of the Drainage Channel and North Portal. Submittal date: 04/20/1994.

GS940708314211.032. Summary of Lithologic Logging of New and Existing Boreholes at Yucca Mountain, Nevada, March 1994 to June 1994. Submittal date: 07/08/1994.

GS940908314211.045. Graphical Lithologic Log of the Paintbrush Group for Borehole USW SD-12. Submittal date: 09/12/94.

GS941108314211.052. Graphical Lithologic Log of Borehole USW SD-9 from the Base of the Paintbrush Group to Total Depth. Submittal date: 11/03/1994.

GS980608314221.002. Revised Bedrock Geologic Map of the Yucca Mountain Area, Nye County, Nevada. Submittal date: 06/09/1998.

MO0001SEPRADSD.000. Downhole Seismic Data. Submittal date: 01/11/2000.

MO0008GSC00286.000. Exploratory Studies Facility (ESF) North Portal Pad, Waste Handling Building (WHB) Profile Sections #3, #4, #5, #6, #7, and #8. Submittal date: 08/17/2000.

MO0012GSC00405.000. Waste Handling Building (WHB) Site Investigations, As-Built Surveys for Test Pit #1 through #4. Submittal date: 12/22/2000.

MO0101COV00396.000. Coverage: Bores 3. Submittal date: 01/05/2001.

MO0101SEPBGLOG.000. Sample Management & Drilling Department Records Package for Borehole Records (Geologic Logs) from the "Geotechnical Field Investigation for the Waste Handling Building" FWP-SB-00-003. Submittal date: 01/10/2001.

MO0110DVDBOREH.000. Downhole Velocity Data from Boreholes RF-13 and RF-17. Submittal date: 10/17/2001.

MO0110SASWVDYM.000. SASW Velocity Data from the Top of Yucca Mountain. Submittal date: 10/02/2001.

MO0110SASWWHBS.000. SASW Velocity Data from the Waste Handling Building Site Characterization Area. Submittal date: 10/02/2001.

MO0111DVDWHBSC.001. Downhole Velocity Data at the Waste Handling Building Site Characterization Area. Submittal date: 11/08/2001.

MO0112GPLOGWHB.001. Developed Geophysical Log Data from Forensic Evaluation of Geophysical Log Data Collected in Support of the Waste Handling Building. Submittal date: 12/03/2001.

MO0112GSC01170.000. Borrow Pit #1 (Fran Ridge), USBR Sample Locations, for WHB Investigations. Submittal date: 12/04/2001.

MO0202DVDWHBSC.002. Downhole Velocity Data from the Top of Yucca Mountain. Submittal date: 02/11/2002.

MO0202DWAVEATD.000. Downhole S-Wave and P-Wave Interpreted Arrival Time Data from Boreholes RF#13 and RF#17. Submittal date: 02/13/2002.

MO0202GEOSOILP.000. Statistical Summary of Geotechnical Soil Properties by Lithostratigraphical Units. Submittal date: 02/19/2002.

MO0202WHBTMPKS.000. Time Picks for Downhole Seismic Surveys.
Submittal date: 02/13/2002.

MO0203DHRSSWHB.001. Dynamic Laboratory Test Data for Rock and Soil Samples from the Waste Handling Building Site Characterization Area. Submittal date: 03/19/2002.

MO0203EBSCTCTS.016. Compaction and Triaxial Compression Tests of Soil Sample.
Submittal date: 04/01/2002.

MO0203SEPSASWD.000. SASW Velocity Data from the Top of Yucca Mountain. Submittal date: 03/28/2002.

MO02045FTDSUSP.001. Statistics for Shear-Wave Velocity, Compression-Wave Velocity, and Poisson's Ratio by 1.5-Meter Depth Intervals from Suspension Seismic Measurements.
Submittal date: 04/23/2002.

MO020498DNHOLE.000. Shear-Wave and Compression-Wave Velocity Profiles from 1998 Downhole Survey at Borehole UE-25 RF#13. Submittal date: 04/08/2002.

MO0204DENBROCK.000. Statistics for Bulk Density Values by Lithostratigraphic Unit.
Submittal date: 04/23/2002.

MO0204SEISDWHB.001. Suspension Seismic Data for Borehole UE-25 RF#13 at the Waste Handling Building Site Characterization Area. Submittal date: 04/08/2002.

MO0204SEPBSWHB.001. Borehole Suspension Data for Waste Handling Building Site Characterization Area. Submittal date: 04/10/2002.

MO0204SEPFDSSS.000. Profiles of Average Shear-Wave Velocity, Compression-Wave Velocity and Poisson's Ratio from Accumulated Travel Times from Suspension Seismic Surveys at Boreholes UE-25 RF#14 to #26 and RF#28 and RF#29. Submittal date: 04/22/2002.

MO0204SEPGAMDM.000. Statistical Analysis of Gamma-Gamma Density Measurements by Lithostratigraphic Unit. Submittal date: 04/22/2002.

MO0204SEP_SOILP.000. Mean Values of Soil Properties by Lithostratigraphic Unit.
Submittal date: 04/02/2002.

MO0204SEPSWSSS.000. Profile of Average Shear-Wave Velocities from Accumulated Travel Times from a Suspension Seismic Survey at Borehole UE-25 RF#13.
Submittal date: 04/22/2002.

MO0204SUSPSEIS.001. Statistics for Shear-Wave Velocity, Compression-Wave Velocity, and Poisson's Ratio by Lithostratigraphic Unit from Suspension Seismic Measurements. Submittal Date 04/23/2002.

MO0205SEPPRDSV.000. Profiles of Poisson's Ratio from Downhole Seismic Velocity Profiles at Boreholes UE-25 RF#13 to #26 and RF#28 and RF#29. Submittal date: 05/28/2002.

MO0205SWDQRTWF.000. Plots of Average Shear-Wave Velocity Versus Depth and Quarter-Wavelength Amplification Ratio Versus Frequency at Boreholes UE-25 RF#14 to UE-25 RF#19 and UE-25 RF#29. Submittal date: 05/01/2002.

MO0206EBSFRBLT.018. Fran Ridge Borrow Lab Testing. Submittal date: 06/10/2002.

MO0206SASWROCK.000. SASW Velocity Data from Rock Sites on the Crest of Yucca Mountain and in the ESF. Submittal date: 06/19/2002.

MO98PRECLOSURE.000. Design Event Spectra Based on the Results of the Probabilistic Seismic Hazard Analyses for Yucca Mountain and a Velocity Profile for the Repository Block to Support Development of Ground Motion Design Inputs. Submittal date: 02/20/1998.

MO9905LABDYNRS.000. Laboratory Dynamic Rock/Soil Testing for UE-25 RF#13. Submittal date: 05/06/1999.

SNL01A05059301.005. Laboratory Thermal Conductivity Data for Boreholes UE25 NRG-4, NRG-5; USW NRG-6 and NRG-7/7A. Submittal date: 02/07/1996.

SNL02030193001.001. Mechanical Properties for Drill Hole USW NRG-6 Samples from Depth 22.2 ft. to 328.7 ft. Submittal date: 05/17/1993.

SNL02030193001.002. Mechanical Properties Data for Drill Hole USW NRG-6 Samples from Depth 22.2 ft. to 427.0 ft. Submittal date: 06/25/1993.

SNL02030193001.003. Mechanical Properties Data for Drill Hole UE-25 NRG#2 Samples from Depth 170.4 ft. to 200.0 ft. Submittal date: 07/07/1993.

SNL02030193001.004. Mechanical Properties Data for Drill Hole USW NRG-6 Samples from Depth 462.3 ft. to 1085.0 ft. Submittal date: 08/05/1993.

SNL02030193001.005. Mechanical Properties Data for Drill Hole UE-25 NRG#3 Samples from Depth 15.4 ft. to 297.1 ft. Submittal date: 09/23/1993.

SNL02030193001.006. Mechanical Properties Data for Drill Hole UE-25 NRG#2A Samples from Depth 90.0 ft. to 254.5 ft. Submittal date: 10/13/1993.

SNL02030193001.007. Mechanical Properties Data for Drill Hole UE25 NRG#3 Samples from Depth 263.3 ft. to 265.7 ft. Submittal date: 10/20/1993.

SNL02030193001.008. Mechanical Properties Data for Drill Hole USW NRG-6 Sample at Depth of 416.0 ft. Submittal date: 10/20/1993.

SNL02030193001.009. Mechanical Properties Data for Drill Hole UE-25 NRG-5 Samples from Depth 781.0 ft. to 991.9 ft. Submittal date: 11/18/1993.

SNL02030193001.010. Mechanical Properties Data for Drill Hole UE25 NRG-2B Samples from Depth 2.7 ft. to 87.6 ft. Submittal date: 11/18/1993.

SNL02030193001.011. Mechanical Properties Data for Drill Hole UE25 NRG-2A Samples from Depth 135.3 ft. to 166.5 ft. Submittal date: 11/18/1993.

SNL02030193001.012. Mechanical Properties for Drill Hole UE25 NRG-5 Samples from Depth 847.2 ft. to 896.5 ft. Submittal date: 12/02/1993.

SNL02030193001.013. Mechanical Properties Data for Drill Hole UE25 NRG-2B Samples from Depth 2.7 ft. to 87.6 ft. Submittal date: 12/02/1993.

SNL02030193001.014. Mechanical Properties Data for Drill Hole UE25 NRG-4 Samples from Depth 378.1 ft. to 695.8 ft. Submittal date: 01/31/1994.

SNL02030193001.015. Mechanical Properties Data for Drill Hole UE25 NRG-4 Samples from Depth 527.0 ft. Submittal date: 02/16/1994.

SNL02030193001.016. Mechanical Properties Data for Drill Hole USW NRG-7/7A Samples from Depth 18.0 ft. to 472.9 ft. Submittal date: 03/16/1994.

SNL02030193001.017. Mechanical Properties Data for Drill Hole USW NRG-7/7A Samples from Depth 18.0 ft. to 495.0 ft. Submittal date: 03/21/1994.

SNL02030193001.018. Mechanical Properties Data for Drill Hole USW NRG-7/7A Samples from Depth 344.4 ft. Submittal date: 04/11/1994.

SNL02030193001.019. Mechanical Properties Data for Drill Hole USW NRG-7/7A Samples from Depth 507.4 ft. to 881.0 ft. Submittal date: 06/29/1994.

SNL02030193001.020. Mechanical Properties Data for Drill Hole USW NRG-7/7A Samples from Depth 554.7 ft. to 1450.1 ft. Submittal date: 07/25/1994.

SNL02030193001.021. Mechanical Properties Data (Ultrasonic Velocities, Static Elastic Properties, Triaxial Strength, Dry Bulk Density & Porosity) for Drill Hole USW NRG-7/7A Samples from Depth 345.0 ft. to 1408.6 ft. Submittal date: 02/16/1995.

SNL02030193001.022. Mechanical Properties Data for Drill Hole USW NRG-6 Samples from Depth 5.7 ft. to 1092.3 ft. Submittal date: 02/27/1995.

SNL02030193001.023. Mechanical Properties Data (Ultrasonic Velocities, Static Elastic Properties, Unconfined Strength, Triaxial Strength, Dry Bulk Density & Porosity) for Drill Hole USW SD-12 Samples from depth 16.1 ft. to 1300.3 ft. Submittal date: 08/02/1995.

SNL02030193001.024. Elevated Temperature Confined Compression Tests (Ultrasonic Velocities, Static Elastic Properties, Unconfined Strength, Triaxial Strength, Dry Bulk Density & Porosity) for Drill Hole USW SD-9 Samples from 52.6 ft. to 2222.9 ft. Submittal date: 09/05/1995.

SNL02030193001.026. Mechanical Properties Data (Ultrasonic Velocities, Elastic Moduli and Fracture Strength) for Borehole USW SD-9. Submittal date: 02/22/1996.

SNL02030193001.027. Summary Of Bulk Property Measurements Including Saturated Bulk Density For NRG-2, NRG-2A, NRG-2B, NRG-3, NRG-4, NRG-5, NRG-6, NRG-7/7A, SD-9, and SD-12. Submittal date: 08/14/1996.

SNSAND85081500.000. Preliminary Validation of Geology at Site for Repository Surface Facilities, Yucca Mountain, Nevada. Submittal date: 11/01/1986.

SNSAND90249100.000. Summary and Evaluation of Existing Geological and Geophysical Data Near Prospective Surface Facilities in Midway Valley, Yucca Mountain Project, Nye County, Nevada. Submittal date: 01/01/1992.

8.4 SOFTWARE CODES

University of Texas 2002. *Software Code: WinSASW*. V1.23. 10588-1.23-00.

9. ATTACHMENTS

Attachment	Title
I	Logs of Boreholes RF#14 to RF#29
II	Revised Logs of Borehole RF#13
III	Logs of Test Pits TP-WHB-1 to TP-WHB-4
IV	Photomosaic Maps of Test Pits TP-WHB-1 to TP-WHB-4
V	Downhole Seismic Velocity Plots (Redpath) – WHB Area
VI	Downhole Seismic Velocity Plots (GEOVision) – WHB Area
VII	Suspension Seismic Interval Velocity Results
VIII	Suspension Seismic Accumulated Velocity Results
IX	SASW Velocity Plots – WHB Area
X	Borehole Geophysical Surveys
XI	Geotechnical Laboratory Static Testing – WHB Area
XII	Geotechnical Laboratory Dynamic Testing – WHB Area
XIII	SASW Velocity Plots – ESF
XIV	Geotechnical Laboratory Dynamic Testing – ESF
XV	SASW Velocity Plots – Yucca Mountain Crest
XVI	Downhole Seismic Velocity Plots– Yucca Mountain Crest
XVII	Geotechnical Laboratory Dynamic Testing – Fran Ridge
XVIII	Glossary